Fisheries Research
November 2021, Volume 243 Pages 106053 (11p.)
https://doi.org/10.1016/j.fishres.2021.106053
https://archimer.ifremer.fr/doc/00703/81497/

Seasonal and inter-annual variability in abundance of the main tropical tunas in the EEZ of Côte d'Ivoire (2000-2019)

Akia Sosthene [1, 2, 3, *] , Amandé M. [2], Pascual P. [4], Gaertner Daniel [1, 3]

[1] MARBEC, Univ Montpellier, CNRS, Ifremer, IRD, Sète, France
[2] Centre de Recherches Océanologiques (CRO), Abidjan, Cote d'Ivoire
[3] Institut de Recherche pour le Développement (IRD), UMR MARBEC, Av. Jean Monnet, CS 30171, Sète, Cedex, 34203, France
[4] Instituto Español de Oceanografía, Centro Oceanográfico de Canarias, Apdo. de Correos 1373, 38080, Santa Cruz de Tenerife, Islas Canarias, Spain

* Corresponding author : Sosthene Akia, email address : sosthene.akia@ird.fr

Abstract :

The seasonal and inter-annual variability in abundance of the main "local tropical tuna resources" in the EEZ of Côte d'Ivoire was analysed with catch and effort data from French and Spanish purse seiners over the period 2000–2019. A seasonal spatio-temporal model developed by Thorson et al. (2020a) was used to estimate abundance indices for the main tropical tunas by commercial category (<10 kg and> = 10 kg, which correspond roughly to maturity stage: immature and mature respectively), and fishing mode (free school sets and FAD sets). Furthermore, we decomposed the abundance time series into intrinsic mode functions using the CEEMDAN algorithm. The decomposition procedure made it possible to filter out the noise in the signal and extract the seasonal and inter-annual components of the abundance indices. A generalized additive model (GAM) was applied to the abundance indices to reveal the influences of environmental factors on species abundance and spatio-temporal distribution. Biological interpretations of the seasonal and inter-annual variability in tropical tuna abundance were made and the possible effects of environmental variables on this abundance discussed. Our results suggest that there are two main fishing seasons in the EEZ of Côte d'Ivoire. It was also found that mature yellowfin tunas are abundant between the first and second quarter of the year while the best season for skipjack occurs between the third and fourth quarter. In addition, we observed a considerable change over time in the seasonal and inter-annual variability of tropical tunas in this area.

Highlights

► Assessment of the tuna resources in the EEZ of Côte d'Ivoire by estimating abundance indices with a seasonal spatio-temporal model. ► Evidence of two marked seasons of abundance: mature yellowfin from February to June and skipjack from August to December. ► Differences in sensitivity to environmental variables and peak abundance of tuna caught on FAD vs tuna caught on FSC. ► Similarity between the dynamics of some abundance indices and some environmental variables.

Keywords : Abundance indices, Seasonal and inter-annual variation, Spatio-temporal vector autoregressive model, (VAST), Tropical tuna

1. Introduction

Fishing is of paramount importance in Côte d'Ivoire, as it is one of the main sources of animal protein for the country's poorest households due to its relatively affordable price compared to meat. Socio-economically, the tuna industry plays an important role in employment in Côte d'Ivoire (landing activities, canneries) and exports there. A trade and utilization chain for the tuna bycatch, called "faux poissons", retained on-board by purse seiners and landed in Abidjan (Côte d'Ivoire) has been developed since the early 1990s. Romagny et al. (2000) showed that this sector was of great socioeconomic importance for its actors from landing to consumption. A recent study has shown that in addition to the great social and economic importance of this sector for the local population, it contributes substantially towards food security for the Ivorian people (Monin et al., 2017). Côte d'Ivoire furthermore benefits from the incomes generated by fisheries agreements concluded with long-distance foreign vessels.

Given the essential role of fisheries, and mainly tuna fisheries, coastal countries have established fisheries departments to better manage the exploitation of tuna resources in their EEZ. Due to their highly migratory nature, the management of tuna stocks is carried out at a large regional scale by Regional Fisheries Management Organizations (RFMOs). Despite the need to assess the status of tuna resources at the stock level, little information is produced to know the state of the local resources, thus the coastal countries cannot optimize the management of their EEZ. In Côte d'Ivoire, there are two main types of tuna fisheries: industrial and artisanal. Industrial fisheries are dominated by EU purse seiners, with Spain and France predominant (Failler et al., 2014). Fisheries data for the EU industrial fleet are very well collected and monitored, and remain the best sources of information on the sector. The tuna resources of Côte d'Ivoire are mainly exploited by this fleet within the framework of a fishing agreement between Côte d'Ivoire and the European Union (Failler et al., 2014). The production of artisanal tuna fishery remains significant, but the data collected on this segment remain insufficient for a complete analysis of the sector. To date, local abundance of tuna in the EEZ of Côte d'Ivoire has not been specifically assessed (Cofrepeche, Poseidon, 2012; Failler et al., 2014). However, the downward trend in the reference tonnage of the EU/CIV fisheries agreements (supplementary material S1: Table 1:S1) and the global and local effects of climate change highlight the urgent need for Côte d'Ivoire to study seasonal and inter-annual variation in the tuna resources temporarily found in its EEZ.

Given the lack of direct estimates from scientific surveys, commercial catch per unit of effort (CPUE) is used to derive relative abundance of tuna resources which play an important role in stock assessment and management (Ricker, 1940; Maunder and Langley, 2004; Maunder and Punt, 2004). Nominal CPUEs derived from commercial fisheries are greatly influenced by spatial, temporal, and environmental factors, among others, and need to be standardized (Fonteneau et al., 1999; Maunder and Punt, 2004). Several methods have been applied to standardize CPUE including GLMs and GAMs (Campbell, 2004; Katara et al., 2018); Machine learning and Data mining techniques (Albeare, 2009; Yang et al., 2015), and spatio-temporal models (Thorson et al., 2020a, 2015; Maunder et al., 2020). We use the recent version of the VAST spatio-temporal model developed by Thorson et al. (2020a). This model includes annual, seasonal and spatial variations in density and allows us to capture two important key issues: (i) the standardization of data that are spatially unbalanced over several seasons and (ii) the identification of inter-annual changes in the seasonal chronology of population. The three most important tropical tuna species - skipjack tuna (Katsuwonus pelamis, SKJ), yellowfin tuna

(Thunnus albacares, YFT), and bigeye tuna (Thunnus obesus, BET) - were divided into eight class categories taking into account the species, the maturity stage (immature and mature), and the two main fishing modes in the purse seine fishery (free school sets and floating object sets: hereafter referred to as FSC and FOB, respectively [note that FOB can be natural logs but in the large majority of cases are drifting fish aggregating devices known as dFADs]. The categorization of species by school type is legitimate in the sense that the fishing techniques differ. Fishing on dFADs can be analogous to harvesting and collecting, and fishing on free schools to searching and hunting. dFADs increase the catchability of tuna, as compared to sets on free schools by helping fishers locate fish (reducing search time) and allowing a high percentage of successful sets (Moreno et al., 2007). Free schools are dominated by large yellowfin whereas dFADs schools are mainly composed of skipjack and juveniles of the two others species. This distinction will enable evaluation of this aspect in the study area. Several studies have highlighted the major effects of climatic cycles on the distribution and availability of tuna resources in a local area (Maury et al., 2001; Lehodey et al., 2006; Ménard et al., 2007; Marsac, 2017). The variability of climatic conditions can be a non-negligible indicator of the variability in tuna abundance and spatial distribution and consequently justify the analysis of the relationship between environmental variables and tuna abundance indices. The following environmental variables have been selected for this study: sea surface temperature (SST), dissolved oxygen at a depth of 100 m (DO2_100), chlorophyll concentration (CHL), sea surface salinity (SSS), mixed layer thickness (MLD), sea surface height (SSH) and SST-based coastal upwelling index (CUI_sst). Indeed, some studies showed that upwelling indices are important in explaining the fluctuations of tuna and tuna-like species abundance.

To analyse the seasonal and inter-annual variation in the European purse seiners CPUEs in the Ivorian EEZ, we first estimated the abundance indices using a Thorson et al. (2020a) seasonal spatio-temporal model. Thereafter, we used a method adapted to analyse non-linear and non-stationary signals (i.e., the CEEMDAN algorithm), with the aim to decompose the CPUE series into a finite and exhaustive number of components, called intrinsic mode functions (IMFs). Finally, we explored the relationships between the estimated abundance indices and the environmental variables using GAMs.

2. Materials and methods

2.1. Study area

The study area extends between latitudes 1 °N and 6 °N and longitudes 2 °W and 8 °W (Fig. 1). This is the smallest area that includes the 1° square that pass through the Ivorian EEZ. The area was selected to facilitate future comparisons with data collected by 1° square degrees and to avoid boundary effects. This area is characterized by a seasonal surface temperature signal due to the presence of two cool seasons, each associated with the coastal upwelling (Morlière, 1970). The main cold season takes place in winter between July and September. Winter cooling is then intensified on the coast by upwelling that brings nutrient-rich water to the surface. A second cooling occurs along the coast in January-February; this second cold season is low-amplitude and short-lived (between one and two months; Cury and Roy, 1987)

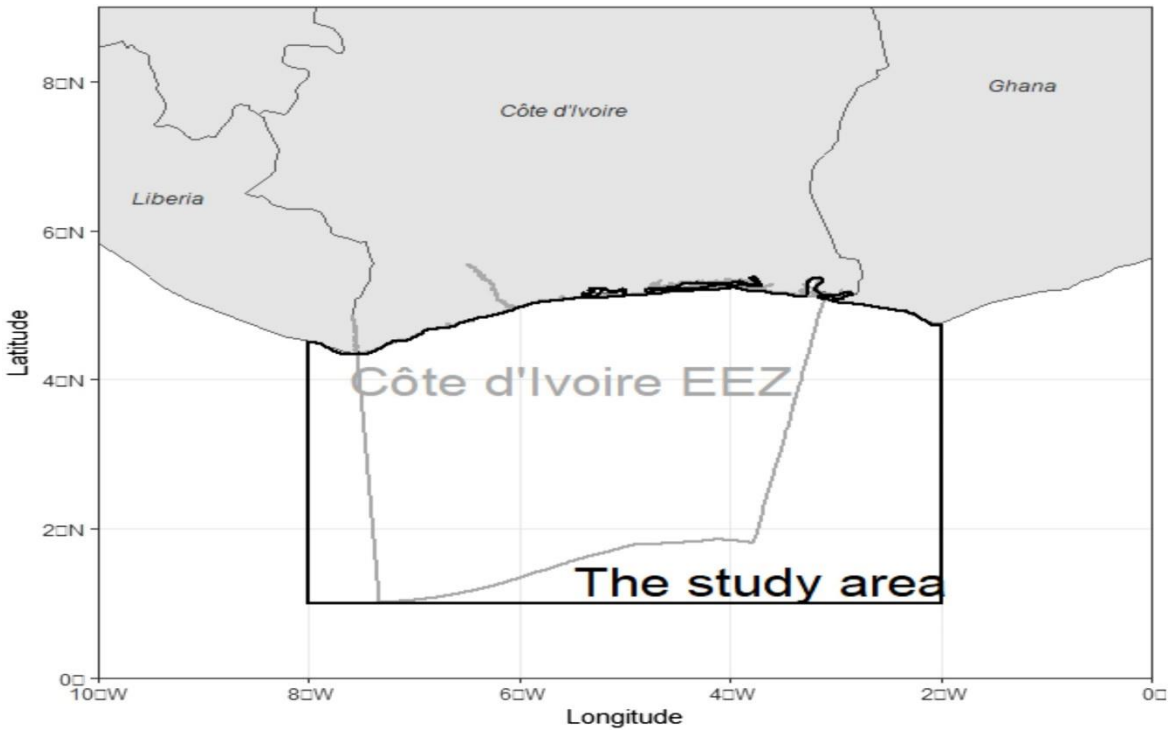

Fig. 1. The EEZ of Côte d'Ivoire and the study area. The area of interest is the square area defined in this figure.

2.2. Catch and effort data

Catch and effort data for EU purse seiners operating in the EEZ of Côte d'Ivoire from 2000 to 2019 were compiled and managed by the Tuna Observatory (Ob7) of the French National Research Institute for Sustainable Development (IRD, UMR MARBEC), and the Spanish Institute of Oceanography (IEO) for the French and the Spanish fleets respectively. The raw logbook data produced by the skippers were corrected by the T3 methodology regarding total catch per set (to account for the difference between reported catch at sea and landed catch) and species composition (based on port size sampling), see Pallarés and Hallier (1997) and Duparc et al., (2020), to generate the level 1 logbook database used in this paper. The commercial size category was used as a discriminant factor at the maturity stage of bigeye and yellowfin tuna. Commercial categories 2 and 3 (tuna > = 10 kg) are classified as mature and category 1 (tuna <10 kg) is classified as immature (except for skipjack which belongs to this category and was not divided by maturity stage). We know from the literature[5] that 50 % size at maturity is reached around 100 cm fork length (that is to say around 20 kg) for yellowfin and bigeye. However, for the sake of simplicity we used the conventional "size" commercial categories reported in purse seiners logbooks by European skippers (category 1: <10 kg; category 2: 10–30 kg; category 3: >30 kg). All sets per boat and per day were combined and assigned to the centroids of these activities. The total number of sets per day per boat has been filtered and days with unrealistic data (over 5 sets per day per boat) deleted. Given that free schools are detected at random at the surface of the sea, the unit of effort associated with this fishing mode was expressed as the searching time (i.e., the time spent on the fishing ground less the duration of all setting operations). In contrast, many dFADs are not encountered randomly, specifically

5 See ICCAT manual, chapter 2 at https://www.iccat.int/en/iccatmanual.html

when they are equipped with a GPS buoy and continuously tracked remotely by the purse seiner. In such a case we used the number of dFADs sets as a measurement of the fishing effort. The data were then divided into eight categories according to the species, the maturity stage and the fishing mode. Only catch and effort data from sets conducted out in the study area were selected in this study.

2.3. Environmental data

Six candidate environmental variables were extracted from the EU's Copernicus Marine Environment Monitoring Service (CMEMS) (https://marine.copernicus.eu/) at a monthly mean resolution (Table 1): sea surface temperature (SST), sea surface height (SSH), chlorophyll concentration (CHL), salinity (SSS), mixed-layer thickness (MLD), and dissolved oxygen at a depth of 100 m (DO2_100). The spatial resolution of the model grid for SSS, SSH, SST, and MLD is 1/12° (0.083° x 0.083°, about 8 km), while the spatial resolution for CHL, DO2_100 is 1/4° (0.25° x 0.25°, about 24 km).

2.4. Coastal upwelling index (CUI_SST)

A seventh environmental variable, the monthly SST-based coastal upwelling index (CUI_SST) was calculated for the Ivorian EEZ. The SST-based coastal upwelling indices are obtained by taking the thermal difference (ΔT) between the coast and the offshore SST at the same latitude. In practice, CUI_SST has been defined as the thermal difference between cold coastal waters and warmer offshore waters at the same latitude (Benazzouz et al., 2014). The general formulation is as follows:

$$CUI_{SST\ (lat,\ time)} = SST_{offshore\ (lat,\ time)} - SST_{coastal\ (lat,\ time)} \quad (1)$$

The general calculation formula is very simple, but the challenge is to study the best way to define the coastal and offshore zones and to correctly extract the two thermal references to be used for the calculation. The resulting SST-based coastal upwelling index is characterized by a seasonal signal with peaks in the first and third quarter of the year (Fig. 2)

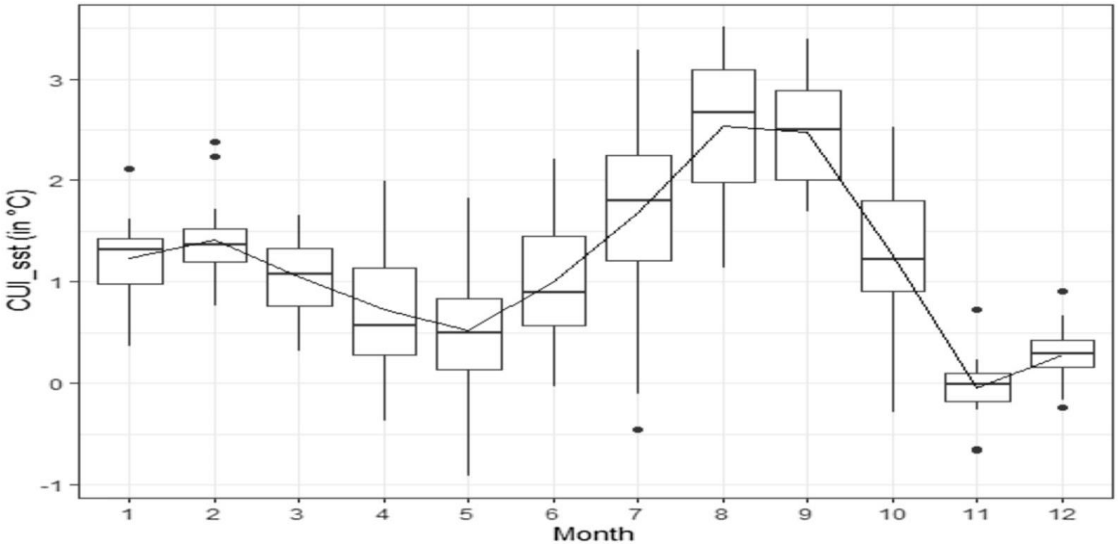

Fig. 2. Seasonal variations in the SST-based coastal upwelling index in the Ivorian EEZ

Table 1 : Summary of the candidate environmental variables included in this present study

Variable acronym	Variable name	Unit
SST	Sea surface temperature	°C
SSH	Sea surface height	meter
CHL	Chlorophyll concentration	mg. m-3
DO2_100	Dissolved oxygen concentration at 100 meters of depth	mmol.m-3
SSS	Salinity	PSU
MLD	Mixed layer thickness	meter
CUI_sst	Coastal upwelling index	°C

2.5. Methods

2.5.1. The seasonal spatio-temporal model

We applied a vector-autoregressive spatio-temporal delta-generalized linear mixed model to the catch and effort data, using the R package VAST (Thorson, 2019). Recently, VAST has been expanded to account for seasonal and inter-annual variability (Thorson et al., 2020a). This allows an understanding how species distribution and abundance varies within a year by month or season, and also within a month or season across years. It offers reasonable performance even when data are not fully available for one or more combinations of years and seasons, which is common in commercial catch data. In order to work at a finer scale temporal resolution (monthly, bi-monthly, quarterly…), the estimates in year-season t are shrunk towards predicting density in adjacent year-seasons (*t-1* and *t + 1*), as well as towards estimating density in other seasons in a given year and density in other years for a given season. This specification implies that the model includes a "main effect" for a season and year, as well as an autocorrelated "interaction" of season and year. We present below a brief summary of the principal parameters and philosophy of the model but readers are encouraged to refer to supplementary materials S2 for more technical details.

The VAST model is being implemented using the Poisson-link delta model as recommended by Thorson (2018). The Poisson-link delta model includes the probability p_i that sample i encounters a given species [i.e. $\Pr(B > 0)$], and also the expected measurement r_i given that species is encountered, $\Pr(B \mid B > 0)$:

$$\Pr(B = b_i) = \begin{cases} 1 - p_i & \text{if } B = 0 \\ p_i \times g\{B \mid r_i, \sigma_m^2\} & \text{if } B > 0' \end{cases} \quad (2)$$

where we specify a lognormal distribution for positive catches. This Poisson-link delta model predicts encounter probability p_i and positive catch rate r_i by modeling two log-linked linear predictors, $\log(n_i)$ and $\log(w_i)$ for each sample i; n_i and w_i are then transformed to yield p_i and r_i :

$$p_i = 1 - \exp(-a_i \times n_i)\,, r_i = \frac{a_i \times n_i}{p_i} \times w_i\,, \quad (3)$$

where a_i is the area-swept offset for sample i. This model structure is designed so that expected density d_i is the product of encounter probability and positive catch rate and also the product of transformed linear predictors (i.e $d_i = p_i * r_i = n_i * w_i$). These predictors can be interpreted as numbers-density n_i (with units numbers per area) and average weights w_i (with units biomass per number). n_i always enters via the product $a_i * n_i$ such that n_i is expressed as density. We consider effort as a catchability factor in the model. The Poisson-link delta model is useful relative to other delta models because both linear predictors use a log-link function so that all effects are additive in their impact on the predicted log-density. Specifically, we specify that:

$$\log(n_i) = \underbrace{\beta_n^*(t_i)}_{\substack{Year-season\\ intercept}} + \underbrace{\omega_n^*(s_i)}_{\substack{Spatial\\ main\ effect}} + \underbrace{\xi_{nu}^*(s_i,u_i)}_{\substack{Season\\ spatial\ effect}} + \underbrace{\xi_{ny}^*(s_i,y_i)}_{\substack{Year\\ spatial\ effect}} + \underbrace{\varepsilon_{nu}^*(s_i,t_i)}_{\substack{Year-season\\ spatial\ effect}} + \underbrace{\zeta_n^*(i)}_{\substack{Catchability\\ covariates}} \quad (4)$$

$$\log(w_i) = \underbrace{\beta_w^*(t_i)}_{\substack{Year-season\\ intercept}} + \underbrace{\omega_w^*(s_i)}_{\substack{Spatial\\ main\ effect}} + \underbrace{\xi_{wu}^*(s_i,u_i)}_{\substack{Season\\ spatial\ effect}} + \underbrace{\xi_{wy}^*(s_i,y_i)}_{\substack{Year\\ spatial\ effect}} + \underbrace{\varepsilon_{wu}^*(s_i,t_i)}_{\substack{Year-season\\ spatial\ effect}} + \underbrace{\zeta_w^*(i)}_{\substack{Catchability\\ covariates}} \quad (5)$$

The French purse seiners were targeting mainly free schools while the Spanish purse seiners were targeting drifting FADs. This difference in fishing strategy is less pronounced in the recent years as the use of dFADs-fishing increased in both fleets. There is likely also a vessel size category component in the choice of the fishing strategy. Both covariates (flag and vessel size category [carrying capacity]) have been introduced in the analysis as catchability covariates as suggested by Thorson (2019).

Key model parameters for abundance indices are density predicted, area-weighted density sum, and abundance-weighted mean density. The model estimates the density prediction per year at each fine spatial resolution:

$$\begin{aligned} d(s,t) &= n(s,t) \times w(s,t) \\ &= \exp\{\beta_n^*(t) + \omega_n^*(s) + \xi_{nu}^*(s,u) + \xi_{ny}^*(s,y) + \varepsilon_n^*(s,t)\} \\ &\quad \times \exp\{\beta_w^*(t) + \omega_w^*(s) + \xi_{wu}^*(s,u) + \xi_{wy}^*(s,y) + \varepsilon_w^*(s,t)\} \end{aligned} \quad (6)$$

We use density to calculate the total abundance for the entire domain as the area-weighted sum of density $d\ (s,t)$ predicted at a fine spatial resolution:

$$I(t) = \sum_{s=1}^{n_s} a(s)d(s,t) \quad (7)$$

Where n_s is the number of fine-scale predictions and a_s is the spatial area associated with each prediction.
See the supplementary material S2 for more details on the model, its implementation and results.

2.5.2. Statistical analyses

We decomposed the abundance indices into intrinsic mode functions to extract their seasonal and inter-annual components using the Complete Ensemble Empirical Mode Decomposition with adaptive noise (CEEMDAN) algorithm. The CEEMDAN algorithm belongs to the broad family of Empirical Mode Decomposition (EMD) algorithms (Huang et al., 1998). Torres et al. (2011) introduced this algorithm as a variation of EEMD algorithm (Wu and Huang, 2009) that allows exact reconstruction of the original signal and better spectral separation of intrinsic mode functions. We used the package "Rlibeemd" (Luukko et al., 2016) to decompose the eight abundance indices with the CEEMDAN algorithm. See the supplementary material S1 for more details on the CEEMDAN algorithm application.

The seasonal and inter-annual components of the abundance indices estimated in this paper are extracted from the CEEMDAN intrinsic mode functions (IMFs). The residual component represents the long-term component (inter-annual component), and the IMFs with annual frequency represent the seasonal (intra-annual) component. Three types of time series in the different IMFs can be observed: (i) some sub-annual (periodic) time series showing at least two local minimum and two local maximum by year (ii) the annual (periodic) time series that had no more than three local peaks (maximum + minimum) and (iii) some supra-annual (periodic) time series. In situations when there was more than one annual frequency component, we considered the average between them to construct the seasonal component. The seasonal component was used for two purposes in this study. First, we calculated the average abundance per season (month or two months in the case of immature yellowfin tuna caught on dFADs) over the entire study period. This allowed us to have the average seasonal factors. Then, we examined the dynamics of seasonality over the entire study period. The packages seasonal (Sax and Eddelbuettel, 2018) and forecast (Hyndman et al., 2008) were used for plotting the inter-annual variation of the seasonalities of each abundance index.

A Principal Component Analysis (PCA) was used to understand the common variability of the environmental variables used and to characterize environmental conditions of tropical tunas in the EEZ of Côte d'Ivoire.

GAMs (Hastie and Tibshirani, 1987) was used to study the links between the abundance indices by category and the environmental factors because they make it possible to take into account the non-linearity of such relationships (Maury et al., 2001). GAMs allowed the quantification

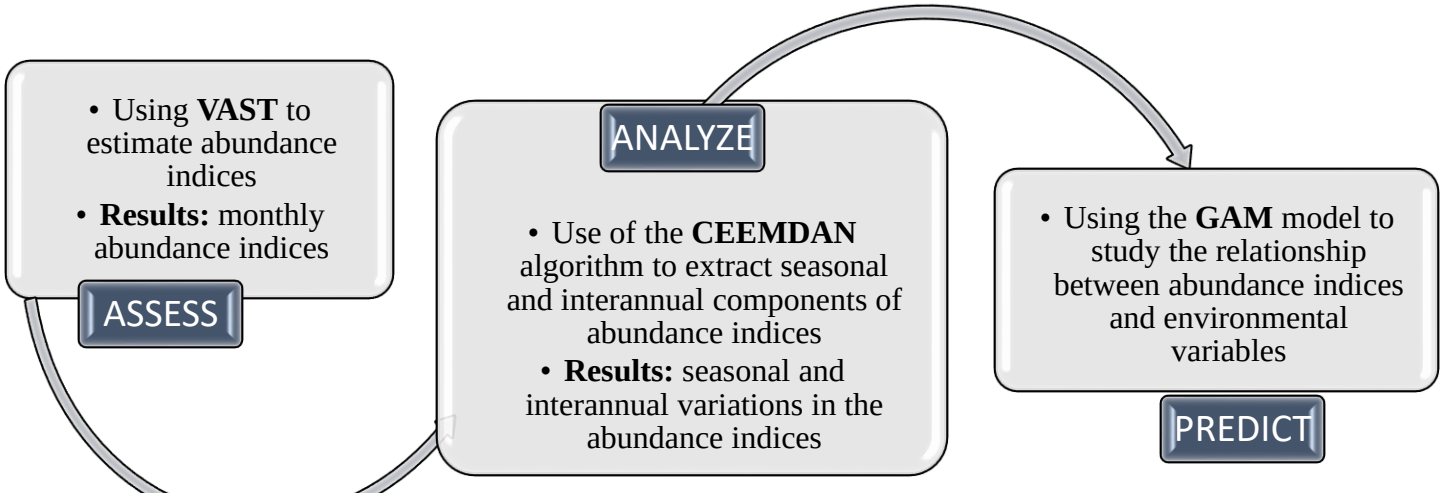

Fig. 3. Schematic representation of the methodology used in this study

of the percentage of deviance that can be explained by habitat, and to determine the relative contribution of the environmental variables. All statistical analyses were conducted with R 4.2. (R Core Team, 2019). The packages FactoMineR 1.34 (Husson, 2008) and mgcv 1.8–31 (Wood, 2017) were used for PCAs and for GAMs ,respectively. The entire data processing and analysis procedure is summarized in Fig.3

3. Results

Supplementary material S2 presents the estimated abundance indices and the decomposition of each abundance index into intrinsic mode functions using the CEEMDAN algorithm. All these results were analysed to obtain the factors related to the seasonal and inter-annual variation in the abundance of tropical tunas in the area of the EEZ of Côte d'Ivoire.

3.1. Seasonality of abundance indices

Mature yellowfin tuna captured on FSC and skipjack tuna captured on dFADs in the Ivorian EEZ are the categories showing the most obvious seasonality (Fig. 4). The seasonality of the tuna fisheries in the EEZ of Côte d'Ivoire is largely due to these two species. Two main tuna-abundance seasons can be identified. The first, characterized by an abundance of mature yellowfin tuna, takes place between March and July, and the second, characterized by an abundance of skipjack tuna, takes place between August and December (Fig. 4; Table 2). Some shrinkage of the seasonality factor is evident for SKJ on FSC, with amplitude ranging from 23 at the start of the study period to almost 5 over the last years (Fig. 5). The seasonality of the other abundance indices is almost constant throughout the study period (Fig. 5, Fig. 6).

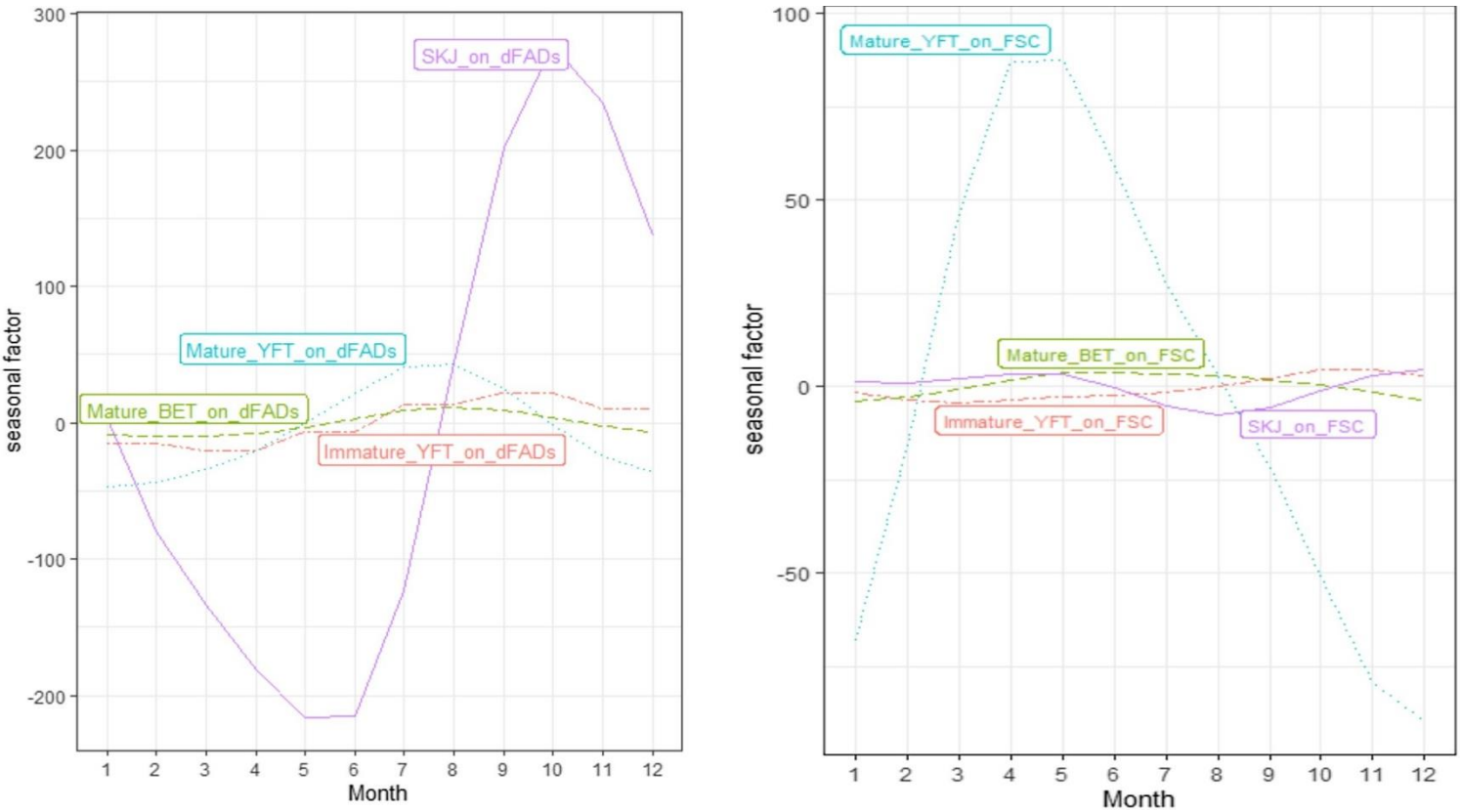

Fig. 4: Average monthly changes in abundance indices for the eight categories of tropical tuna analyzed for the 2000-2019 period.

Table 2 : Summary of the seasonal variability of abundance indices in the EEZ of Côte d'Ivoire (2020-2019).

Period	Seasonal factor (Peak-lowest)	Peak month	Peak abundance season	Low abundance season	Change in seasonality over the study period
Mat_BET_dFADs	21.03	August	June-October	Novemb-May	Slight shrinkage
Mat_BET_FSC	7.73	June	April-October	Novemb-March	Almost constant
SKJ_dFADs	492.3	October	August-Decem	January-July	Almost constant
SKJ_FSC	11.97	December/ April	October-Decem/ March-May	May-September	Shrinkage
Imm_YFT_ dFADs	42.9	October	July-December	January-June	Almost constant
Imm_YFT_FSC	8.95	November	August-Septem	January-July	Almost constant
Mat_YFT_dFADs	90.2	August	June-September	November-April	Almost constant
Mat_YFT_FSC	177.13	April	March-July	October-January	Almost constant

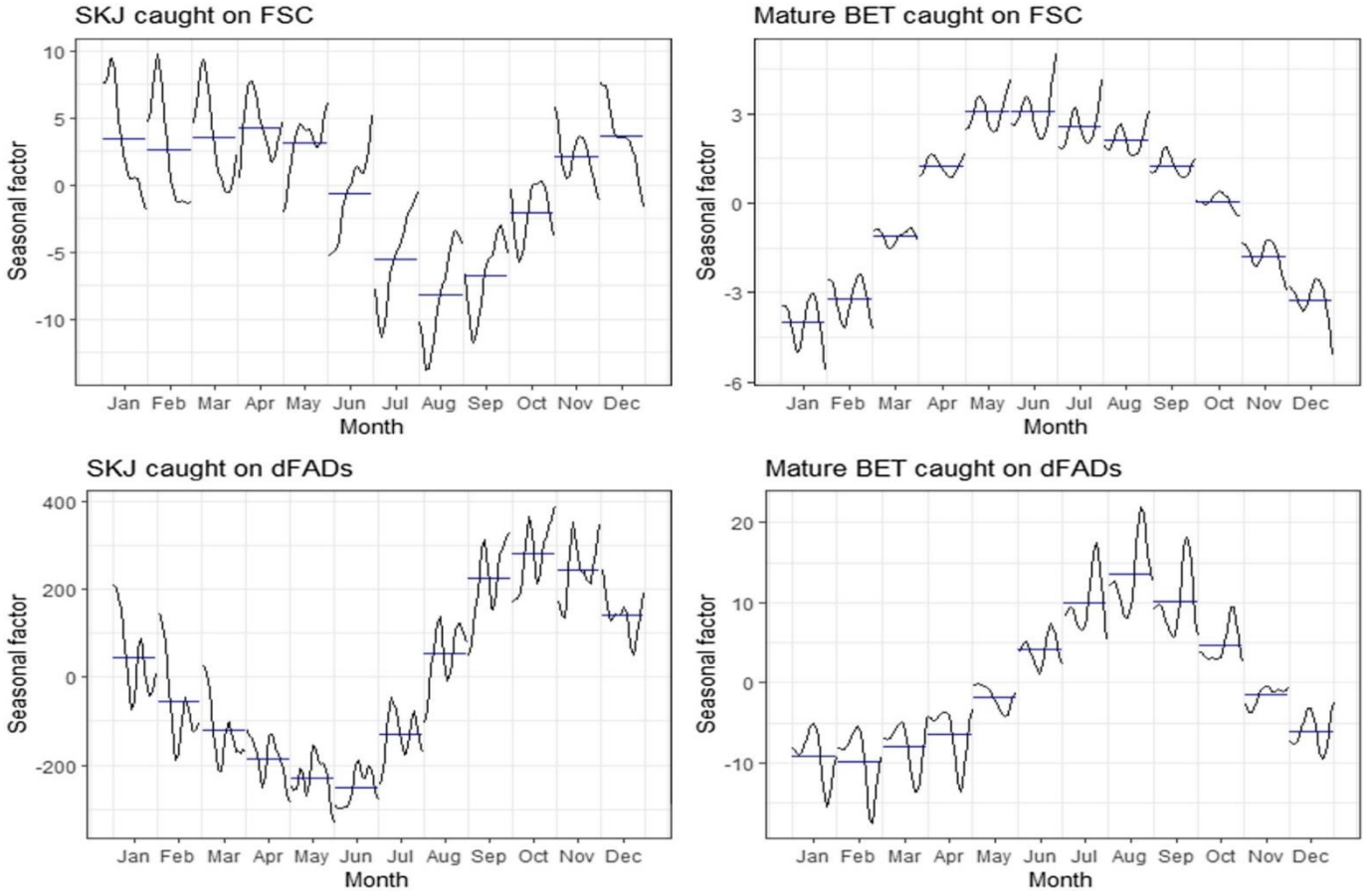

Fig. 5. Interannual variations in monthly abundance indices of skipjack and mature bigeye tuna. The curves observed for each month correspond to the interannual variability of abundance over that month and the horizontal dashes correspond to the monthly average (in trend) over the study period.

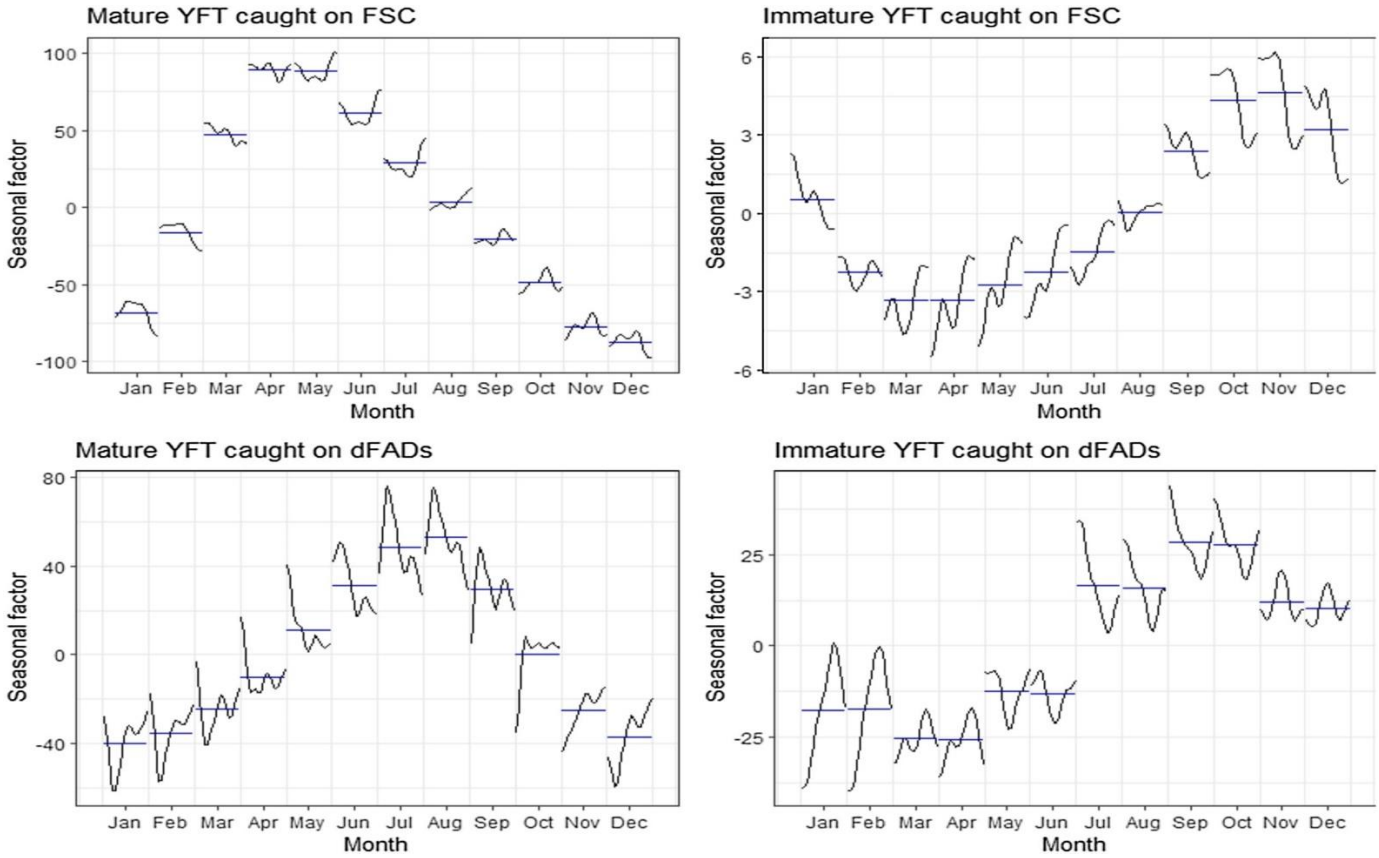

Fig. 6. Interannual variations in monthly abundance indices of yellowfin tuna. The curves observed for each month correspond to the interannual variability of abundance over that month and the horizontal dashes correspond to the monthly average (in trend) over the study period

3.2. Inter-annual variations of abundance indices

For sets on dFADs, there is a general downward trend in abundance indices for the majority of the categories (Fig. 7). The abundance indices for mature bigeye tuna show a downward trend from 2000 to 2009 and an upward trend since 2009.

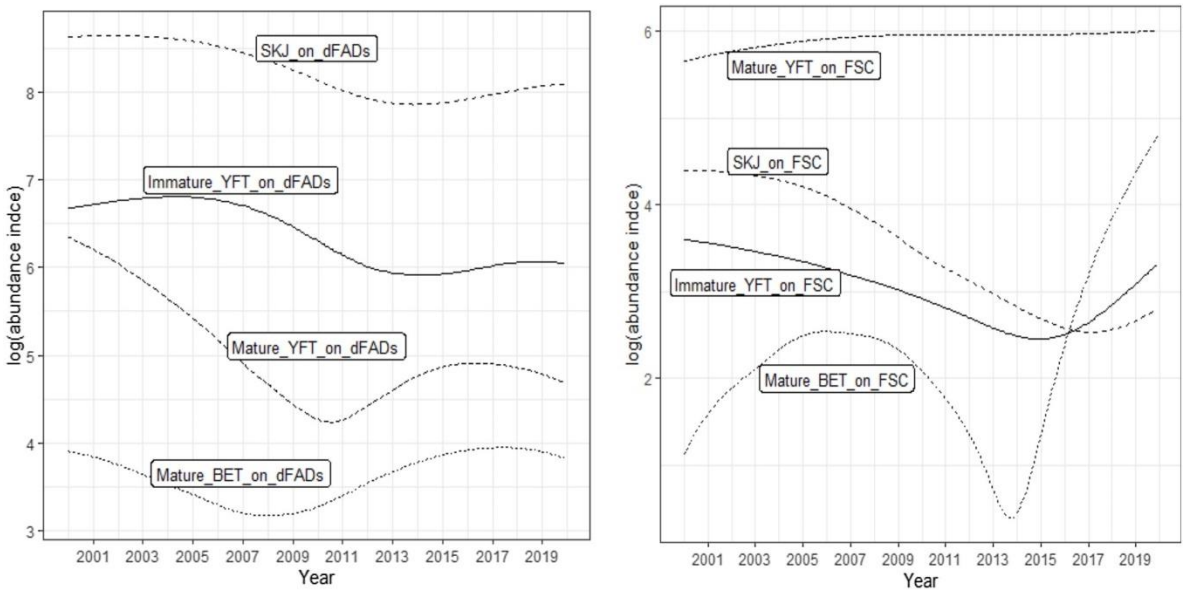

Fig. 7 : Interannual variations of abundance indices by fishing mode over the period 2000-2019.

For sets on FSC, there is an overall downward trend in the abundance indices for immature yellowfin tuna and skipjack tuna from 2000 to 2016/2017 and an upward trend from 2016/2017 onwards (Fig. 7). Mature yellowfin tuna increase over the study period. Mature bigeye tuna tend to increase from 2000 to 2006, then decrease to a local minimum in 2014 and increase from 2015 to 2019. Mature yellowfin tuna is the predominant category in the FSC species composition.

3.3. Environmental variability in the study area (PCA results)

The criterion of Kaiser (1960) enables the selection of the first three axes that represent 82.9 % of the total variability contained in the environmental variables. PCA showed correspondence between chlorophyll concentration (CHL), coastal upwelling index (CUI_sst) and sea surface salinity (SSS), which were strongly correlated to the positive semi axis of the first principal component, and opposed to sea surface temperature (SST) and sea surface height (SSH) (Table 3; Fig. 8). The first principal component (Dim 1), explained 53.6 % of the global variability of the data, highlights the great difference in environmental conditions between the primary cold season characterized by the upwelling phenomena and the primary warm season. From the projection of the months over the first two axes, it can be seen that July, August, and September are on the positive semi axis of the first principal component (Dim1), and April and May are on the negative semi axis of that first component (Supplementary material S1: Fig. 9:S1).

Table 3: Correlation between variables and dimensions (Dim1), square cosine (cos), contribution (contrib), and eigenvalue (inertia) of the first three principal components from the PCA analysis for the environmental variables selected in the study.

Variable	Dim.1	contrib	Cos2	Dim.2	contrib	Cos2	Dim.3	contrib	Cos2
SST	-0.90	21.62	0.811	-0.059	0.309	0.004	-0.095	1.044	0.009
SSS	0.654	11.40	0.428	0.431	16.34	0.186	0.386	17.36	0.149
MLD	0.195	1.015	0.038	0.907	72.40	0.823	-0.223	5.815	0.05
CHL	0.914	22.27	0.835	-0.171	2.56	0.029	0.093	1.018	0.009
CUI_sst	0.820	17.95	0.673	-0.280	6.918	0.079	0.073	0.623	0.005
DO2_100	-0.516	7.093	0.266	0.08	0.561	0.006	0.797	74	0.635
SSH	-0.836	18.646	0.7	0.102	0.909	0.01	0.034	0.135	0.001
% Inertia		53.58			16.24			12.62	

The second component of this PCA explained 16.2% of the global variability of the data. It was strongly correlated to the mixed-layer thickness (MLD) on the positive semi-axes (Table 3). This second component (Dim 2) was interpreted as a mixed layer depth gradient. From the projection of the months over the first two axes, it can be seen that June is on the positive semi axis of the second principal component (Dim2) (Supplementary material S1: Fig. 9:S1).

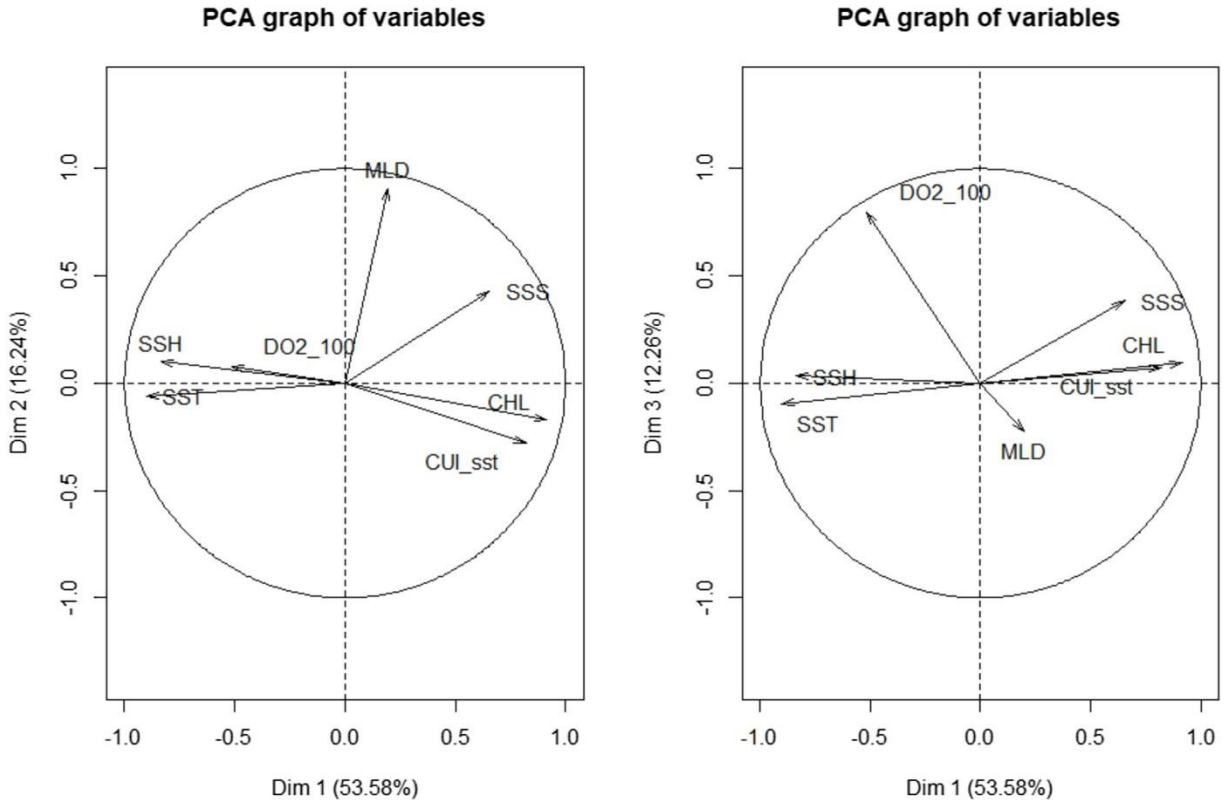

Fig. 8. First (Dim 1), second (Dim 2) and third (Dim 3) axes of the principal component analysis of the sea surface temperature (SST), sea surface height (SSH), sea surface salinity (SSS), chlorophyll concentration (CHL), dissolved oxygen at a depth of 100 meters (DO2_100), mixed-layer thickness (MLD) and Coastal upwelling index (CUI_sst) in the EEZ of Côte d'Ivoire.

The third component of this PCA explained 12.3% of the global variability of the data (Fig. 8). It was strongly correlated to the dissolved oxygen at a depth of 100 m (DO2_100) on the positive semi-axis (Table 3). This third component (Dim 3) was interpreted as a dissolved oxygen gradient which is a sub-surface variable.

3.4. Results of GAM models

All environmental variables were significant in terms of explaining the variability of skipjack abundance indices. There are however some differences between the abundance on FSC that is better explained by dissolved oxygen at a depth of 100 m (DO2_100), salinity, sea surface temperature (SST), chlorophyll concentration (CHL) and mixed-layer thickness (MLD), while abundance indices on dFADs are better explained by dissolved oxygen at 100 m depth (DO2_100) (Table 4).

Abundance index for adult yellowfin tunas on dFADs is explained by sea surface height (SSH), sea surface temperature (SST), chlorophyll concentration (CHL) and coastal upwelling index (CUI_sst) while abundance on FSC is linked to sea surface temperature (SST) only, with a higher proportion of the deviance explained for dFADs (Table 4).

Only the dissolved oxygen at a depth of 100 m (DO2_100) better explains abundance indices for juvenile yellowfin tunas (on dFADs and on FSC). It must be stressed that the deviance explained by environmental factors on the abundance on dFADs is higher than those FSC (Table 4).

For mature bigeye tunas, abundance indices on dFADs are better explained by sea surface temperature (SST) and chlorophyll concentration (CHL) while for FSC sea surface temperature (SST) and mixed-layer thickness (MLD) are the two environmental factors that most impact on the abundance.

Table 4 : Generalized additive models (univariate) of the eight categories of tuna as functions of the seven environmental variables. Deviance explained (in percentage) of log(abundance indices) by each variable are shown. The symbol * means that the coefficient is significant at 5% (p-value <0.05)

Variable	SKJ_FAD	SKJ_FS	YFT_Mat FAD	YFT_Mat FSC	YFT_Imm FAD	YFT_Imm FSC	BET_Mat FAD	BET_Mat FSC
SST	1.60	12.8*	25.5*	25.7*	1.87	2.14*	37.7*	18.1*
DO2_100	25.1*	32.7*	7.72*	3.94e-05	30.6*	19.8*	17.7*	3.13*
SSH	1.28	5.29*	31.9*	1.85*	3.23*	4.99*	20*	10*
CHL	0.32	12*	24.6*	1.46	0.84	4.05*	31.8*	8.6*
SSS	0.81	13.2*	8.91*	4.46*	0.01	3.87*	17*	11.3*
MLD	2.92*	11*	4.61*	4.26*	0.65	0.72	4.32*	18.1*
CUI_sst	0.14	9.58*	15*	2.24*	7.29e-06	0.63	16*	7.22*

4. Discussion

The need for coastal countries to evaluate their local resources is gaining importance. Andriamahefazafy (2020) highlighted that the inability for coastal countries to evaluate their tuna resources was frustrating for their governments. This highlights their willingness and need to gain an idea of the variability of the abundance of tuna transiting their EEZs as a complement to the regional assessments carried out by tuna RFMOs. We assess the “local tuna stocks” in the EEZ of Côte d'Ivoire by estimating abundance indices. The abundance indices obtained by using VAST served as inputs to other methods to characterize their seasonal and inter-annual variability. In this study, for the sake of simplicity, we used the term “local tuna stock” somewhat inappropriately, because tuna are migratory so the stock concept is more complex than a spatial boundary. We agree with Amon Kothias and Bard (1993) when they define the tuna resources of Côte d'Ivoire as a component of the tropical Atlantic tuna stocks. The estimated abundance indices are therefore interpreted as the tuna outflow remaining in the study area at a given time. In addition, the study area is imperfectly assigned to the Ivorian EEZ, but

the selected area extends beyond the Ivorian EEZ and considers boundary effects. One of the major limitations of this study is the selection of the fishery. Several fleets and gear types exploit the tuna resources of the Ivorian EEZ, but our study was limited to the French and Spanish purse seiners. This choice enhances consistency due to the relatively better quality and availability of the data, but interpretations may be affected by gear selectivity. It is important to consider these factors in the conclusions of this research, but as far as we know, this study is the first to estimate a local abundance of tunas with such levels of disaggregation (maturity level and school type) in the Gulf of Guinea region.

Another major limitation of this study is the use of commercial catch and effort information to estimate abundance indices. The relationship between standardized CPUEs and real abundance can be subject to hyperdepletion or hyperstability, depending on the fishing gear (Hilborn and Walters, 1992; Walters, 2003). Tropical purse seine tuna fisheries rely on many factors such as the concentration of schools in clusters (Fonteneau et al., 2017, 2008; Orensanz et al., 1998), and on the continuous introduction of technological developments (e.g., FADs equipped with echosounders) that contribute to the increase in vessels' fishing power (Fonteneau et al., 1999; Torres-Irineo et al., 2014). However, due to the difficulties in obtaining information on new fishing technology introduced on board each vessel, the conventional standardization methods do not really capture the impact of these factors. We know that the estimated abundance indices in this paper are not immune to the biases from which the approximation of abundance by standardized CPUE suffers. However, we have chosen to disaggregate the data by school type and maturity stage to avoid some biases.

With regards to the effects of the environmental conditions on tuna resources, studies have shown that in comparison with other tuna species, skipjack tuna vertical movements are limited and restricted to surface waters because they have a limited tolerance to low levels of dissolved oxygen and very low temperatures (Graham and Dickson, 2004). The fact that the dissolved oxygen at a depth of 100 m, MLD and SST better explain the variability in skipjack catch rate is due in part to this species-specific characteristic. Our results showed that the peak season of skipjack tuna in Côte d'Ivoire (August – December) coincides with the presence of upwelling, rich in nutrients, during the third quarter of the year. Skipjack tuna are most concentrated inside the EEZ of Côte d'Ivoire during the months with low SST and high CHL (i.e. from August to December with a peak in September) (supplementary material S1: Fig. 2:S1 and Fig. 9:S1). Bard et al. (1988) suggested that the equatorial migration of skipjack tuna is particularly driven by foraging and thus driven by particularly productive zones. The delay of 1–2 months from the peak of the upwelling to the peak of skipjack abundance provides further evidence confirming these general aspects already analysed in the Gulf of Guinea. Indeed, Mendelssohn and Roy (1986) found that higher concentrations of skipjack occur when there was an upwelling one month prior to fishing, followed by a relative warming of the waters two weeks prior to fishing. Our results reinforce this observation while highlighting the differences observed between dFADs and FSC fishing. Mature yellowfin tuna are most concentrated inside the EEZ of Côte d'Ivoire during the months with high SST and high SSH (i.e., from March to July with a peak in April - May) (supplementary material: Fig. 2: S1 and Fig. 9:S1). Several studies have shown that there is significant yellowfin spawning activity in the Gulf of Guinea from December through April (ICCAT, 2019a). The seasonality of adult yellowfin tuna in this study is consistent with previous findings in this sub-area of the Gulf of Guinea. The peak in abundance is due to a mixture of genetic migrations related to reproduction which takes place in the first quarter of the year in the study area (Albaret, 1977) and trophic migrations related

to the enrichment of the study area in food generated by the presence of coastal upwelling which takes place from January to February (Binet, 1976). In conclusion, the seasonality of tuna abundance in the EEZ of Côte d'Ivoire is consistent with the patterns of tropical tuna characteristics observed at regional scales and a function of local environmental conditions (Mendelssohn and Roy, 1986).

The recent stock assessments of Atlantic tropical tunas have revealed that (1) yellowfin tuna is not overfished and not subject to overfishing, (2) bigeye tuna has been overfished since 1994 and overfishing has been undergoing since 1997, and (3) skipjack tuna are not likely overfished and not subject to overfishing (ICCAT, 2019a). When stocks are overfished, one can expect a reduction in biomass, the impact of which is greater at the periphery of the spatial distribution of the stock (e.g., in the EEZ of Côte d'Ivoire) than in the core area, as postulated by the McCall's basin hypothesis (MacCall, 1990). For bigeye, the tropical tuna species most impacted by exploitation, our results suggest a declining trend during the first decade and an increasing trend from 2009 onwards on dFADs and 2014 on FSC components. The overall trend of bigeye caught on FSC varies slightly from 2000 to 2017 followed by a sudden increase in the last two years (Fig. 3 S1). It is very unlikely to see such an abrupt change in the abundance of a long-lived species such as bigeye. The resulting overall trend could be due to a change in catchability compared to previous years. We reserve the right to interpret it as a change in the abundance of this species. However, since bigeye is rare in this area, a peak in moderate catches could generate such observations. The situation is somewhat different for catches on dFADs. More specific analyses could help better understand the phenomenon observed in the abundance indices of mature bigeye tuna in this study area. The situation is different for yellowfin and skipjack as both species show a general downward trend, with the exception of yellowfin captured on FSC. As we have seen, CHL and SST are responsible for seasonality in abundance indices of skipjack and mature yellowfin. The global trend of these variables over the study period could have affected the overall dynamics of the abundance of both species. Indeed, there is an overall upward trend in SST, and a downward trend in the coastal upwelling index and chlorophyll concentration over the years (Fig. 9). Future analyses more specific to this topic will explain the similarity between trends in these variables and those of some abundance indices estimated in this paper.

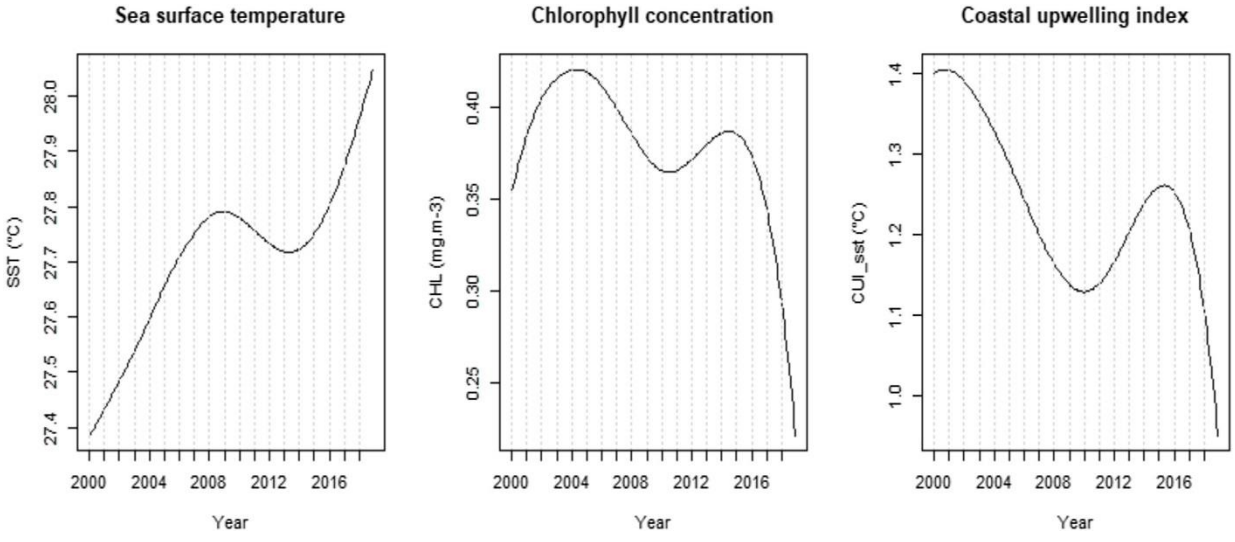

Fig. 9. Interannual variations (global trend) of three environmental variables over the period 2000-2018. The decomposition has been done by using the CEEMDAN's algorithm

Several studies have examined the difference between the behaviour of tropical tuna captured on dFADs or on FSC, and differences in several biological parameters and migrating patterns have been reported (Hallier and Gaertner, 2008). Ménard et al. (2000) suggested that the dFADs fishery may have wide-ranging effects on the migration of tuna in general and on the productivity of skipjack in particular. Coming back to the results of the univariate analysis of the relationship of tuna abundance with environmental variables (Table 5), the importance of the dissolved oxygen at 100 m depth (DO2_100) on the abundance of skipjack can be seen by the percentage of the variance explained: 35.7 % on FSC against only 23.3 % on dFADs.

Table 5: Summary of the relationships between environnemental variables and abundance indices. Only factors with explained deviance higher than 10% have been selected and ranked by decreasing order of explained deviance (e.g. Mature BET on FSC, SST > MLD > SSS > SSH).

Species	**Fishing in dFADs**	**Fishing in FSC**
SKJ	DO2_100	D02_100 ; SSS ; SST ; CHL ; MLD
Mature YFT	SSH ; SST ; CHL and CUI_sst	SST
Immature YFT	DO2_100	DO2_100
Mature BET	SST ; CHL ; SSH ; DO2_100 ; SSS ; CUI_sst	SST ; MLD ; SSS and SSH

In addition, CHL explains 9.58 % of the catches on FSC but very little (0.14 %) on dFADs. Consequently, as skipjack caught on dFADs are comparable in size with individuals caught on FSC, this suggests that dFADs decrease the dependence of skipjack on several environmental factors that is to say modify its habitat. Moreover, the peak abundance of skipjack catches on dFADs take place one to two months before the peak abundance of catches on free school in a period which could be less favourable in terms of habitat. Some differences in deviance explained (by environmental variables) were also observed between catches on dFADs and catches on FSC for the other categories studied.

Our results suggest that, at the same level of maturity for the same species, the effect of environmental variables on abundance indices differ between dFADs and FSC. These differing effects of environmental variables on tuna abundance have been observed in several studies(Druon et al., 2017; Putri et al., 2019; Zainuddin et al., 2019) without reaching a definitive conclusion on how large is the effect of dFAD use on tuna populations.

5. Conclusion

This study highlighted the details of local resources of regionally managed highly migratory species like tropical tunas. General trend and seasonality of such local resources has been assessed and analysed. In an international context where competitiveness is at stake, such analyses with complementary characteristics are essential to better take advantage of the share of global resources over which a country has some rights. This study constitutes one of the proofs of the possibility for some coastal countries to evaluate the variations in abundance of tunas in the waters under their jurisdiction in addition to the broad-scale patterns which are analysed within RFMOs. It revealed changes in abundance indices over the study period (Fig. 7); reductions in amplitude of the seasonality for some combination of species-size categories (Fig. 5) and differences in peak abundance and sensitivity to environmental variability between dFADs and free school fishing (Table 4, Table 5). For skipjack, our results indicate that dFAD-associated schools are less dependent on the variation of several environmental factors than free schools. Our results suggest a strong relationship between the dynamics of some environmental variables and the abundance indices for skipjack and adult yellowfin tunas. This study made it possible to isolate the particularities of the local resource and thus to lay the first bases for possible analyses of the influence of global phenomena (overfishing, climate change, etc.) on the local resource at the EEZ level, thus providing the basis for future management measures.

CRediT authorship contribution statement

S. AKIA: Conceptualization, Methodology, Software, Validation, Visualization, Investigation, Writing - original draft.

M. Amande: Conceptualization, Supervision, Writing - review & editing, Supervision.

P. Pascual: Data Curation, Writing - review & editing.

D. Gaertner: Conceptualization, Resources, Validation, Writing - review & editing, Supervision, Funding acquisition, Project administration.

Declaration of Competing Interest

The authors report no declarations of interest.

Acknowledgements

This project was co-funded by IRD (ARTS funding) and the “Observatoire des Ecosystèmes Pélagiques Tropicaux exploités” (Ob7) from IRD/MARBEC. We sincerely thank the contribution of the staff of the Ob7 for providing data on the French fleet. The authors also thank Lorelei Guery, Francis Marsac and Hervé Demarq (IRD-MARBEC) for many helpful suggestions, advices and methodological tools regarding our analyses.

Our gratitude also goes to the reviewers of this manuscript for their comments, corrections and suggestions for its improvement.

References

Albaret, J.-J., 1977. La reproduction de l'albacore (Thunnus albacares) dans le golfe de Guinée. O.R.S.T.O..M. série Oceanogr.

Albeare, S.M., 2009. Comparisons of Boosted Regression Tree, GLM And GAM Performance In The Standardization Of Yellowfin Tuna Catch-Rate Data From The Gulf Of Mexico Lonline Fishery. Thesis.

Amon Kothias, J., Bard, F., 1993. Les ressources thonières de Côte d'Ivoire 323–352.

Andriamahefazafy, M., 2020. The politics of sustaining tuna, fisheries and livelihoods in the Western Indian Ocean.

Bard, F.X., Cayré, P., Diouf, T., 1988. Les migrations (des thons). Chapitre 5. Ressources, pêche Biol. des thonidés Trop. l'Atlantique Centre-Est. FAO Doc. Tech. Pêches 292, 391.

Benazzouz, A., Mordane, S., Orbi, A., Chagdali, M., Hilmi, K., Atillah, A., Lluís Pelegrí, J., Hervé, D., 2014. An improved coastal upwelling index from sea surface temperature using satellite-based approach - The case of the Canary Current upwelling system. Cont. Shelf Res. https://doi.org/10.1016/j.csr.2014.03.012

Binet, D., 1976. Contribution à l'écologie de quelques taxons du zooplancton de Côte d'Ivoire. 2-Dolioles, Salpes, Appendiculaires. Doc. Sci. Cent. Rech. Océanographiques, Abidjan 7, 45–61.

Campbell, R.A., 2004. CPUE standardisation and the construction of indices of stock abundance in a spatially varying fishery using general linear models. Fish. Res. https://doi.org/10.1016/j.fishres.2004.08.026

Cofrepeche, Poseidon, M.& N., 2012. Évaluation ex-post du protocole de l'accord de partenariat dans le domaine de la pêche entre l> Union européenne et la Côte-d> Ivoire (Contrat cadre MARE/2011/01-Lot 3, contrat spécifique 2).

Cury, P., Roy, C., 1987. Upwelling et pêche des espèces pélagiques côtières de Côte-d'Ivoire: une approche globale. Oceanol. acta 10, 347–357.

Druon, J.-N., Chassot, E., Murua, H., Lopez, J., 2017. Skipjack tuna availability for purse seine fisheries is driven by suitable feeding habitat dynamics in the Atlantic and Indian Oceans. Front. Mar. Sci. 4, 315.

Duparc, A., Depetris, M., Floch, L., Cauquil, P., Bach, P., Lebranchu, J., 2020. (T3) SOFTWARE A redesign for the T3 code 22, 1–5. https://doi.org/10.5281/zenodo.3878125.Changes

Failler, P., El Ayoubi, H., Konan, A., 2014. Industrie des pêches et de l'aquaculture en Côte d'Ivoire.

FAO, 2021a. ICCAT Standing Committee on Research and Statistics (ICCAT- SCRS). Stock status report 2014. Skipjack tuna - East Atlantic. FIRMS Reports. Fish. Resour. Monit. Syst. [online]. Rome. Updat. 29 January 2015. [Cited 26 January 2021]. http//firms.fao.org/firms/resource/15/en.

FAO, 2021b. ICCAT Standing Committee on Research and Statistics (ICCAT- SCRS). Stock status report 2019. Yellowfin tuna - Atlantic. FIRMS Reports. Fish. Resour. Monit. Syst. [online].]. Rome. Updat. 16 January 2020. [Cited 26 January 2021]. http//firms.fao.org/firms/resource/20/en.

FAO, 2021c. ICCAT Standing Committee on Research and Statistics (ICCAT- SCRS). Stock status report 2018. Bigeye tuna - Atlantic. FIRMS Reports. Fish. Resour. Monit. Syst. [online]. Rome. Updat. 23 May 2019. [Cited 26 January 2021]. http//firms.fao.org/firms/resource/9/en.

Fonteneau, A., Alayón, P.J.P., Marsac, F., 2017. Exploitation of large yellowfin tuna caught in free schools concentrations during the 2013 spawning season (December 2012-May 2013). Collect. Vol. Sci. Pap. ICCAT 73, 868–882.

Fonteneau, A., Gaertner, D., Nordstrom, V., 1999. An overview of problems in the CPUE-abundance relationship for the tropical purse seine fisheries. Collect. Vol. Sci. Pap. ICCAT 49, 259–276.

Fonteneau, A., Lucas, V., Tewkai, E., Delgado, A., Demarcq, H., 2008. Mesoscale exploitation of a major tuna concentration in the Indian Ocean. Aquat. Living Resour. 21, 109–121.

Graham, J.B., Dickson, K.A., 2004. Tuna comparative physiology. J. Exp. Biol. https://doi.org/10.1242/jeb.01267

Hallier, J.P., Gaertner, D., 2008. Drifting fish aggregation devices could act as an ecological trap for tropical tuna species. Mar. Ecol. Prog. Ser. https://doi.org/10.3354/meps07180

Hastie, T., Tibshirani, R., 1987. Generalized additive models: Some applications. J. Am. Stat. Assoc. https://doi.org/10.1080/01621459.1987.10478440

Hilborn, R., Walters, C.J., 1992. Stock and recruitment, in: Quantitative Fisheries Stock Assessment. Springer, pp. 241–296.

Huang, N., Shen, Z., Long, S., Wu, M., Shih …, H., 1998. The empirical mode decomposition and the Hilbert spectrum for nonlinear and non-stationary. Proc. Math.

Husson, F., 2008. FactoMineR: An R Package for Multivariate Analysis. https://doi.org/10.18637/jss.v025.i01

Hyndman, R.J., Khandakar, Y., others, 2008. Automatic time series forecasting: the forecast package for R. J. Stat. Softw. 27, 1–22.

ICCAT, 2019a. Report for Biennial Period, 2018-2019, Part II – Vol. 2. Standing Committee on Research and Statistics (SCRS). Madrid, Spain 470.

ICCAT, 2019b. Report for Biennial Period, 2018-2019, Part I – Vol. 2. Standing Comm. Res. Stat. (SCRS). Madrid, Spain 450.

Kaiser, H.F., 1960. The application of electronic computers to factor analysis. Educational and Psychological Measurement. Educ. Psychol. Meas.

Katara, I., Gaertner, D., Marsac, F., Grande, M., Kaplan, D., Agurtzane, U., Loreleï, G., Mathieu, D., Antoine, D., Laurent, F., Jon, L., Francisco, A., 2018. Standardisation of yellowfin tuna CPUE for the EU purse seine fleet operating in the Indian Ocean., 19th Working Party on Tropical Tunas.

Lehodey, P., Alheit, J., Barange, M., Baumgartner, T., Beaugrand, G., Drinkwater, K., Fromentin, J.M., Hare, S.R., Ottersen, G., Perry, R.I., Roy, C., van der Lingen, C.D., Werner, F., 2006. Climate variability, fish, and fisheries. J. Clim. https://doi.org/10.1175/JCLI3898.1

Luukko, P.J.J., Helske, J., Räsänen, E., 2016. Introducing libeemd: a program package for performing the ensemble empirical mode decomposition. Comput. Stat. https://doi.org/10.1007/s00180-015-0603-9

MacCall, A.D., 1990. Dynamic geography of marine fish populations. Washington Sea Grant Program Seattle, WA.

Marsac, F., 2017. The Seychelles Tuna Fishery and Climate Change, in: Climate Change Impacts on Fisheries and Aquaculture. https://doi.org/10.1002/9781119154051.ch16

Maunder, M.N., Langley, A.D., 2004. Integrating the standardization of catch-per-unit-of-effort into stock assessment models: testing a population dynamics model and using multiple data types. Fish. Res. 70, 389–395.

Maunder, M.N., Punt, A.E., 2004. Standardizing catch and effort data: A review of recent approaches. Fish. Res. https://doi.org/10.1016/j.fishres.2004.08.002

Maunder, M.N., Thorson, J.T., Xu, H., Oliveros-Ramos, R., Hoyle, S.D., Tremblay-Boyer, L., Lee,

H.H., Kai, M., Chang, S.-K., Kitakado, T., others, 2020. The need for spatio-temporal modeling to determine catch-per-unit effort based indices of abundance and associated composition data for inclusion in stock assessment models. Fish. Res. 229, 105594.

Maury, O., Gascuel, D., Marsac, F., Fonteneau, A., Rosa, A.-L. De, 2001. Hierarchical interpretation of nonlinear relationships linking yellowfin tuna (*Thunnus albacares*) distribution to the environment in the Atlantic Ocean. Can. J. Fish. Aquat. Sci. https://doi.org/10.1139/cjfas-58-3-458

Ménard, F., Fonteneau, A., Gaertner, D., Nordstrom, V., Stéquert, B., Marchal, E., 2000. Exploitation of small tunas by a purse-seine fishery with fish aggregating devices and their feeding ecology in an eastern tropical Atlantic ecosystem, in: ICES Journal of Marine Science. https://doi.org/10.1006/jmsc.2000.0717

Ménard, F., Marsac, F., Bellier, E., Cazelles, B., 2007. Climatic oscillations and tuna catch rates in the Indian Ocean: A wavelet approach to time series analysis. Fish. Oceanogr. https://doi.org/10.1111/j.1365-2419.2006.00415.x

Mendelssohn, R., Roy, C., 1986. Environmental influences on the French, Ivory-Coast, Senegalese and Moroccan tuna catches in the Gulf of Guinea, in: Proceedings of the ICCAT Conference on the International Skipjack Year Program. Edited by EK Symons, PM Miyake, and GT Sakagawa. ICCAT, Madrid. pp. 170–188.

Monin, J.A., Amalatchy, J.N.C., Goran, D.K.N., Chris, M.N.C., Kouadio, F.K., Kouadio, C., Nadège, A., Dewals, P., Restrepo, V., 2017. UTILIZATION AND TRADE OF FAUX POISSON LANDED IN ABIDJAN 73, 749–754.

Moreno, G., Dagorn, L., Sancho, G., Itano, D., 2007. Fish behaviour from fishers ' knowledge : the case study of tropical tuna around drifting fish aggregating devices (DFADs) 1528, 1517–1528. https://doi.org/10.1139/F07-113

Morlière, A., 1970. Les saisons marines devant Abidjan. Doc. Sci. Cent. Rech. Océanographiques, Abidjan 1, 1–15.

Orensanz, J.M., Parma, A.M., Hall, M.A., 1998. The analysis of concentration and crowding in shellfish research. Can. Spec. Publ. Fish. Aquat. Sci. 143–158.

Pallarés, P., Hallier, J.P., 1997. Analyse du schéma d'échantillonnage multispécifique des thonidés tropicaux. Rapp. Sci. IEO/ORSTOM, Program. 95, 37.

Putri, A.R.S., Zainuddin, M., Musbir, M., Mustapha, M.A., Hidayat, R., 2019. Effect of oceanographic conditions on skipjack tuna catches from FAD versus free-swimming school fishing in the Makassar Strait, in: IOP Conference Series: Earth and Environmental Science. p. 12008.

R Core Team, 2019. R: A language and environment for statistical computing. R Found. Stat. Comput.

Ricker, W.E., 1940. Relation of "Catch per Unit Effort" to Abundance and Rate of Exploitation. J. Fish. Res. Board Canada. https://doi.org/10.1139/f40-008

Romagny, B., Ménard, F., Dewals, P., Gaertner, D., N'Goran, N., 2000. Le "faux-poisson" d'Abidjan et la pêche sous DCP dérivants dans l'Atlantique tropical Est : circuit de commercialisation et rôle socio-économique. Pêche thonière Dispos. Conc. Poisson. Caribbean-Martinique, 15-19 Oct 1999 634–652.

Sax, C., Eddelbuettel, D., 2018. Seasonal Adjustment by {X-13ARIMA-SEATS} in {R}. J. Stat. Softw. 87, 1–17. https://doi.org/10.18637/jss.v087.i11

Thorson, J. T., 2019. VAST model structure and user interface 1–19.

Thorson, James T., 2019. Guidance for decisions using the Vector Autoregressive Spatio-Temporal (VAST) package in stock, ecosystem, habitat and climate assessments. Fish. Res. https://doi.org/10.1016/j.fishres.2018.10.013

Thorson, J.T., 2018. Three problems with the conventional delta-model for biomass sampling data, and a computationally efficient alternative. Can. J. Fish. Aquat. Sci. https://doi.org/10.1139/cjfas-2017-0266

Thorson, J.T., Adams, C.F., Brooks, E.N., Eisner, L.B., Kimmel, D.G., Legault, C.M., Rogers, L.A., Yasumiishi, E.M., 2020. Seasonal and interannual variation in spatio-temporal models for index standardization and phenology studies. ICES J. Mar. Sci. https://doi.org/10.1093/icesjms/fsaa074

Thorson, J.T., Shelton, A.O., Ward, E.J., Skaug, H.J., 2015. Geostatistical delta-generalized linear mixed models improve precision for estimated abundance indices for West Coast groundfishes. ICES J. Mar. Sci. https://doi.org/10.1093/icesjms/fsu243

Torres-Irineo, E., Gaertner, D., Chassot, E., Dreyfus-León, M., 2014. Changes in fishing power and fishing strategies driven by new technologies: The case of tropical tuna purse seiners in the eastern Atlantic Ocean. Fish. Res. https://doi.org/10.1016/j.fishres.2014.02.017

Torres, M.E., Colominas, M.A., Schlotthauer, G., Flandrin, P., 2011. A complete ensemble empirical mode decomposition with adaptive noise, in: ICASSP, IEEE International Conference on Acoustics, Speech and Signal Processing - Proceedings. https://doi.org/10.1109/ICASSP.2011.5947265

Walters, C., 2003. Folly and fantasy in the analysis of spatial catch rate data. Can. J. Fish. Aquat. Sci. 60, 1433–1436.

Wood, S.N., 2017. Generalized additive models: An introduction with R, second edition, Generalized Additive Models: An Introduction with R, Second Edition. https://doi.org/10.1201/9781315370279

Wu, Z., Huang, N.E., 2009. Ensemble empirical mode decomposition: A noise-assisted data analysis method. Adv. Adapt. Data Anal. https://doi.org/10.1142/S1793536909000047

Yang, S., Zhang, Y., Zhang, H., Fan, W., 2015. Comparison and analysis of different model algorithms for CPUE standardization in fishery. Nongye Gongcheng Xuebao/Transactions Chinese Soc. Agric. Eng. https://doi.org/10.11975/j.issn.1002-6819.2015.21.034

Zainuddin, M., Ridwan, M., Putri, A.R.S., Hidayat, R., others, 2019. The Effect of Oceanographic Factors on Skipjack Tuna Fad vs Free School Catch in The Bone Bay, Indonesia: An Important Step Toward Fishing Management. J. Ilmu Dan Teknol. Kelaut. Trop. 11, 123–130.

S1: Online supplementary material for 'Seasonal and inter-annual variability in abundance of the main tropical tunas in the EEZ of Côte d'Ivoire (2000-2019)'

Akia S., Amandé M., Pascual P. and Gaertner D.

31/05/2021

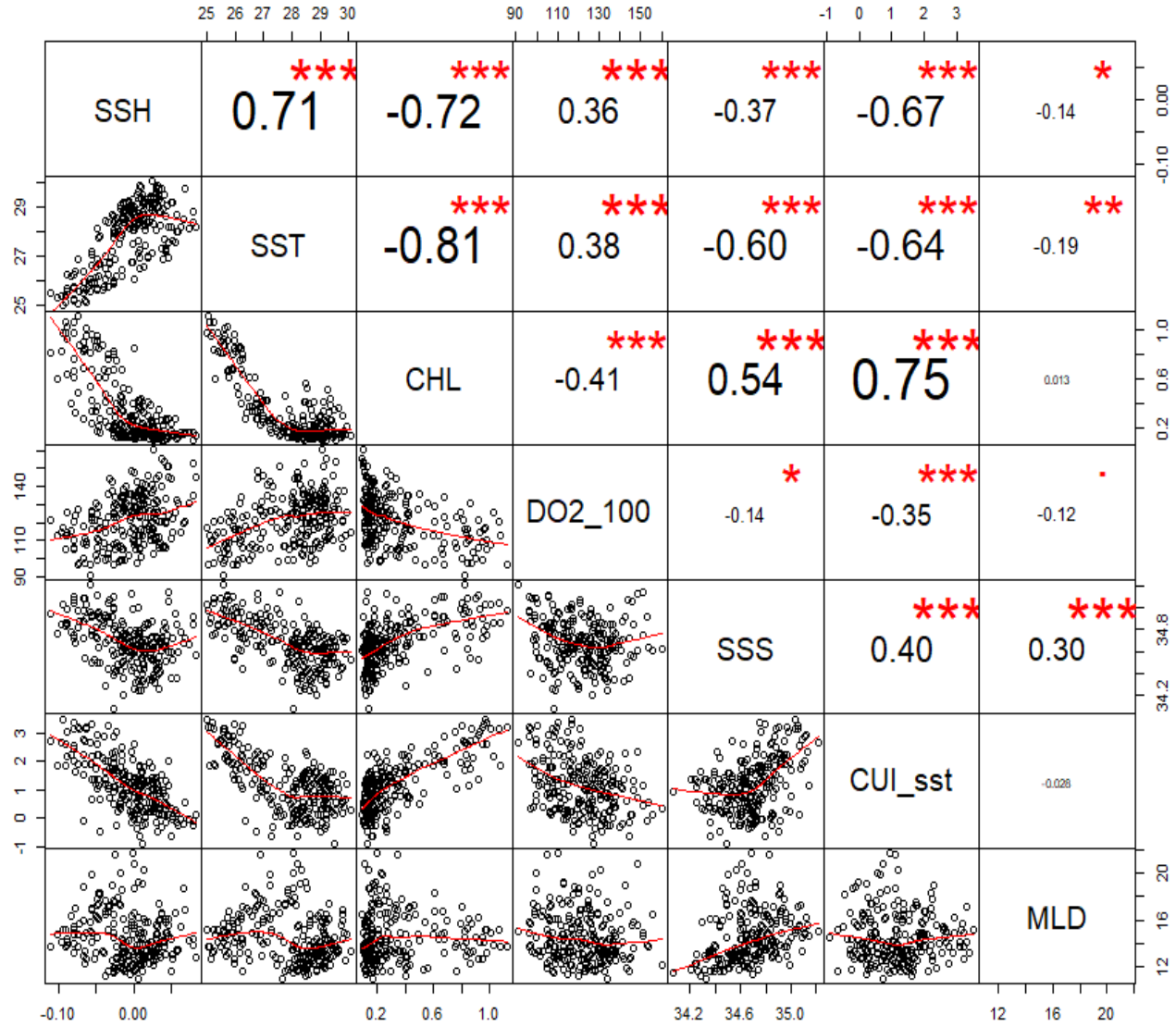

Fig. 1.S1 Cross-correlation matrix of the environmental variables included in this study.

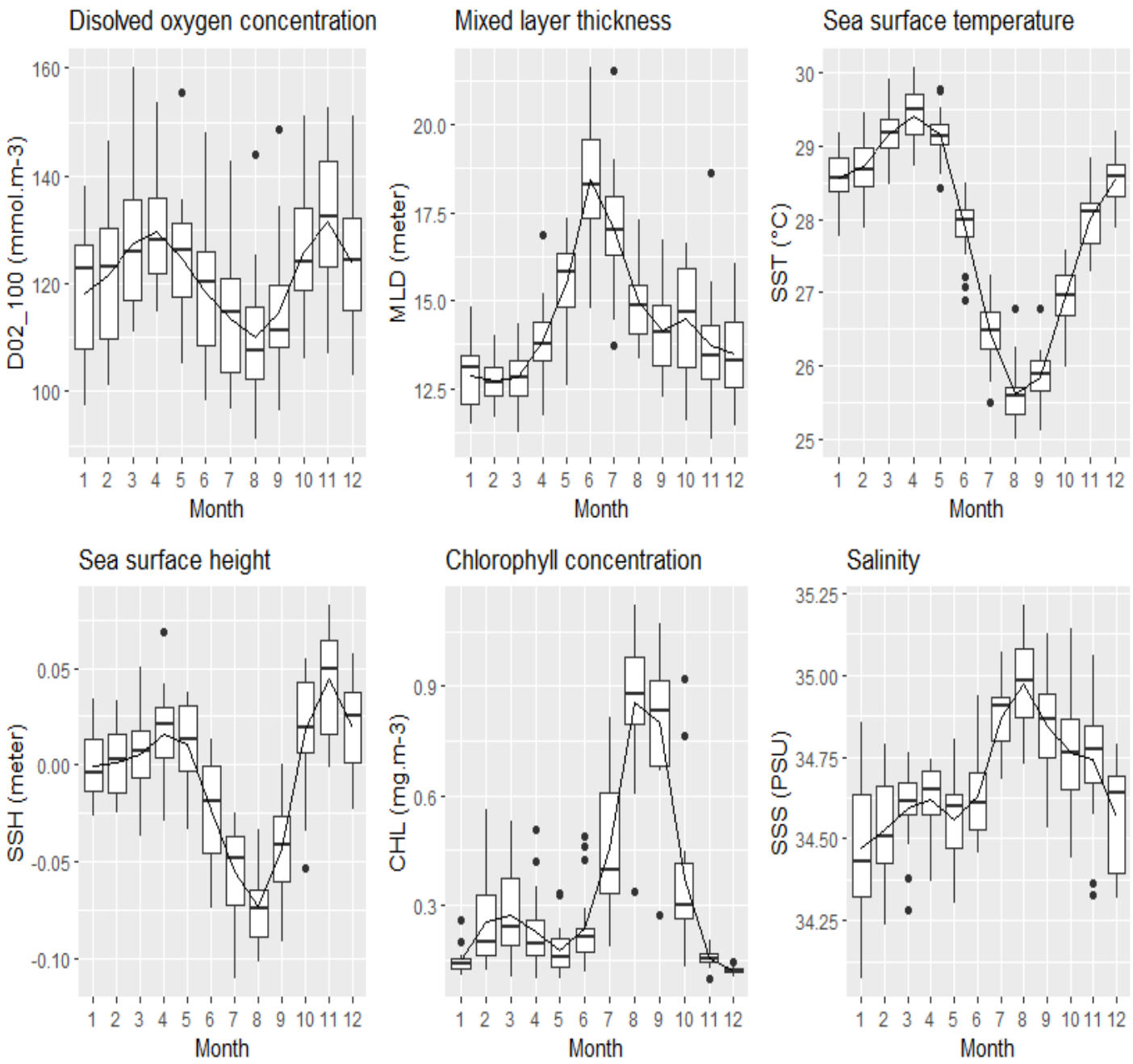

Fig. 2.S1 Seasonal variation in the environmental variables included in this study.

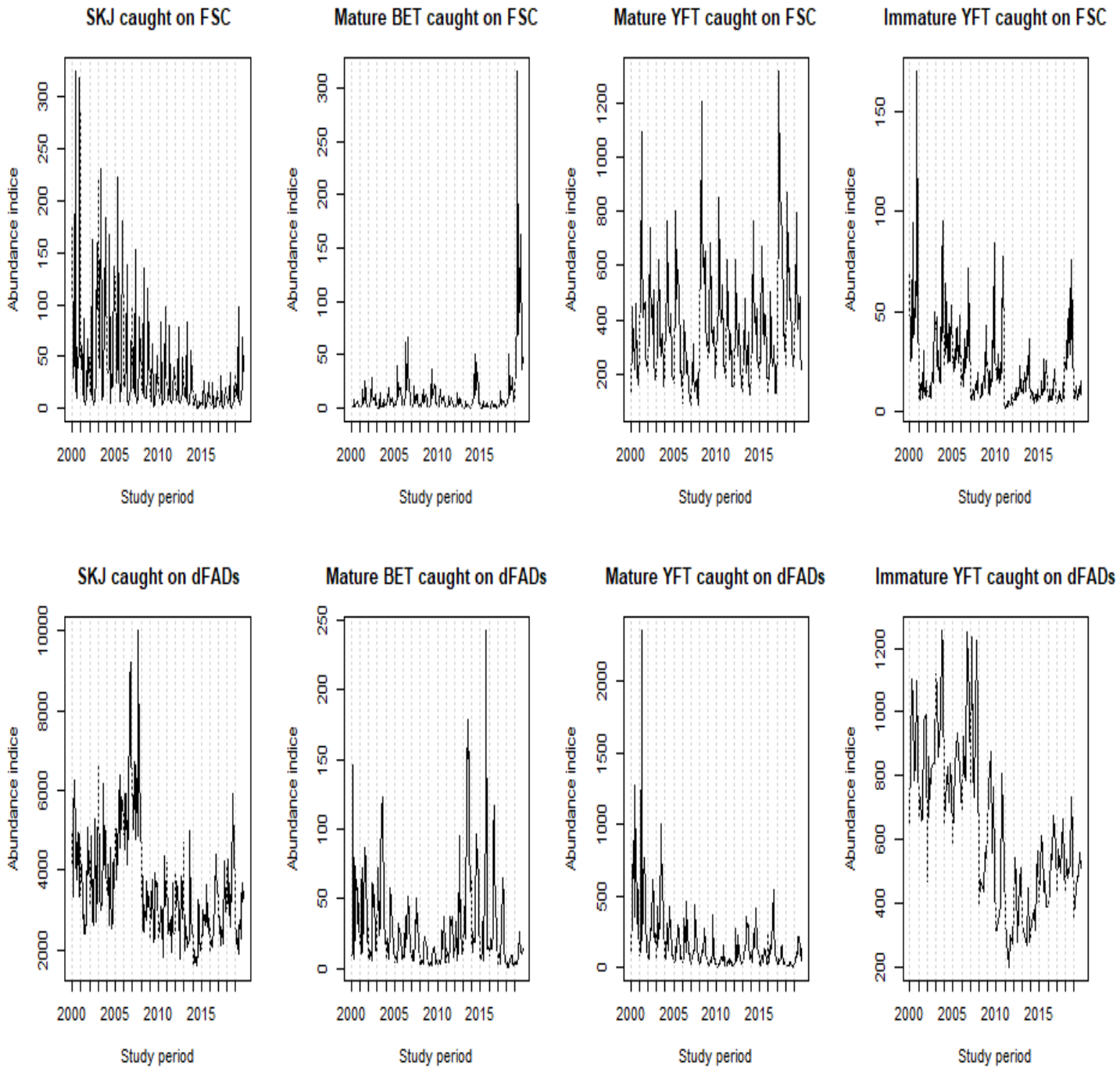

Fig. 3.S1 Monthly abundance indices of the eight categories of tropical tunas analysed in this study.

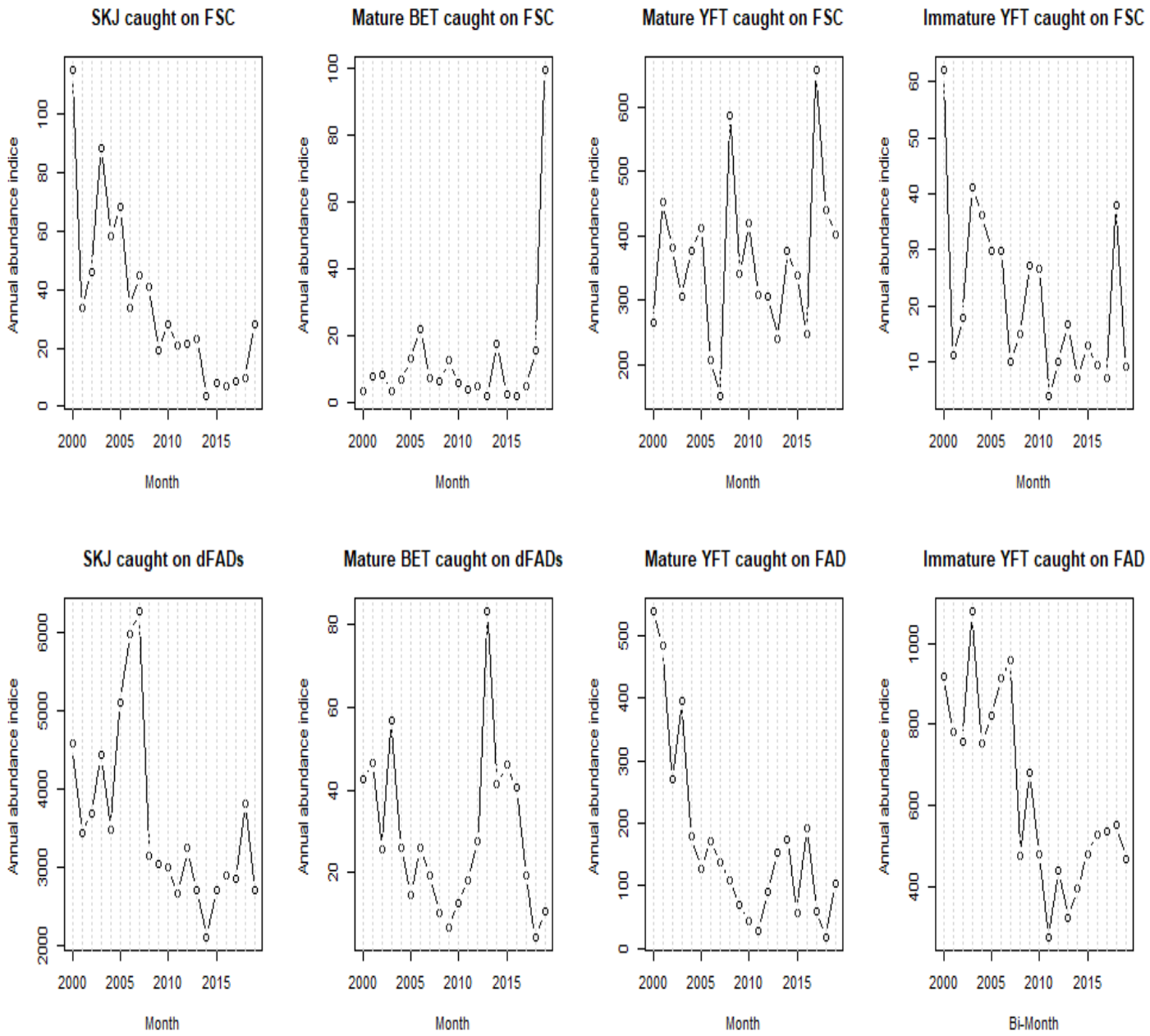

Fig. 4.S1 Annual abundance indices of the eight categories of tropical tunas analysed in this study. Abundance indices are expressed in tons per km2 per searching hour (tons/h.km2) for catches on FSC, and in tons per km2 per set (tonnes/set.km2) for catches on FAD. It is a simple sum of the monthly abundance indices resulting from the seasonal spatio-temporal model.

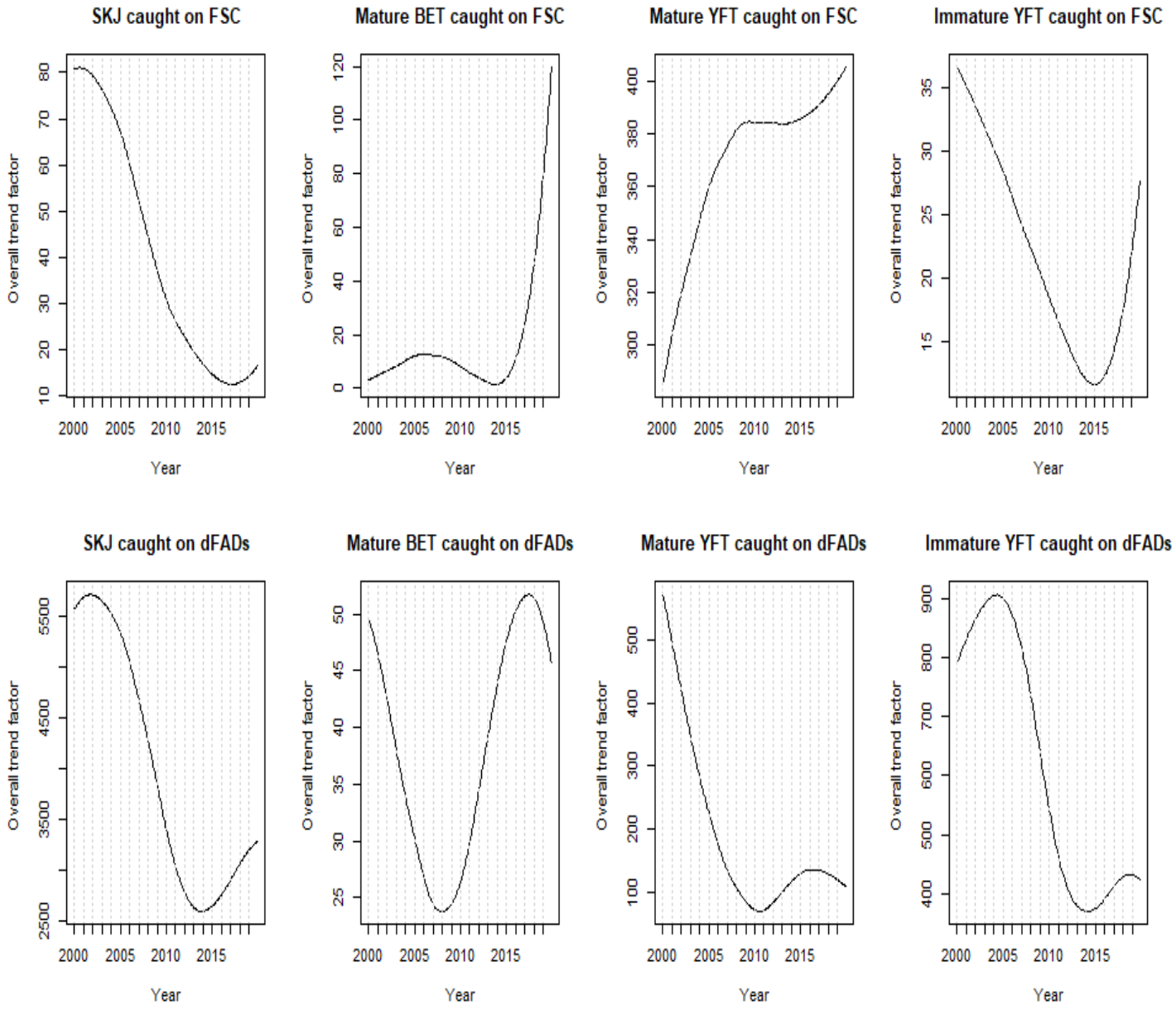

Fig. 5.S1 Inter-annual variations in abundance indices over the study period. This global trend is derived from the decomposition of the abundance indices using the CEEMDAN algorithm.

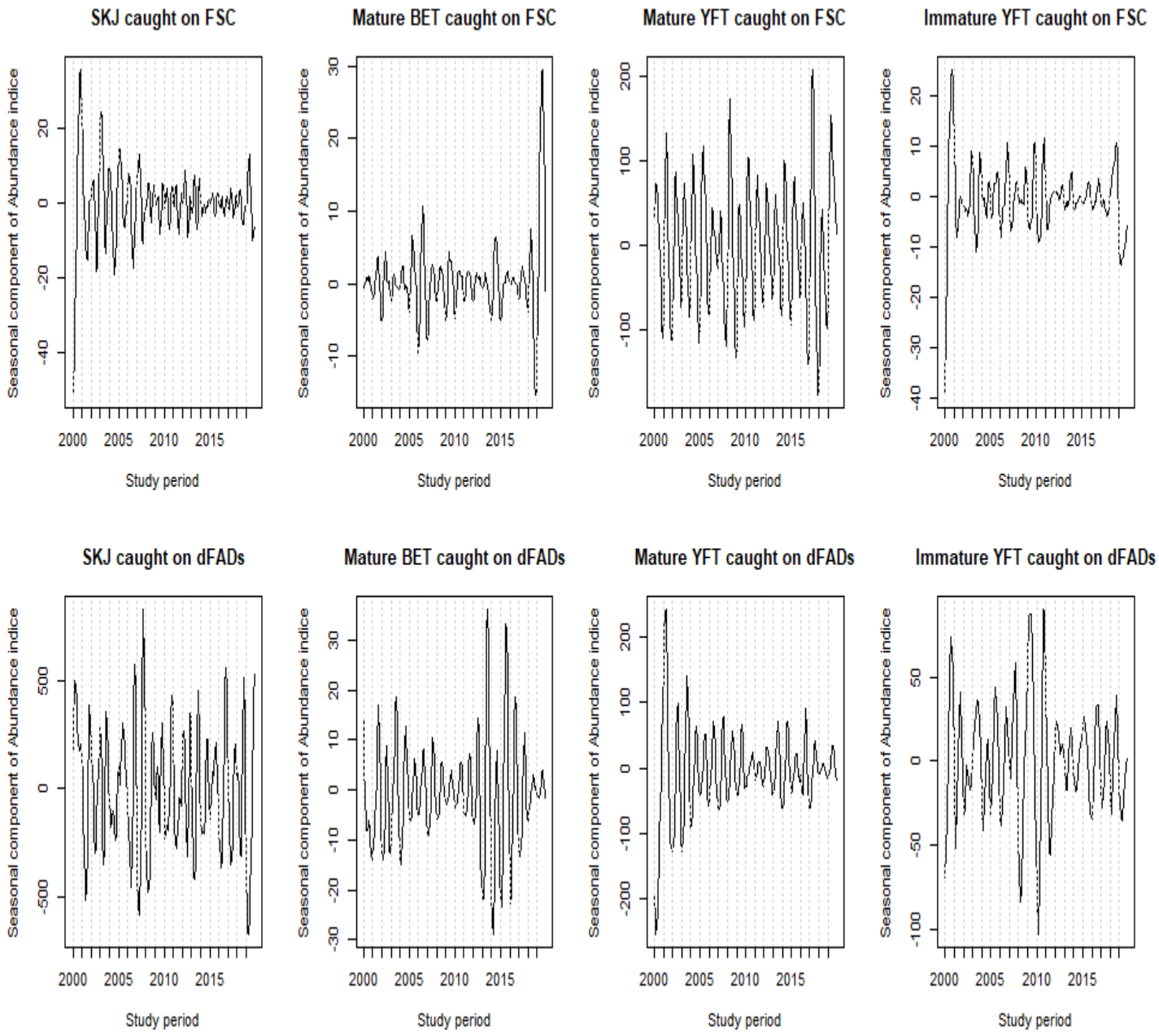

Fig. 6.S1 Seasonal component of the abundance indices of the eight categories of tropical tunas analysed in this study.

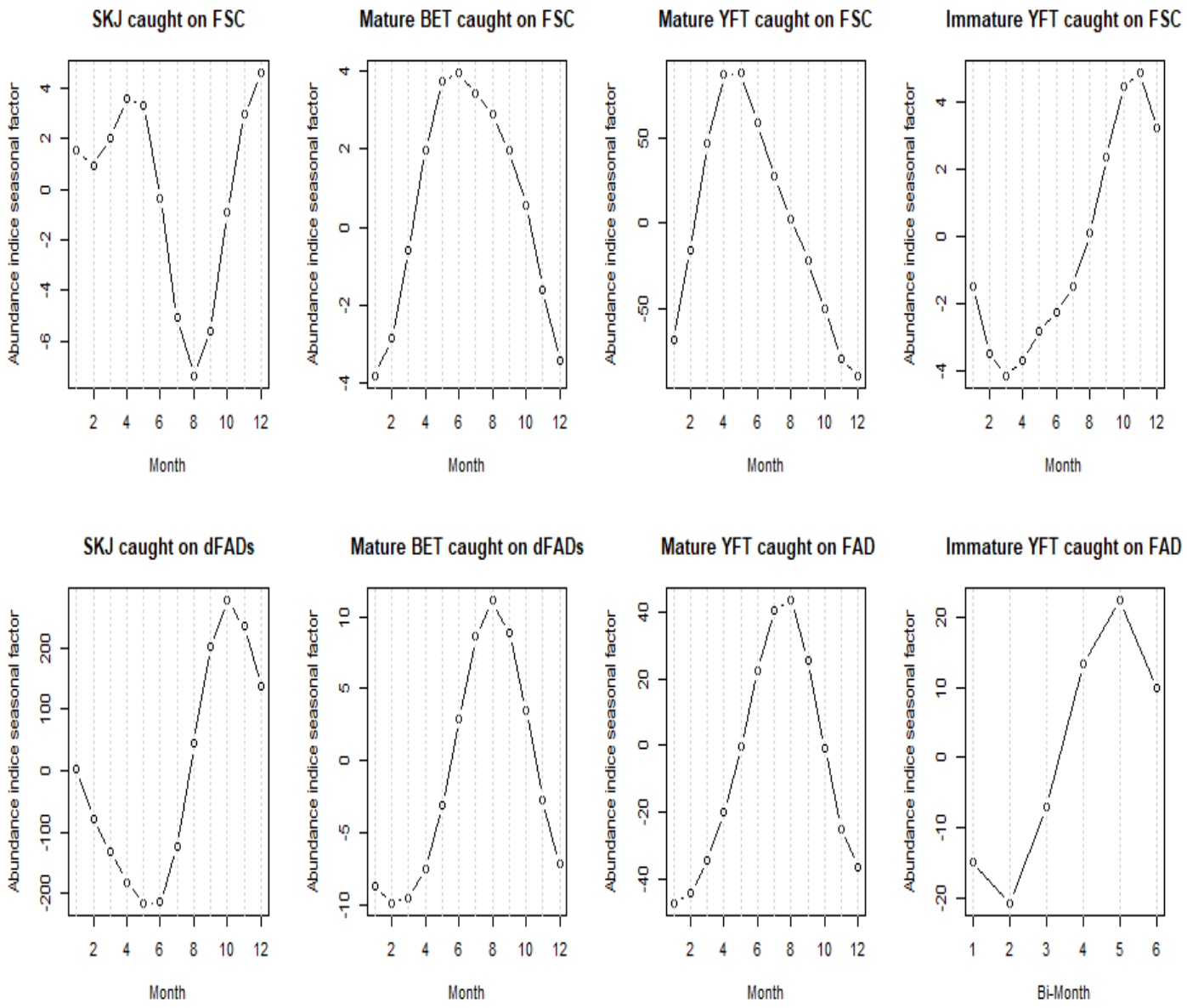

Fig. 7.S1 Mean average seasonal variations in abundance indices for the eight categories of tropical tunas analysed in this study (over the study period). There are seasonal factors and therefore might have negative values.

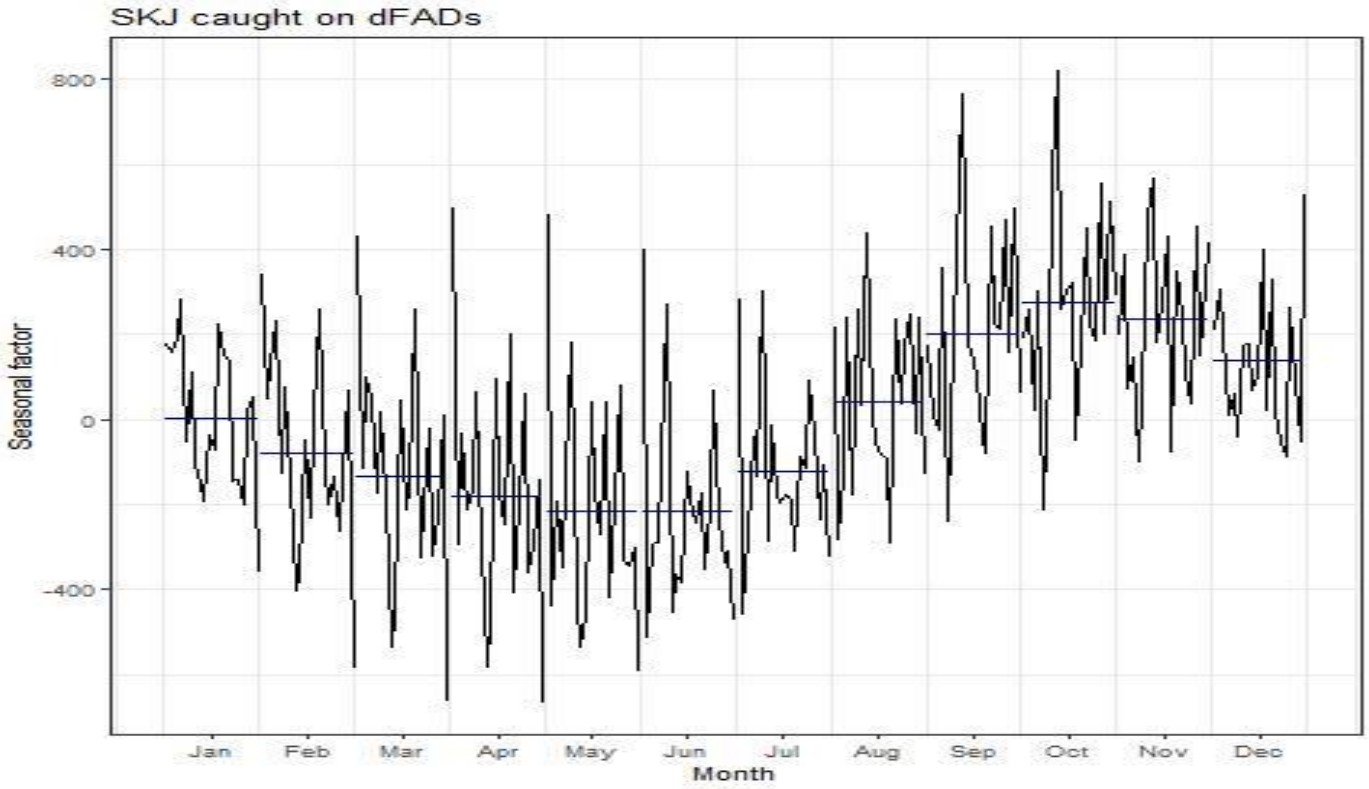
SKJ caught on dFADs
800
400
0
-400
Seasonal factor
Jan
Feb
Mar
Apr
May
Jun
Jul
Aug
Sep
Oct
Nov
Dec
Month

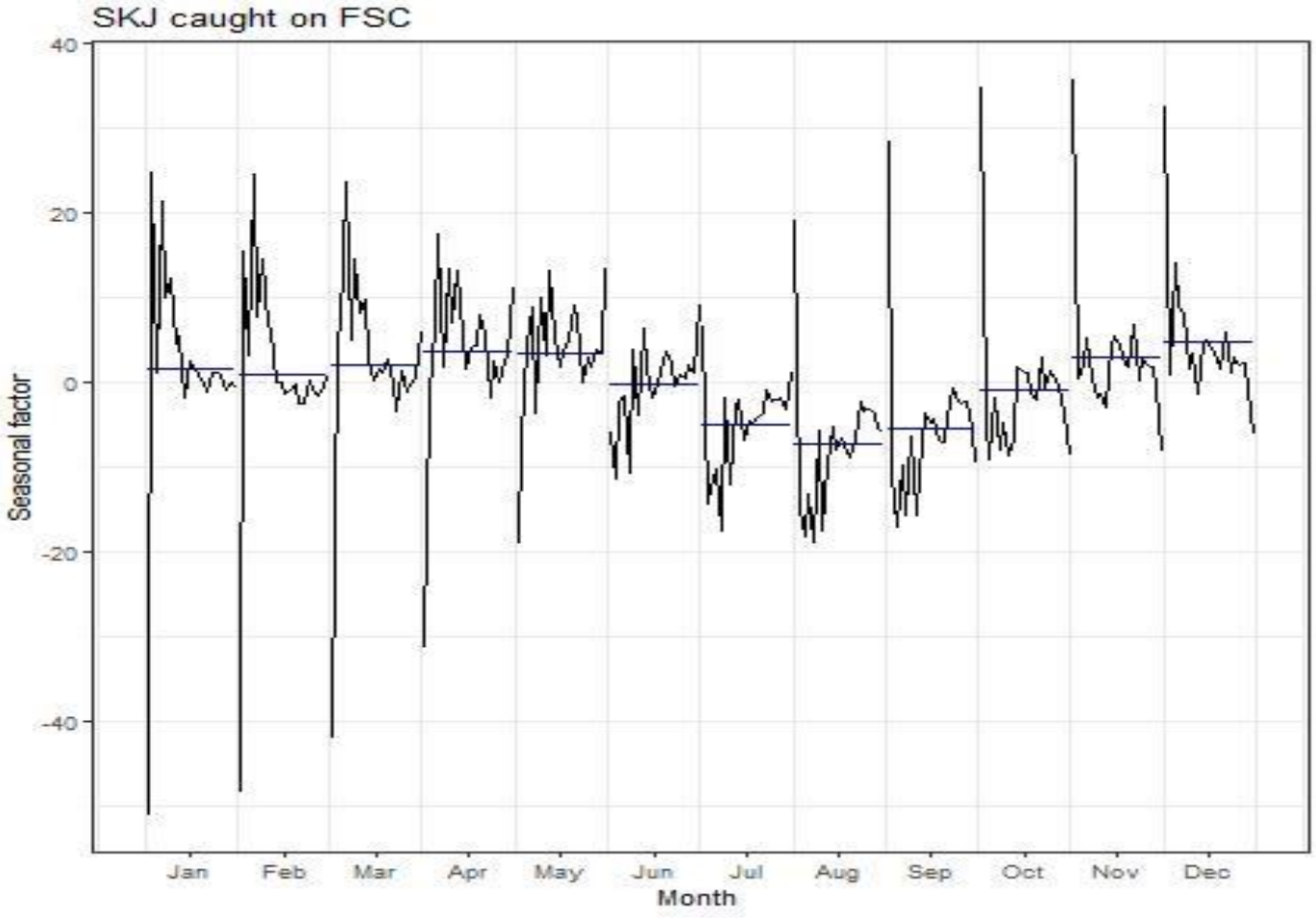
SKJ caught on FSC
40
20
0
-20
-40
Seasonal factor
Jan
Feb
Mar
Apr
May
Jun
Jul
Aug
Sep
Oct
Nov
Dec
Month

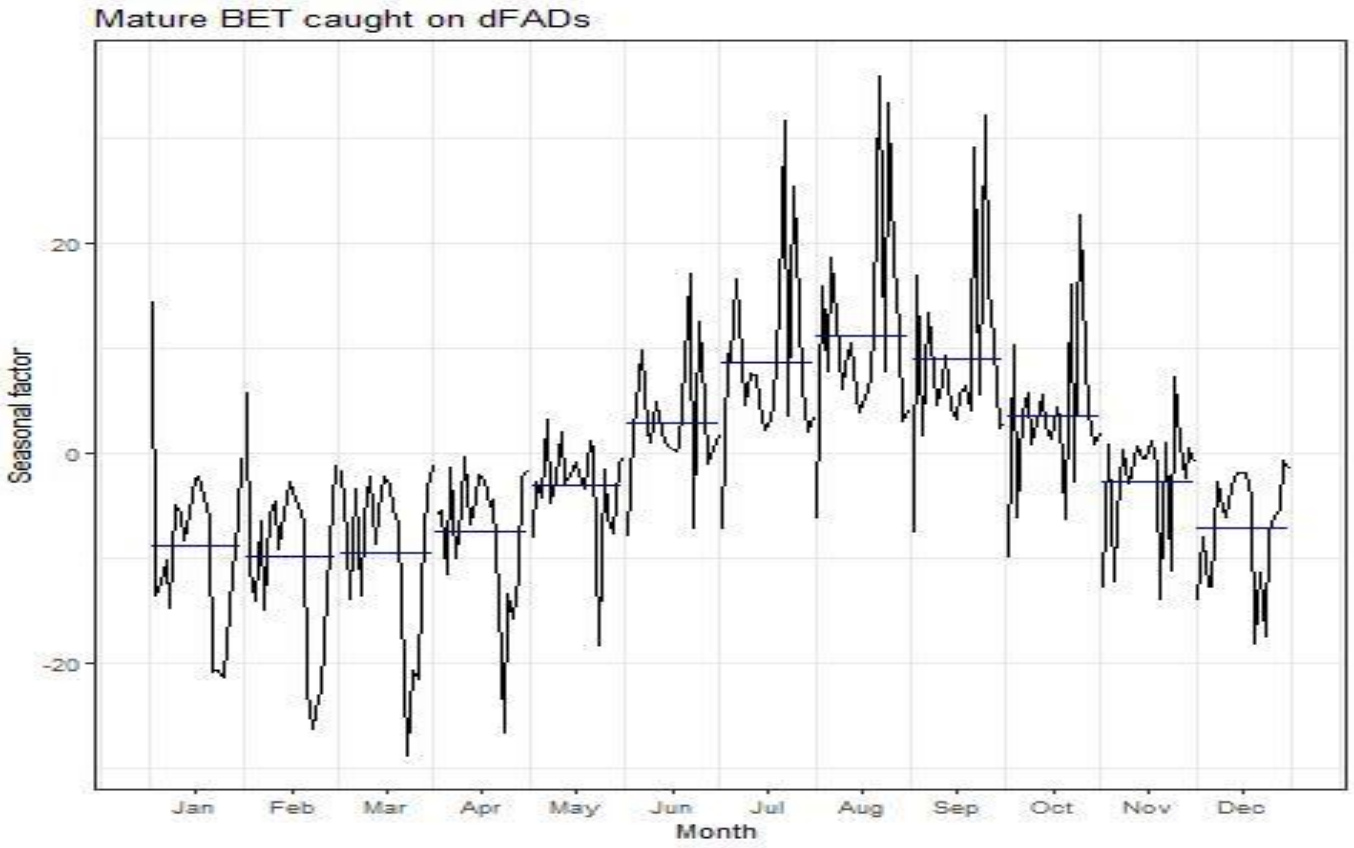
Mature BET caught on dFADs
Seasonal factor
20
0
-20
Jan
Feb
Mar
Apr
May
Jun
Jul
Aug
Sep
Oct
Nov
Dec
Month

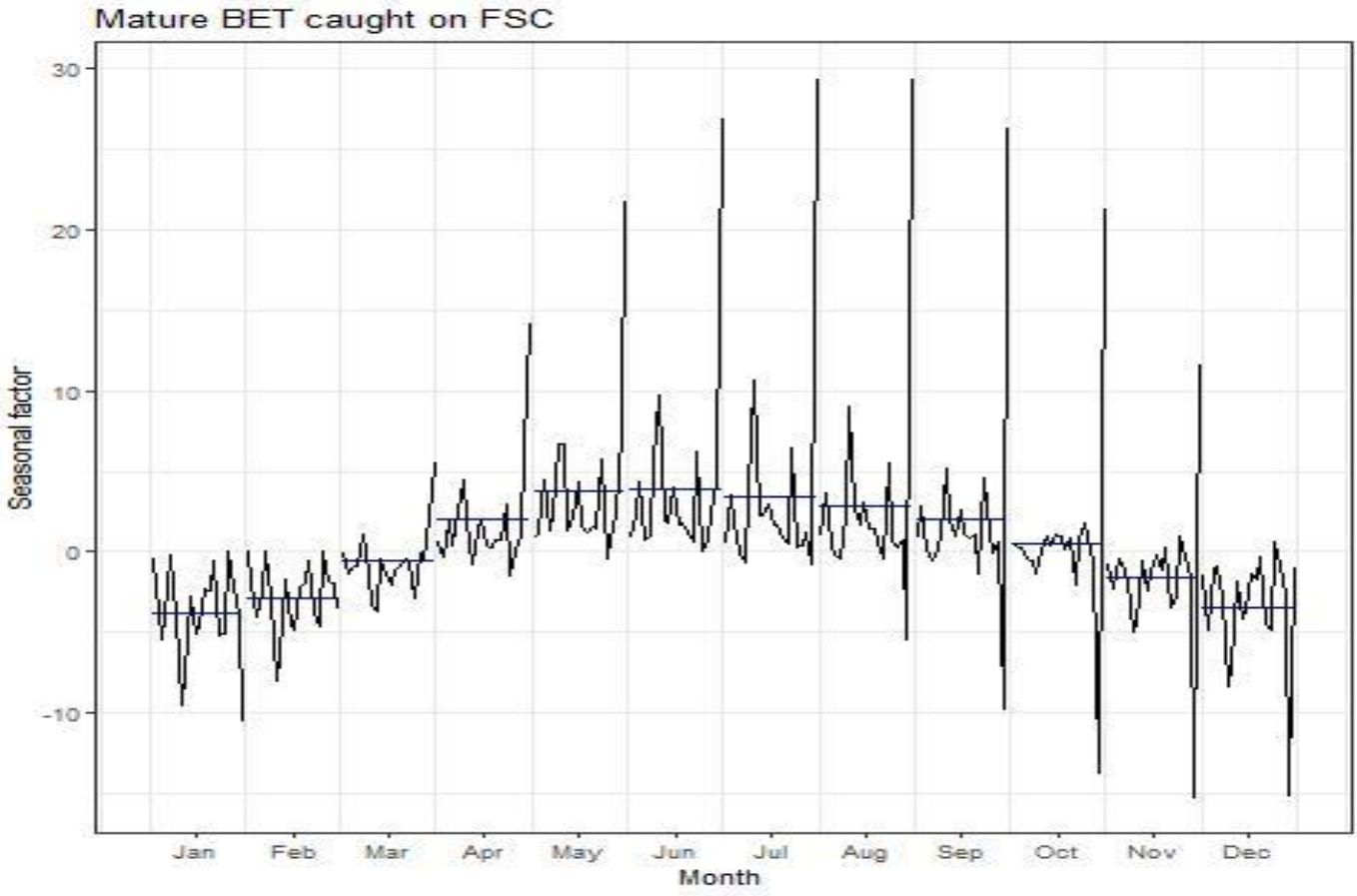
Mature BET caught on FSC
Seasonal factor
30
20
10
0
-10
Jan
Feb
Mar
Apr
May
Jun
Jul
Aug
Sep
Oct
Nov
Dec
Month

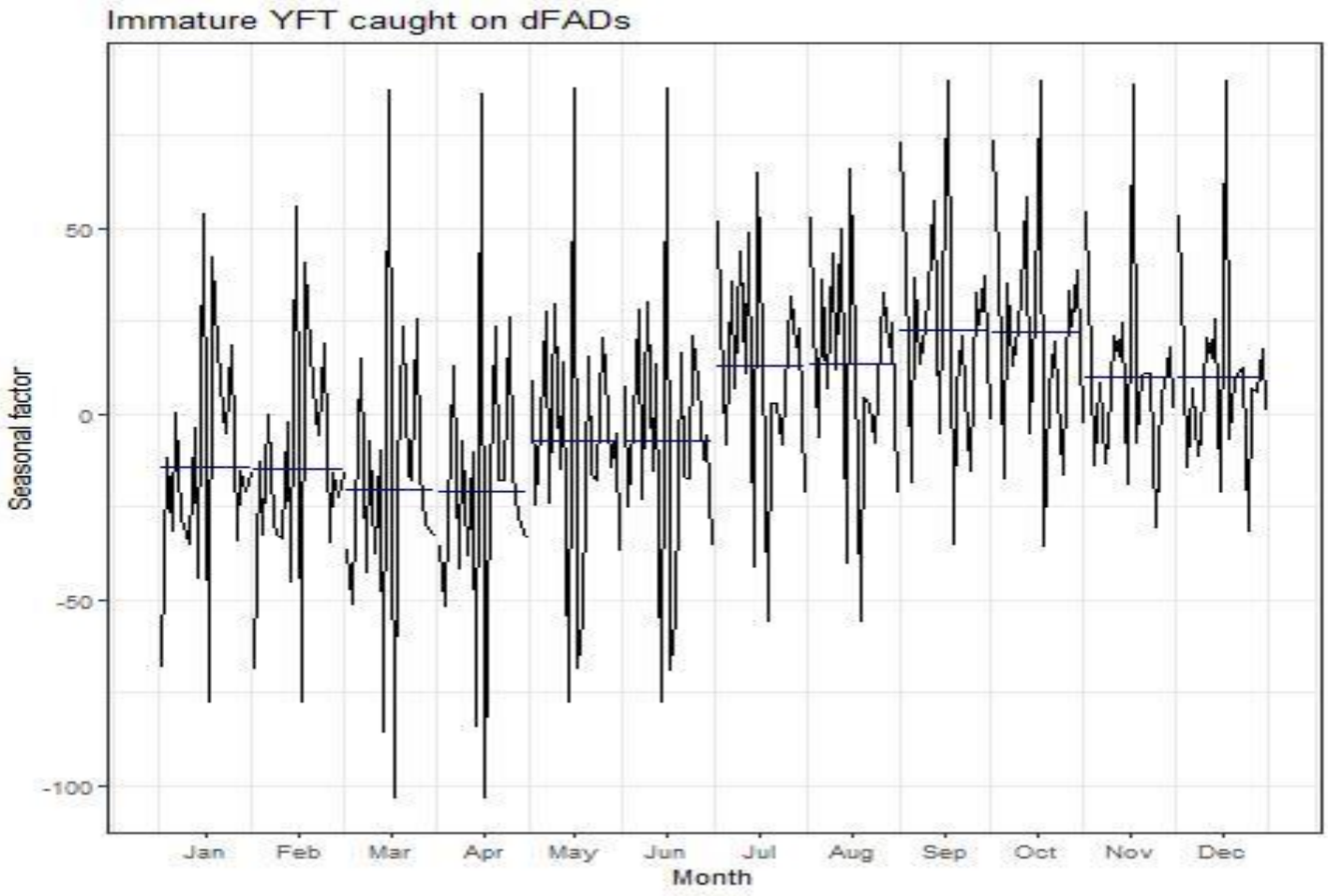
Immature YFT caught on dFADs
Seasonal factor
50
0
-50
-100
Jan
Feb
Mar
Apr
May
Jun
Jul
Aug
Sep
Oct
Nov
Dec
Month

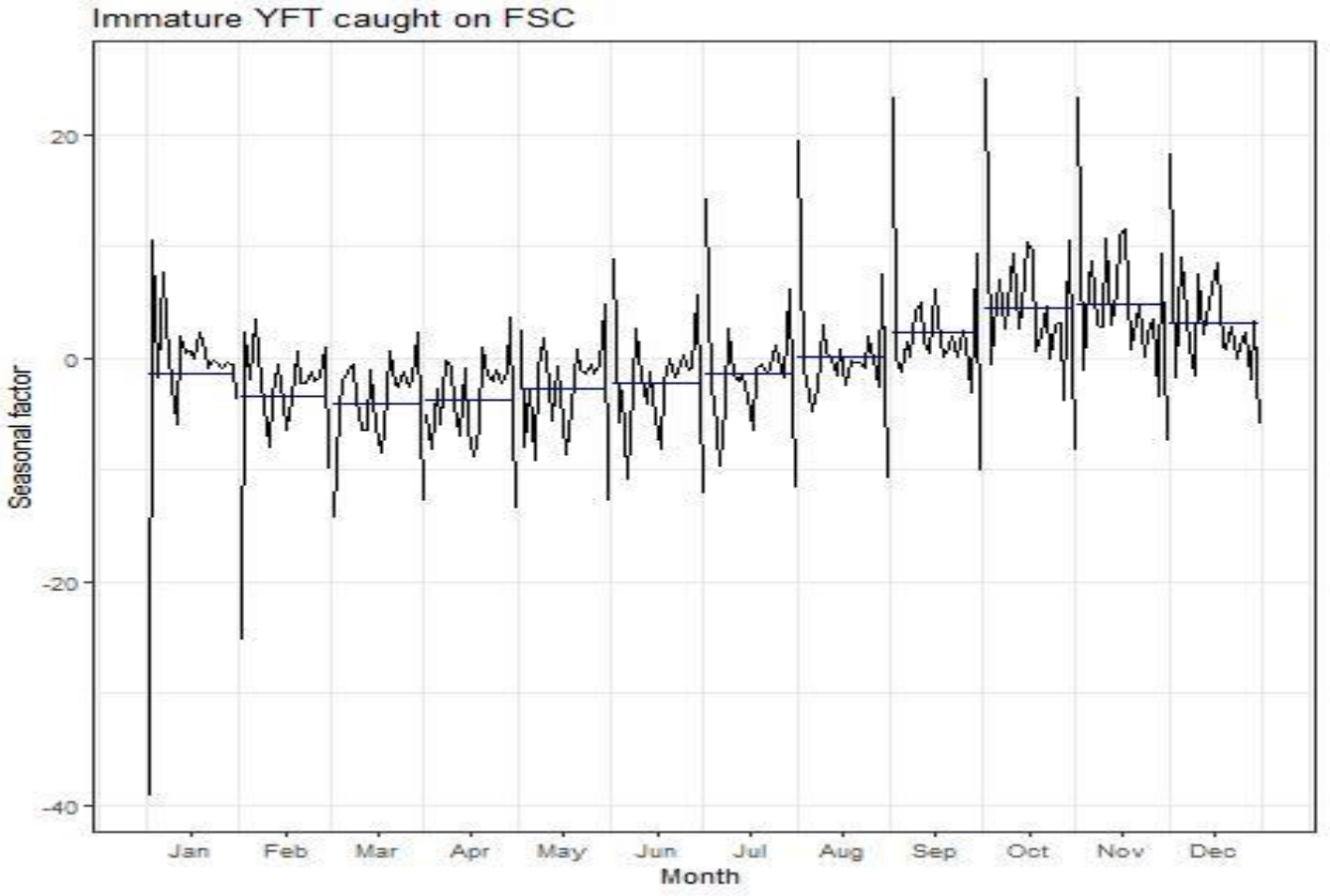
Immature YFT caught on FSC
Seasonal factor
20
0
-20
-40
Jan
Feb
Mar
Apr
May
Jun
Jul
Aug
Sep
Oct
Nov
Dec
Month

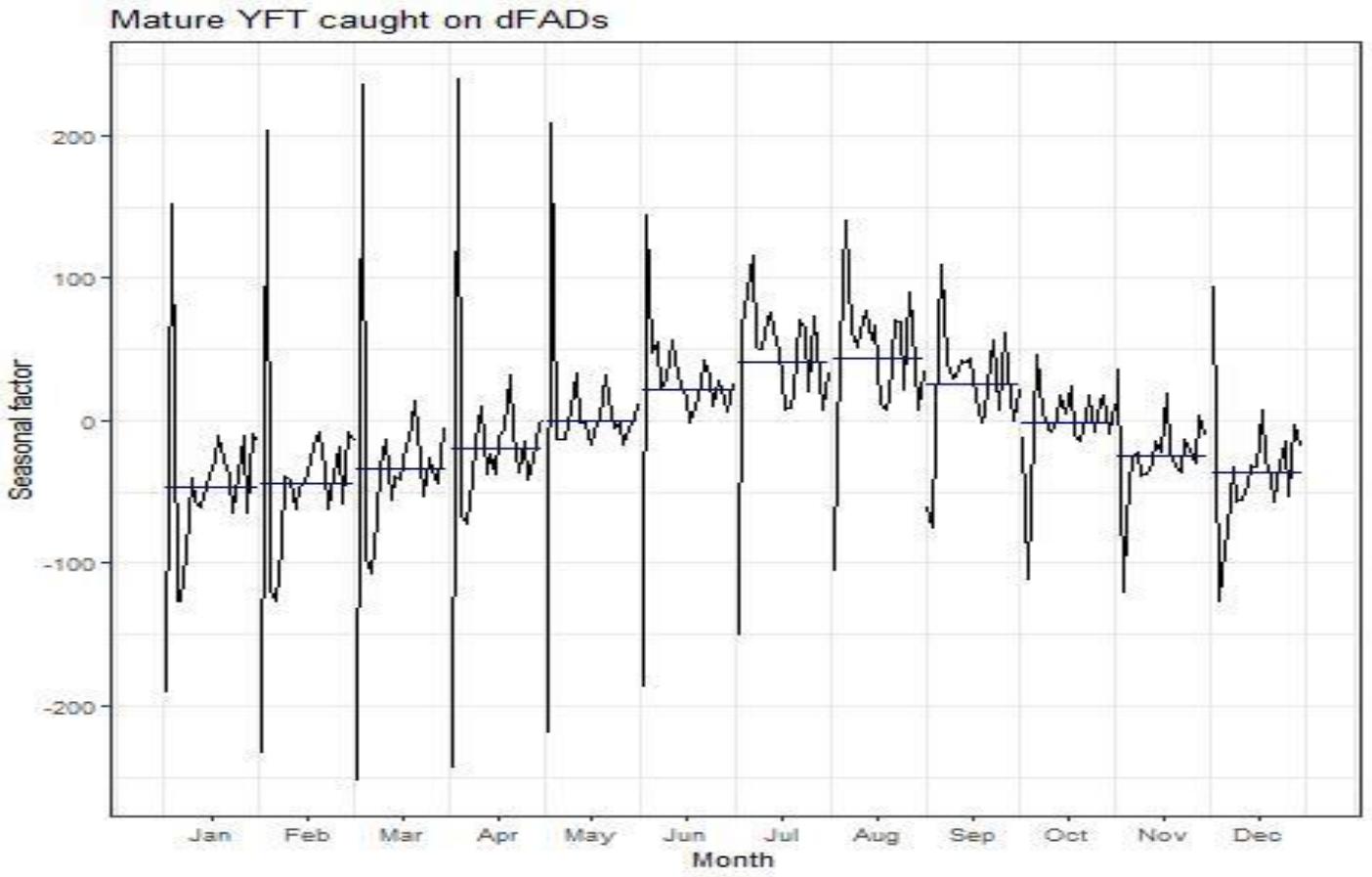

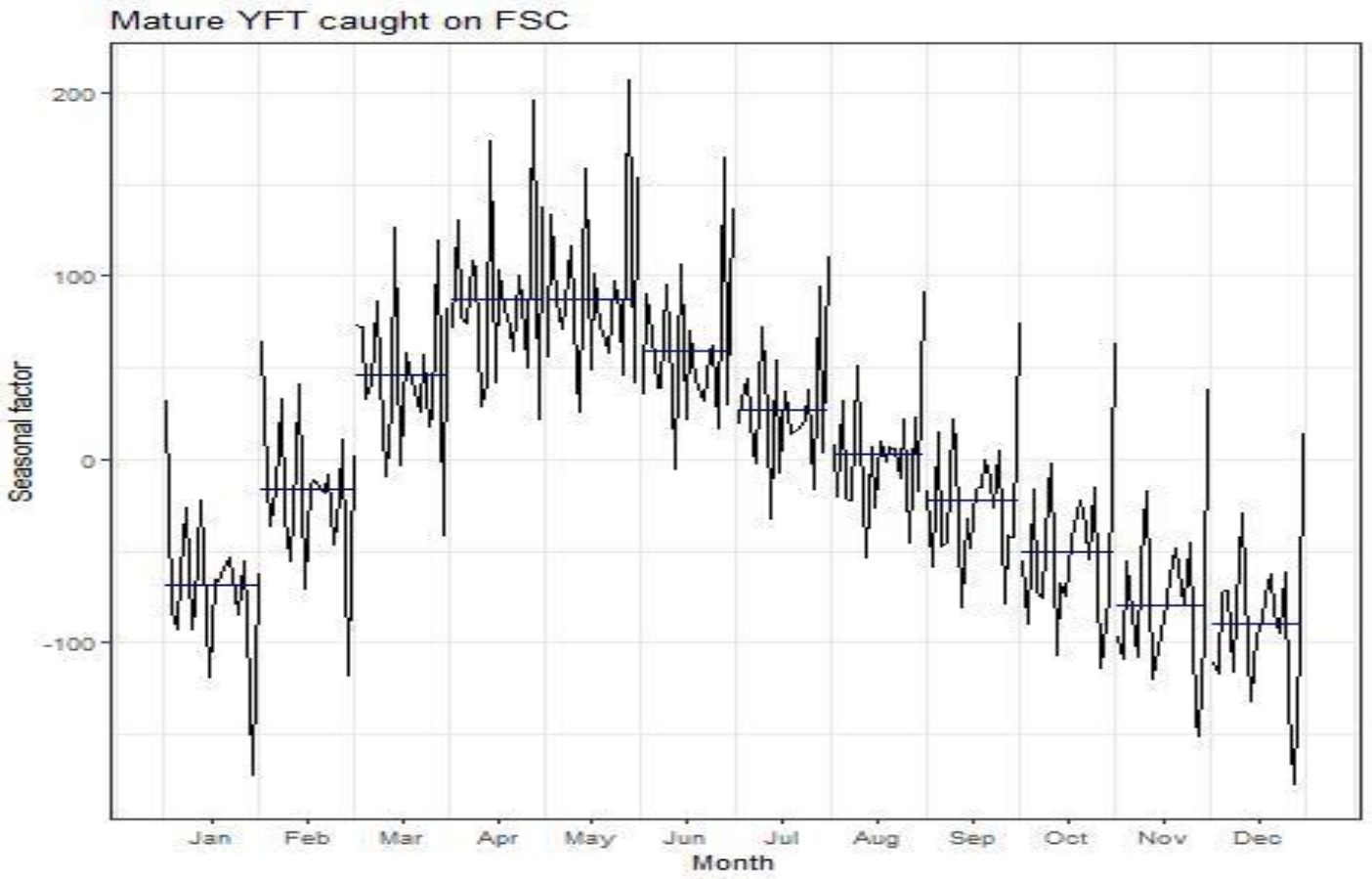

Fig. 8:S1 Inter-annual variations in seasonal abundance indices over the study period. The comment is the same for the 8 figures.

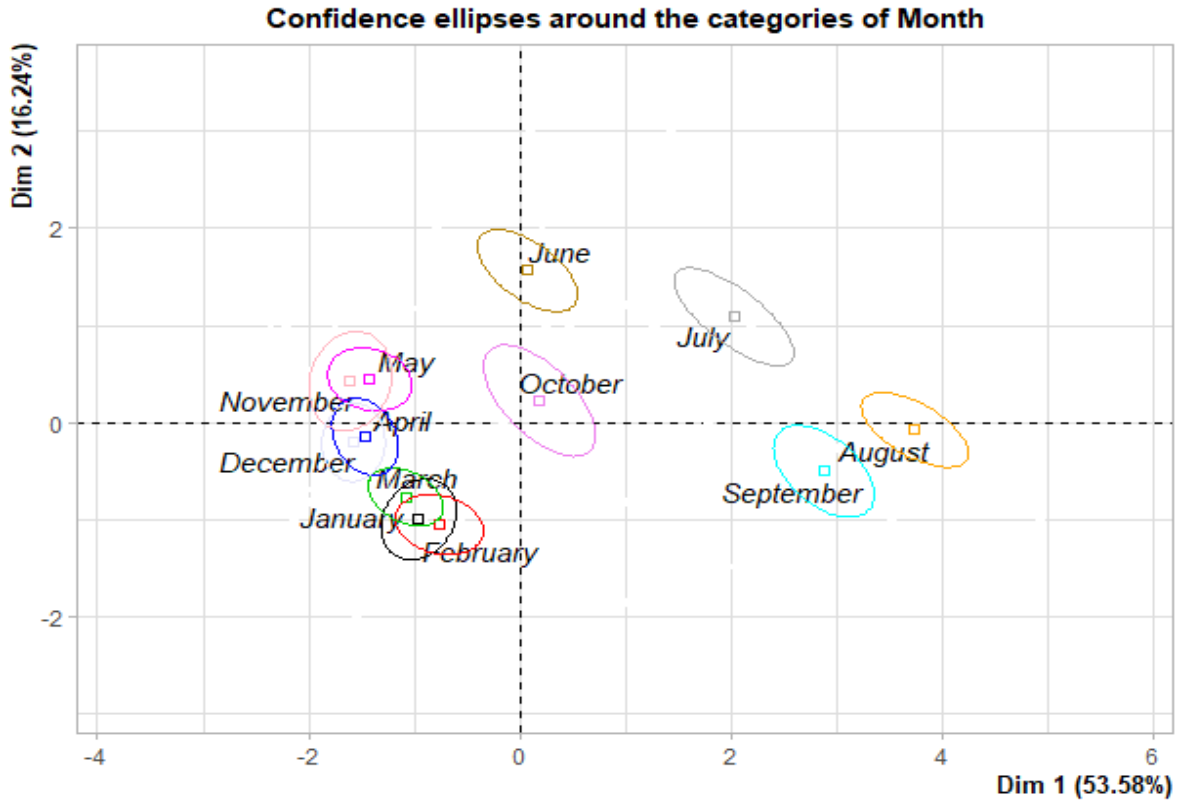

Fig. 9.S1 Ordination diagram of the principal component analysis (first and second principal components) showing variability of environmental conditions in the EEZ of Côte d'Ivoire. The diagram shows the average projection of the months (used as a qualitative supplementary variable) in the plane defined by the first two axes.

Table 1 :S1

Fisheries agreement concluded between the EU and Côte d'Ivoire from 1997 to date. The data were collected on the website https://ec.europa.eu/fisheries/cfp/international/agreements and were synthesized by period.

Period	Reference tonnage (Tonnes/year)	Tuna seiners	Surface longliners	Other like seiners	Other like longliners	Vessels total
1997 - 2000	**8500**	39	14	7	3	**63**
2000 – 2003	**8500**					**71**
2004 – 2007	**8400**	34	11	3	0	**48**
2007 – 2013	**7000**	25	15	0	0	**40**
2013 – 2018	**6500**	28	10	0	0	**38**
2018 - 2024	**5500**	28	8	0	0	**36**

S2: Online supplementary material for 'Seasonal and inter-annual variability in abundance of the main tropical tunas in the EEZ of Côte d'Ivoire (2000-2019)'

Akia S., Amandé M., Pascual P. and Gaertner D.

31/05/2021

MODELS STRUCTURE AND OTHERS RESULTS

We chose to present a summarized version of the seasonal spatio-temporal model developed by Thorson et al. (2020a) in the paper. In addition, we presented only the abundance indices estimated using this method without giving the full set of estimated parameters, model implementation and model outputs. In this section, we will present the complete structure of the model as detailed in Thorson et al. (2020a), the implementation of the model (choice of parameters and estimation using the r packages VAST and FishStatsUtils) as well as the set of model outputs. We will also show the results of CEEMDAN decomposition. In order to present the method in its entirety without any intention of plagiarism, we would like to inform you that the presentation of the methods will be almost identical to that of the authors in order to ensure a good understanding when reading this paper.

1 Seasonal spatio-temporal (VAST) model structure

The Seasonal spatio-temporal model developed by Thorson represents spatial variation in population density, and how density changes both among years (inter-annual variation) and within years (seasonal variation). The commercial fisheries catch and effort data used in this kind of analysis concern field-sampling of sets i records the biomass (Tons) or abundance (numbers) bi encountered by the ith sets, occurring at location s_i (within a fixed and pre-defined spatial domain), year y_i (between a minimum and maximum year $y \in \{y_{\min}, \dots, y_{\max}\}$), and season u_i (among an ordered set of intervals occurring within a year, $u_i \in \{u_1, \dots, u_U\}$). These seasons could be quarters (winter, spring, summer, fall), months (January-December), weeks (1-52), or any intervals defined within a year (whether having even or uneven spacing and duration). In this notation, the combination of year y_i and season u_i is sufficient to define the time of a given sample and the term t to describe this combination, $t \in \{y_{\min}u_1, y_{\min}u_2, \dots, y_{\max}u_U\}$, where seasons and years are ordered such that $t+1$ is the year-season combination occurring immediately after t and $t-1$ is the year-season combination preceding t. This model has reasonable performance even when data are entirely unavailable for one or more combinations of year and season. That is why estimates in year-season t are shrunk towards predicted density in adjacent year-seasons ($t-1$ and $t+1$), as well as towards estimated density in other seasons for a given year (other u for a given y) and density in other years for a given season (other y for a given u). This specification implies that the model will include a "main effect" for season and year, as well as an autocorrelated "interaction" of season and year.

The implementation of these criteria has been done using a Poisson-link delta model (Thorson, 2018) that specifies a probability distribution for random variable B, corresponding to the likelihood of response variable b_i for each sample (set) i, $\Pr(B = b_i)$. This Poisson-link delta model

includes the probability p_i that sample i encounters a given species [i.e. $\Pr(B > 0)$], and also the expected measurement r_i given that the species is encountered, $\Pr(B \mid B > 0)$:

$$\Pr(B = b_i) = \begin{cases} 1 - p_i & \text{if } B = 0 \\ p_i \times g\{B \mid r_i, \sigma_m^2\} & \text{if } B > 0 \end{cases}$$

where we specify a lognormal distribution for the distribution of positive catches. This Poisson-link delta model predicts encounter probability p_i and positive catch rate r_i by modelling two log-linked linear predictors, $\log(n_i)$ and $\log(w_i)$ for each sample i; n_i and w_i are then transformed to yield P_i and r_i :

$$p_i = 1 - \exp(-a_1 \times n_i), \qquad r_i = \frac{a_i \times n_i}{p_i} \times w_i$$

where a_i is the area-swept offset for sample i. This model structure is designed such that expected density d_i is the product of encounter probability and positive catch rate and also the product of transformed linear predictors (i.e. $d_i = p_i r_i = n_i w_i$). When the response variable b_i is in units biomass, these predictors can be interpreted as numbers-density n_i (with units numbers per area) and average weights w_i (with units biomass per number). Alternatively, if the response variable is in units numbers, n_i (with units numbers per area) and w_i (with dimensionless units) describe a parametric link between expected encounter probability and expected numbers given an encounter, but they are not specifically interpretable as describing numbers-density and biomass per number. In both interpretations, n_i always enters via the product $a_i \times n_i$ such that n_i is expressed as density.

The Poisson-link delta model is useful relative to other delta models because both linear predictors use a log-link function, so that all effects are additive in their impact on predicted log-density. Specifically, we specify that:

$$\log(n_i) = \underbrace{\beta_n^*(t_i)}_{\substack{Year-season \\ intercept}} + \underbrace{\omega_n^*(s_i)}_{\substack{Spatial \\ main\ effect}} + \underbrace{\xi_{nu}^*(s_i, u_i)}_{\substack{Season \\ spatial\ effect}} + \underbrace{\xi_{ny}^*(s_i, y_i)}_{\substack{Year \\ spatial\ effect}} + \underbrace{\varepsilon_{nu}^*(s_i, t_i)}_{\substack{Year-season \\ spatial\ effect}} + \underbrace{\zeta_n^*(i)}_{\substack{Catchability \\ covariates}}$$

$$\log(w_i) = \underbrace{\beta_w^*(t_i)}_{\substack{Year-season \\ intercept}} + \underbrace{\omega_w^*(s_i)}_{\substack{Spatial \\ main\ effect}} + \underbrace{\xi_{wu}^*(s_i, u_i)}_{\substack{Season \\ spatial\ effect}} + \underbrace{\xi_{wy}^*(s_i, y_i)}_{\substack{Year \\ spatial\ effect}} + \underbrace{\varepsilon_{wu}^*(s_i, t_i)}_{\substack{Year-season \\ spatial\ effect}} + \underbrace{\zeta_w^*(i)}_{\substack{Catchability \\ covariates}}$$

where the other linear predictor w_i is defined identically except that the subscript n is replaced by w for all coefficients. In applications with limited information (either due to low sample sizes or small variance), the variance of one or more of these terms may be estimated near zero such that the corresponding term is then dropped from the model. Specifying an additive structure in log-space for both variables (n_i and w_i) simplifies interpretation of estimated terms where $\omega_n^*(s_1) = 0.1$ indicates that $n(s_1, t)$ is expected to be 10% higher at location s_1 than at location s_1 where $\omega_n^*(s_2) = 0$. We also hypothesize that this additive structure in log-space will be more parsimonious than a conventional delta model, although testing this is an empirical question for future research. Spatial terms are estimated using a predictive-process framework (Banerjee et al., 2008), such that we estimate the value of each spatial variable at a set of "knots", where the number of knots n_x is specified by the user in a balance between computational speed and spatial resolution. In the case of spatial variation, we specify a Gaussian Markov random field for vector ω_n^* containing the value of the spatial variable $\omega_n(s)$ at each knot:

$$\boldsymbol{\omega}_{\mathrm{n}} \sim MVN(\mathbf{0}, \sigma_{n\omega}^2 \mathbf{R}_n)$$

where $\mathbf{R}_n$ is the correlation matrix and $\sigma_{n\omega}^2$ is the pointwise variance such that $\sigma_{n\omega}^2 \mathrm{R}_n$ is the spatial covariance. We then project from the values ω_n at knots to the values ω_n^* at the location of available data. The correlation matrix, in turn, is calculated based on a vector of distance $\mathrm{d}(s_1, s_2)$ between any pair of locations s_1 and s_2, and we use a sparse precision matrix that approximates a Matérn correlation function :

$$\mathbf{R}_n(s_1, s_1) = \frac{1}{2^{\nu-1}\Gamma(\nu)} \times (\kappa_n \mathbf{d}(s_1, s_2)\mathbf{H})^{\nu} \times K_{\nu}(\kappa_n \mathbf{d}(s_1, s_2)\mathbf{H})$$

where we estimate a linear transformation H involving estimated parameters (representing geometric anisotropy) and decorrelation rate κ_n. Given the value of a spatial variable at each knot, the value at any given location s within spatial domain Ω is then calculated using bilinear interpolation, using a projection matrix calculated by the R package R-INI.A (Lindgren, 2012). Season and year main spatial effects are specified similarly, except the probability of $\xi_{\mathrm{nu}}(u)$ is calculated independently for every season u and the probability of $\xi_{\mathrm{ny}}(y)$ is calculated independently for each year y. However, the year-season interaction $\varepsilon_n(s,t)$ is autocorrelated across the ordered year-season index t :

$$\boldsymbol{\varepsilon}_n(s,t) \sim \begin{cases} MVN(\mathbf{0}, \mathbf{Q}^{-1}) & \text{if } t = t_{min} \\ MVN(\rho_{n\varepsilon}\varepsilon_n(s, t-1), \mathbf{Q}^{-1}) & \text{if } t > t_{min} \end{cases}$$

where the degree of autocorrelation $\rho_{n\varepsilon}$ in spatio-temporal variation $\mathcal{E}_n(s,t)$ is also estimated. We here assume that the decorrelation-rate parameters κ_n and κ_w are identical for spatial and spatio-temporal components and different between the two linear predictors n and w. Similarly, intercepts $\beta_n(t)$ are specified such that they can be interpolated for season–year combinations without any data using information from adjacent season–years, other years of the same season, or other seasons of the same year. This is again accomplished by including season and year main effects, and an autocorrelated interaction of season and year:

$$\beta_n^*(t) = \mu_\beta + \beta_{nu}(u) + \beta_{ny}(y) + \beta_{nt}(t)$$

where μ_β is the average intercept across all seasons and years, $\beta_{nu}(u)$ captures differences in expected intercept among seasons $u, \beta_{ny}(y)$ captures differences in expected intercepts among years y, and $\beta_{nt}(t)$ represents an autocorrelated season-year interaction:

$$\beta_{nt}(t) \sim \begin{cases} N\left(0, \sigma_{n\beta}^2\right) & \text{if } t = t_{min} \\ N\left(\rho_{n\beta}\beta_{nt}(t-1), \sigma_{n\beta}^2\right) & \text{if } t > t_{min} \end{cases}$$

and where the magnitude of autocorrelation is again estimated from available data. We ensure identifiability for $\mu_\beta, \beta_{nu}(u)$, and $\beta_{ny}(y)$ by imposing a corner constraint on the season and year effects (i.e. $\beta_{nu}(u) = 0$ and $\beta_{ny}(y) = 0$ for the first season and year y). This corner constraint is necessary for intercepts but not spatial terms because the season and year intercepts are treated as fixed effects, while the season and year spatial terms are treated as random effects. We note that this model structure imposes no constraints on the expected "shape" of seasonal variation; that is the model can capture unimodal or multimodal distribution of abundance across seasons within a year.

Parameters are estimated using release 3.7.1 of the Vector Autoregressive Spatio-Temporal (VAST) package (Thorson, 2019b), which is publicly available online (https://github.com/ James-Thorson/VAST) and runs within the R statistical environment (R Core Team, 2017). VAST estimates fixed effects while approximating their marginal likelihood using the Laplace approximation (Skaug and Fournier, 2006). The Laplace approximation is implemented in turn using R package TMB (Kristensen et al., 2016), and computational efficiency is improved using automatic differentiation (Fournier et al., 2012) and the SPDE approximation to spatial correlation matrices (and associated projection matrices) from R-INLA (Lindgren and Rue, 2015). Standard errors are calculated using a generalization of the delta method (Kass and Steffey, 1989), and standard errors are available for predictions of local density after estimating all fixed and random effects:

$$\begin{aligned} d(s,t) = &\quad n(s,t) \times w(s,t) \\ = &\quad \exp\{\beta_n^*(t) + \omega_n^*(s) + \xi_{nu}^*(s,u) + \xi_{ny}^*(s,y) + \varepsilon_n^*(s,t)\} \\ &\times \exp\{\beta_w^*(t) + \omega_w^*(s) + \xi_{wu}^*(s,u) + \xi_{wy}^*(s,y) + \varepsilon_w^*(s,t)\} \end{aligned}$$

where density can then be visualized or further processed to yield derived statistics. For example, total abundance is calculated as the area-weighted sum of density $d(s,t)$ predicted at a fine spatial resolution:

$$I(t) = \sum_{s=1}^{n_s} a(s)d(s,t)$$

where n_s is the number of fine-scale predictions and $a(s)$ is the spatial area associated with each prediction.

2 Seasonal spatio-temporal (VAST) model specifications

We define a 625 (25*25) km2 as spatial area of each fine scale, lead to a 594 fines scales were density prediction has been done. We make the choice to use fine scales prediction rather than knots aggregation, but we define 30 knots to meet the 1*1 square degrees of fisheries data. The use of 30 knots did not converge the model for skipjack caught on dFADs. Thus, we increased the grid size and re-estimated the model as we went along. This allowed us to obtain a convergence with six knots for this category.
We used month as seasonal dimension for each model except for immature yellowfin tuna caught on dFADs, for which we considered bimonthly as seasonal dimension. We used Flag (2 modalities) and carrying capacity (4 modalities) as catchability co-variables in this model.

The parameters, diagnostics and derived quantities of each model can be seen on the next section. Catchability covariates are captured by the $\lambda_i(k)$_p parameter in the model. Find below the definition of each $\lambda_i(k)$_p :

$\lambda_i(k)$_4 is the catchability effect of Spanish vessels relative to the effect of French vessels (as reference);

$\lambda_i(k)$_6 is the catchability effect of vessels with tonnage between 601 and 800 tons relative to the effect of vessels with tonnage between 401 and 600 tons (as reference);

$\lambda_i(k)$_7 is the catchability effect of vessels with tonnage between 801 and 1200 tons relative to the effect of vessels with tonnage between 401 and 600 tons (as reference); and

$\lambda_i(k)$_8 is the catchability effect of vessels with tonnage greater than 1200 tons relative to the effect of vessels with tonnage between 401 and 600 tons (as reference).

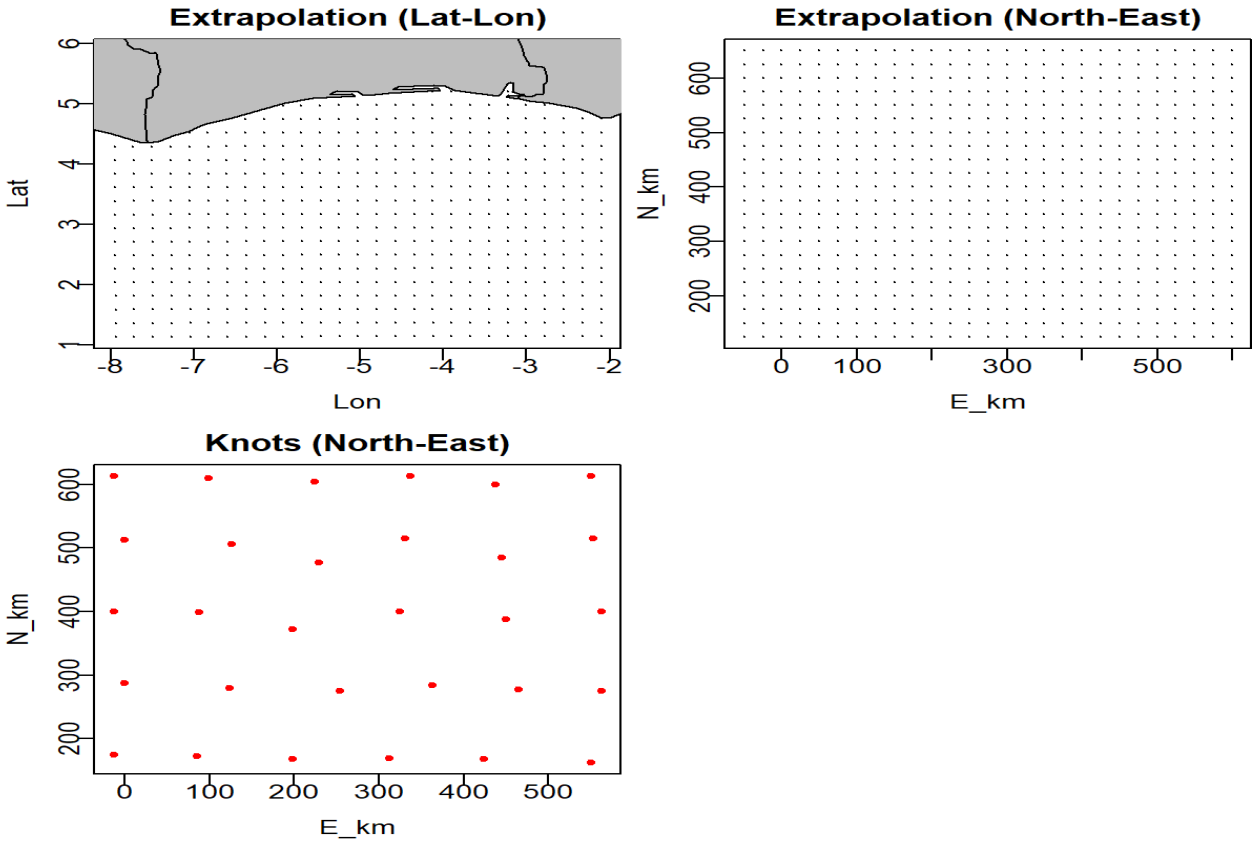

Fig. 1.S2 Visualization of spatial structure used to approximate spatial variation in each case-study (except for SKJ caught on dFADs), after projecting Latitude/Longitude to UTM coordinates measured in eastings (x-axis) and northings (y-axis). The red circles show the location of 30 interior knots where this number was chosen a priori and knots were then allocated using a k-means algorithm in proportion to available sampling data. Black points represent the extrapolation-grid used when approximating the integral across the survey domain.

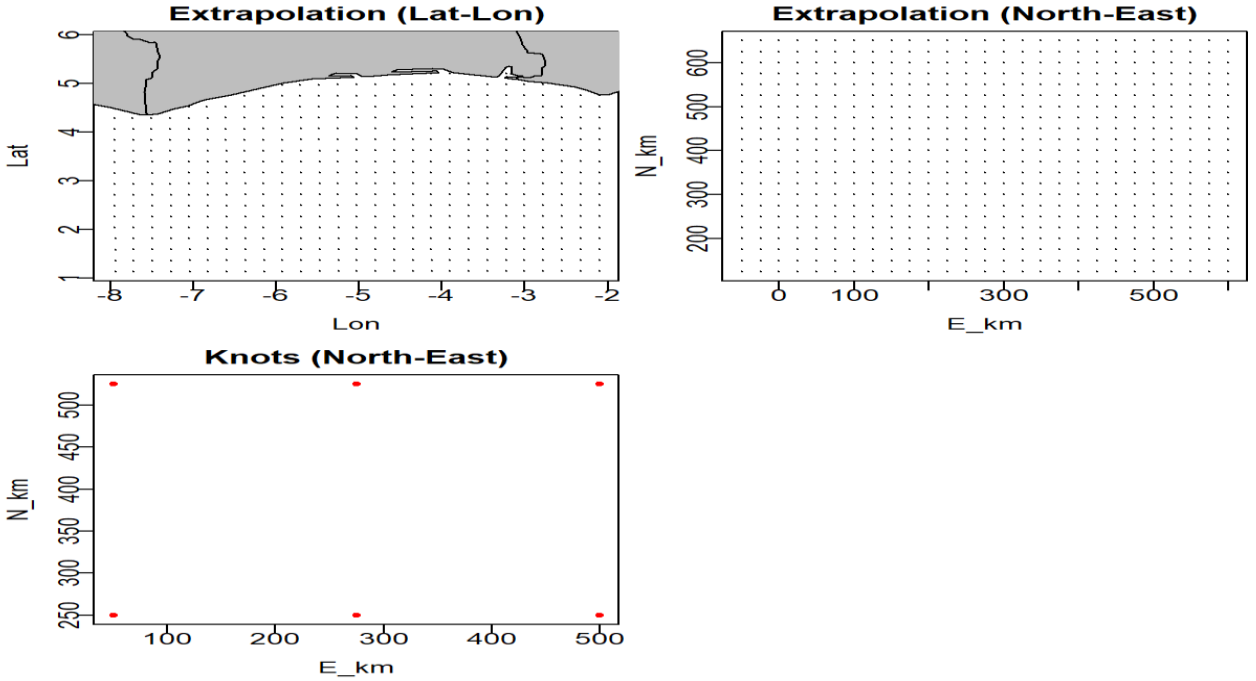

Fig. 2.S2 Visualization of spatial structure used to approximate spatial variation in the case of Skipjack caught on dFADs.

3 Seasonal spatio-temporal (VAST) model results

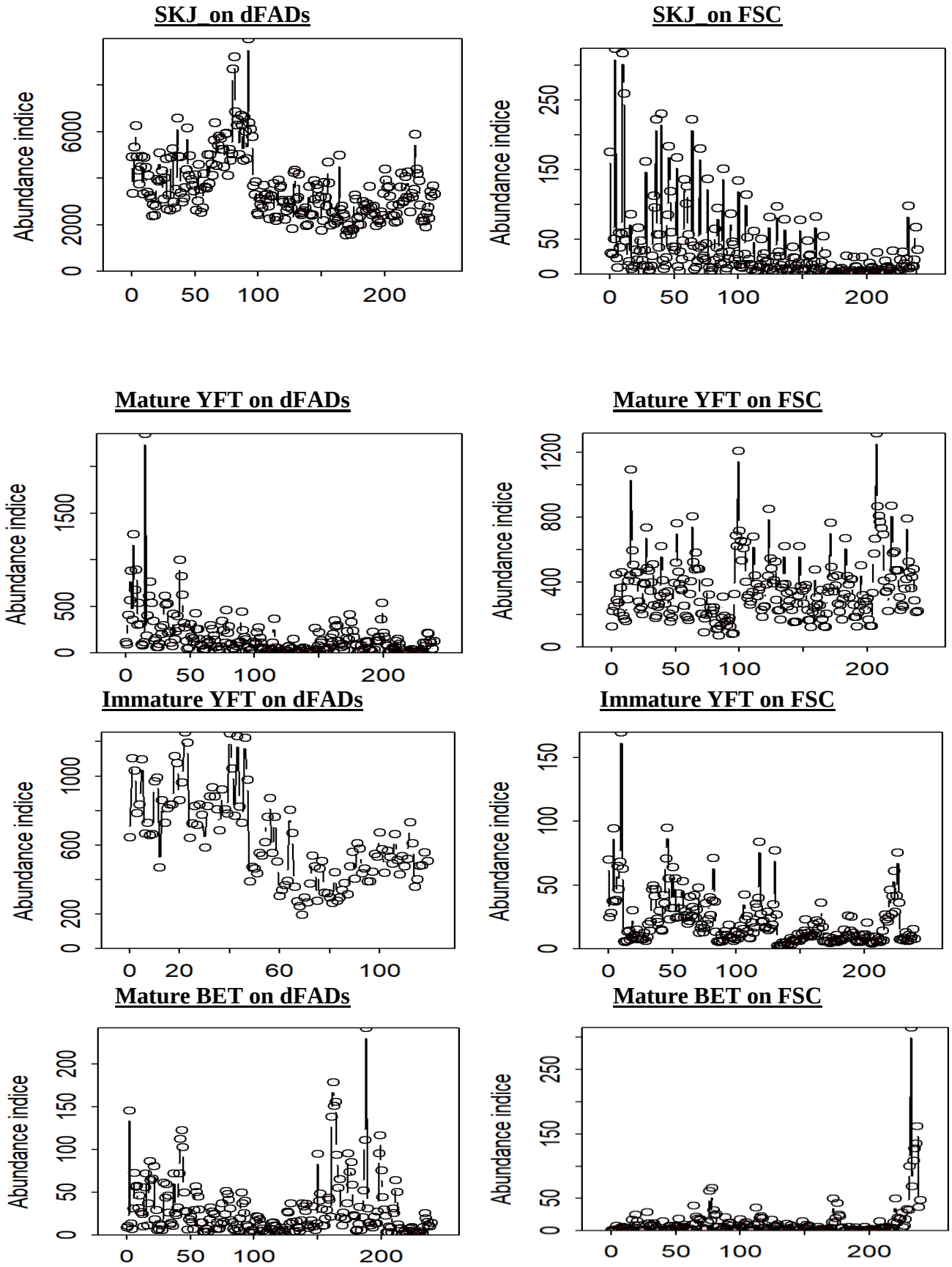

Fig. 3:S2 Estimated abundance indices of the eight categories of tropical tunas analysed in this study. Each showing bias-corrected maximum likelihood estimate (circles) and +/- one standard error for each month (20*12 month=240; 20*6= 120 in the case of immature yellowfin tuna caught on dFADs).

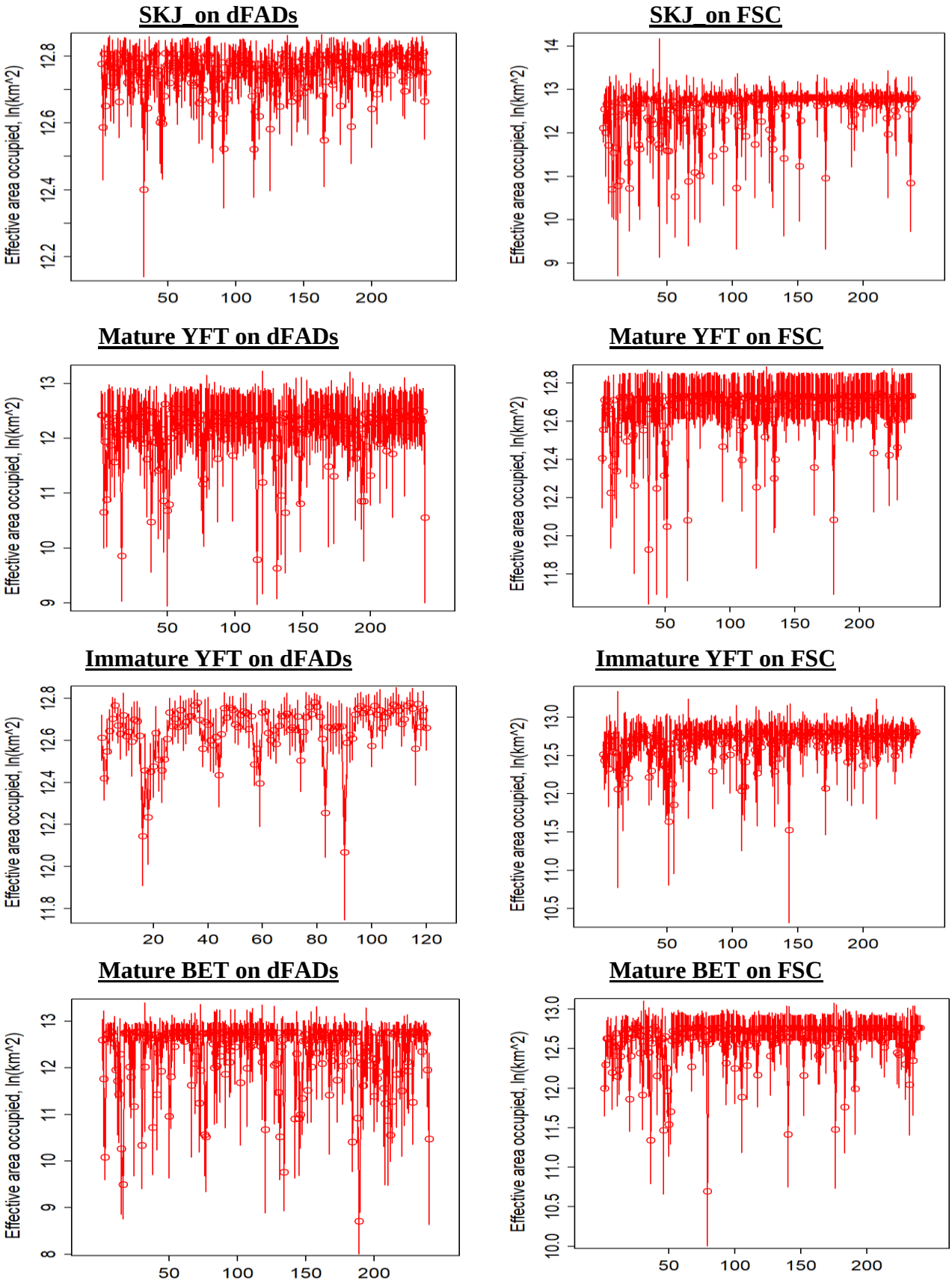

Fig. 4:S2 Estimated effective area occupied (representing area needed to contain the population at average biomass-density) of the eight categories of tropical tunas analysed in this study

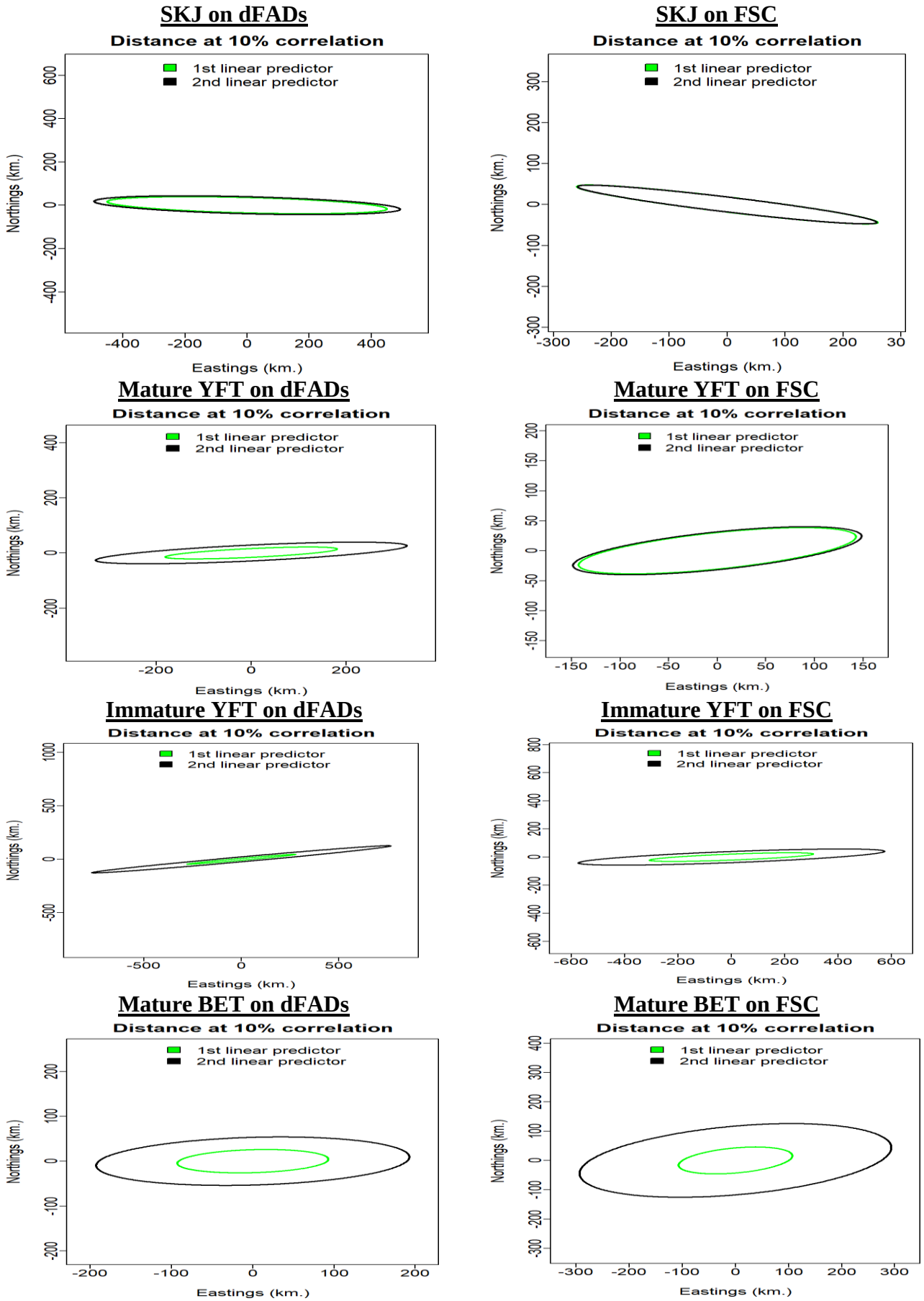

Fig. 5:S2 Ellipses representing estimates of geometric anisotropy for each species (green line: spatial variation in encounter probability; black line: spatial variation in positive catch rate).They represent the decorrelation distance for different directions.

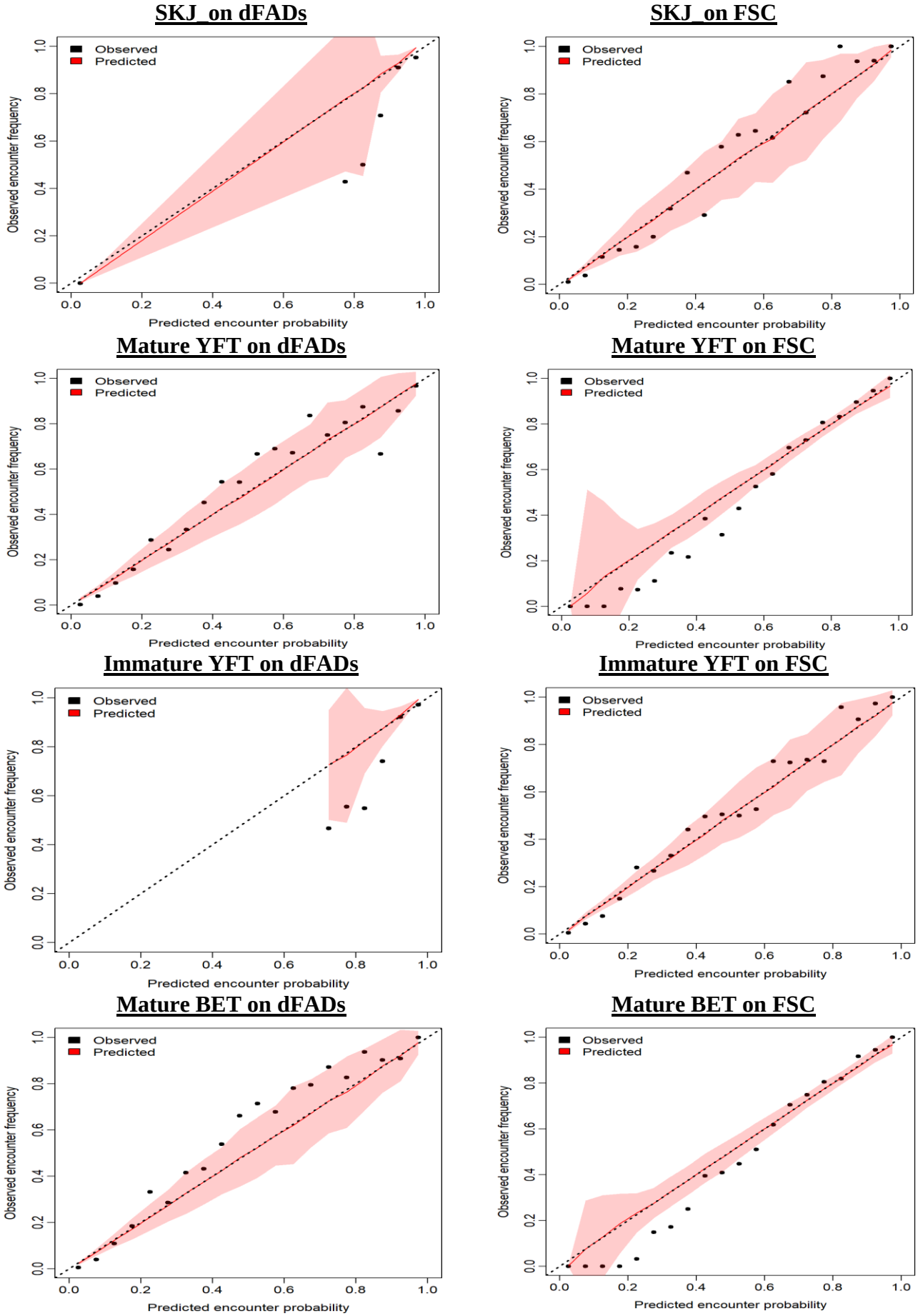

Fig. 6:S2 Expected probability and observed frequency of encounter for "encounter probability" component of the eight categories of tropical tunas analysed in this study.

Table 1: S2

List of estimated parameters (and associated symbols) governing spatial and temporal variance (listing estimate "Est." and standard error "SE") each case study application; this corresponds to all estimated fixed effects except intercepts $\mu_\beta, \beta_{nu}(u)$, and $\beta_{ny}(y)$.

		SKJ caught on dFADs		SKJ caught on FSC	
	Symbol	Est	S.E.	Est	S.E.
Parameter # 1 in H	--	1.26	0.38	1.31	0.46
Parameter # 2 in H	--	-0.12	0.42	-0.58	0.74
SD for spatial variation in n	$\sigma_{n\omega}$	0.01	0.20	-1.2e-6	0.25
SD for spatial season–year interaction in n	$\sigma_{n\varepsilon}$	-0.55	0.28	-3.36	0.69
Natural log. for decorrelation rate in n	$\ln(\kappa_n)$	-3.80	0.57	-3.19	0.24
SD for intercept season–year interaction in n	$\sigma_{n\beta}$	--		--	
Autocorrelation for intercepts in n	$\rho_{n\beta}$	--		--	
Autocorrelation for spatial season–year interaction in n	$\rho_{n\varepsilon}$	--		0.4	0.11
Natural log. for SD in spatial season and year effects in n	$\ln(\sigma_{n\xi})$	-1.89	0.91	6.61e-3	0.66
SD for spatial variation in w	$\sigma_{w\omega}$	0.26	0.09	3.5e-8	0.36
SD for spatial season–year interaction in w	$\sigma_{w\varepsilon}$	0.81	0.22	1.76	0.44
Natural log. for decorrelation rate in w	$\ln(\kappa_w)$	-3.89	0.31	-3.19	0.31
SD for intercept season–year interaction in w	$\sigma_{w\beta}$	--		--	
Autocorrelation for intercepts in w	$\rho_{w\beta}$	--		--	
Autocorrelation for spatial season–year interaction in w	$\rho_{w\varepsilon}$	0.24	0.09	0.27	0.19
Natural log. for SD in spatial season and year effects in w	$\ln(\sigma_{w\xi})$	--		--	
Natural log. for SD of measurement error	$\ln(\sigma_m)$	-0.31	0.01	-0.12	0.03
Impact of catchability covariates on 1st linear predictor	$\lambda_1(k)$_4	-0.04	0.12	0.50	0.14
Impact of catchability covariates on 1st linear predictor	$\lambda_1(k)$_6	0.19	0.12	-0.6	0.15
Impact of catchability covariates on 1st linear predictor	$\lambda_1(k)$_7	1.82	280	-0.6	0.16
Impact of catchability covariates on 1st linear predictor	$\lambda_1(k)$_8	0.09	0.10	-1.05	0.49
Impact of catchability covariates on 2nd linear predictor	$\lambda_2(k)$_4	0.10	0.12	0.31	0.15
Impact of catchability covariates on 2nd linear predictor	$\lambda_2(k)$_6	0.05	0.12	0.60	0.17
Impact of catchability covariates on 2nd linear predictor	$\lambda_2(k)$_7	-1.59	280	0.77	0.18
Impact of catchability covariates on 2nd linear predictor	$\lambda_2(k)$_8	0.05	0.10	1.06	0.4

Parameters listed as "--" correspond to terms that are dropped due to the corresponding variance approaching zero. The linear transformation H governing geometric anisotropy involves estimating two parameters which are listed first in the table (Parameter # 1 in H and Parameter # 2 in H).

Table 2: S2

List of estimated parameters (and associated symbols) governing spatial and temporal variance (listing estimate "Est." and standard error "SE") each case study application; this corresponds to all estimated fixed effects except intercepts $\mu_\beta, \beta_{nu}(u)$, and $\beta_{ny}(y)$.

		Mature BET caught on dFADs		Mature BET caught on FSC	
	Symbol	Est	S.E.	Est	S.E.
Parameter # 1 in H	--	0.64	0.28	0.45	0.27
Parameter # 2 in H	--	0.074	0.34	0.17	0.25
SD for spatial variation in n	$\sigma_{n\omega}$	1.5e-7	0.12	0.57	0.15
SD for spatial season–year interaction in n	$\sigma_{n\varepsilon}$	-3.5	0.35	1.28	0.24
Natural log. for decorrelation rate in n	$\ln(\kappa_n)$	-2.85	0.14	-3.17	0.24
SD for intercept season–year interaction in n	$\sigma_{n\beta}$	--		--	
Autocorrelation for intercepts in n	$\rho_{n\beta}$	--		--	
Autocorrelation for spatial season–year interaction in n	$\rho_{n\varepsilon}$	-0.20	0.55	0.27	0.15
Natural log. for SD in spatial season and year effects in n	$\ln(\sigma_{n\xi})$	-9.25	3600	-9.33	1600
SD for spatial variation in w	$\sigma_{w\omega}$	0.52	0.18	-2.6e-6	0.13
SD for spatial season–year interaction in w	$\sigma_{w\varepsilon}$	-1.68	0.33	-1.105	0.11
Natural log. for decorrelation rate in w	$\ln(\kappa_w)$	-3.57	0.27	-4.1	0.00
SD for intercept season–year interaction in w	$\sigma_{w\beta}$	--		--	
Autocorrelation for intercepts in w	$\rho_{w\beta}$	--		--	
Autocorrelation for spatial season–year interaction in w	$\rho_{w\varepsilon}$	-0.25	0.27	0.35	0.097
Natural log. for SD in spatial season and year effects in w	$\ln(\sigma_{w\xi})$	--		-	
Natural log. for SD of measurement error	$\ln(\sigma_m)$	-0.24	0.038	-0.095	0.011
Impact of catchability covariates on 1st linear predictor	$\lambda_1(k)$_4	-0.57	0.12	-0.031	0.053
Impact of catchability covariates on 1st linear predictor	$\lambda_1(k)$_6	0.016	0.15	0.0014	0.064
Impact of catchability covariates on 1st linear predictor	$\lambda_1(k)$_7	-0.22	0.14	-0.084	0.066
Impact of catchability covariates on 1st linear predictor	$\lambda_1(k)$_8	0.55	0.42	-5.44	0.22
Impact of catchability covariates on 2nd linear predictor	$\lambda_2(k)$_4	0.27	0.14	-0.14	0.057
Impact of catchability covariates on 2nd linear predictor	$\lambda_2(k)$_6	0.11	0.19	0.15	0.069
Impact of catchability covariates on 2nd linear predictor	$\lambda_2(k)$_7	0.41	0.2	0.25	0.068
Impact of catchability covariates on 2nd linear predictor	$\lambda_2(k)$_8	0.105	0.48	1.03	0.26

Parameters listed as "--" correspond to terms that are dropped due to the corresponding variance approaching zero. The linear transformation H governing geometric anisotropy involves estimating two parameters which are listed first in the table (Parameter # 1 in H and Parameter # 2 in H).

Table 3: S2

List of estimated parameters (and associated symbols) governing spatial and temporal variance (listing estimate "Est." and standard error "SE") each case study application; this corresponds to all estimated fixed effects except intercepts $\mu_\beta, \beta_{nu}(u)$, and $\beta_{ny}(y)$.

		Mature YFT caught on dFADs		Mature YFT caught on FSC	
	Symbol	Est	S.E.	Est	S.E.
Parameter # 1 in H	--	1.21	0.34	0.76	0.47
Parameter # 2 in H	--	0.248	0.46	0.29	0.49
SD for spatial variation in n	$\sigma_{n\omega}$	-1.7e-7	0.15	0.62	0.17
SD for spatial season–year interaction in n	$\sigma_{n\varepsilon}$	3.44	0.41	1.23	0.26
Natural log. for decorrelation rate in n	$\ln(\kappa_n)$	-2.94	0.14	-3.14	0.27
SD for intercept season–year interaction in n	$\sigma_{n\beta}$	--		--	
Autocorrelation for intercepts in n	$\rho_{n\beta}$	--		--	
Autocorrelation for spatial season–year interaction in n	$\rho_{n\varepsilon}$	-0.14	0.22	0.04	0.18
Natural log. for SD in spatial season and year effects in n	$\ln(\sigma_{n\xi})$	-9.1	2840	-8.26	1194
SD for spatial variation in w	$\sigma_{w\omega}$	1.26	0.35	0.33	0.15
SD for spatial season–year interaction in w	$\sigma_{w\varepsilon}$	-1.26	0.42	1.29	0.24
Natural log. for decorrelation rate in w	$\ln(\kappa_w)$	-3.53	0.32	-3.18	0.23
SD for intercept season–year interaction in w	$\sigma_{w\beta}$	--		--	
Autocorrelation for intercepts in w	$\rho_{w\beta}$	--		--	
Autocorrelation for spatial season–year interaction in w	$\rho_{w\varepsilon}$	-0.69	1.17	0.313	0.17
Natural log. for SD in spatial season and year effects in w	$\ln(\sigma_{w\xi})$	--		--	
Natural log. for SD of measurement error	$\ln(\sigma_m)$	-0.16	0.036	-0.19	0.012
Impact of catchability covariates on 1st linear predictor	$\lambda_1(k)$_4	-0.5	0.12	-0.09	0.054
Impact of catchability covariates on 1st linear predictor	$\lambda_1(k)$_6	-0.17	0.14	-7.4 e-3	0.066
Impact of catchability covariates on 1st linear predictor	$\lambda_1(k)$_7	-0.26	0.13	-0.071	0.067
Impact of catchability covariates on 1st linear predictor	$\lambda_1(k)$_8	0.61	0.43	-0.43	0.20
Impact of catchability covariates on 2nd linear predictor	$\lambda_2(k)$_4	0.079	0.14	0.15	0.052
Impact of catchability covariates on 2nd linear predictor	$\lambda_2(k)$_6	0.092	0.18	0.18	0.064
Impact of catchability covariates on 2nd linear predictor	$\lambda_2(k)$_7	0.37	0.17	0.30	0.064
Impact of catchability covariates on 2nd linear predictor	$\lambda_2(k)$_8	-0.012	0.48	0.23	0.19

Parameters listed as "--" correspond to terms that are dropped due to the corresponding variance approaching zero. The linear transformation H governing geometric anisotropy involves estimating two parameters which are listed first in the table (Parameter # 1 in H and Parameter # 2 in H).

Table 4: S2

List of estimated parameters (and associated symbols) governing spatial and temporal variance (listing estimate "Est." and standard error "SE") each case study application; this corresponds to all estimated fixed effects except intercepts $\mu_\beta, \beta_{nu}(u)$, and $\beta_{ny}(y)$.

		Immature YFT caught on dFADs		Immature YFT caught on FSC	
	Symbol	Est	S.E.	Est	S.E.
Parameter # 1 in H	--	1.74	0.36	1.33	0.58
Parameter # 2 in H	--	0.90	0.65	0.25	0.97
SD for spatial variation in n	$\sigma_{n\omega}$	--		-0.47	0.75
SD for spatial season–year interaction in n	$\sigma_{n\varepsilon}$	0.81	0.17	-2.66	0.69
Natural log. for decorrelation rate in n	$\ln(\kappa_n)$	-2.83	0.27	-3.35	0.28
SD for intercept season–year interaction in n	$\sigma_{n\beta}$	--		--	
Autocorrelation for intercepts in n	$\rho_{n\beta}$	--		--	
Autocorrelation for spatial season–year interaction in n	$\rho_{n\varepsilon}$	-0.18	0.29	0.47	0.11
Natural log. for SD in spatial season and year effects in n	$\ln(\sigma_{n\xi})$	-10.39	59034	0.14	0.41
SD for spatial variation in w	$\sigma_{w\omega}$	-0.36	0.09	6.5e-9	0.21
SD for spatial season–year interaction in w	$\sigma_{w\varepsilon}$	-0.70	0.13	1.27	0.45
Natural log. for decorrelation rate in w	$\ln(\kappa_w)$	-3.85	0.21	-3.97	0.43
SD for intercept season–year interaction in w	$\sigma_{w\beta}$	--		--	
Autocorrelation for intercepts in w	$\rho_{w\beta}$	--		--	
Autocorrelation for spatial season–year interaction in w	$\rho_{w\varepsilon}$	0.39	0.079	0.43	0.27
Natural log. for SD in spatial season and year effects in w	$\ln(\sigma_{w\xi})$	--		--	
Natural log. for SD of measurement error	$\ln(\sigma_m)$	-0.31	0.01	-0.046	0.024
Impact of catchability covariates on 1st linear predictor	$\lambda_1(k)$_4	0.31	0.10	0.67	0.09
Impact of catchability covariates on 1st linear predictor	$\lambda_1(k)$_6	0.06	0.10	-0.802	0.11
Impact of catchability covariates on 1st linear predictor	$\lambda_1(k)$_7	0.36	0.11	-0.56	0.10
Impact of catchability covariates on 1st linear predictor	$\lambda_1(k)$_8	1.73	75	-2.66	0.29
Impact of catchability covariates on 2nd linear predictor	$\lambda_2(k)$_4	-0.17	0.101	-0.080	0.10
Impact of catchability covariates on 2nd linear predictor	$\lambda_2(k)$_6	-0.025	0.109	0.18	0.13
Impact of catchability covariates on 2nd linear predictor	$\lambda_2(k)$_7	-0.11	0.11	0.43	0.13
Impact of catchability covariates on 2nd linear predictor	$\lambda_2(k)$_8	-1.53	75	1.05	0.31

Parameters listed as "--" correspond to terms that are dropped due to the corresponding variance approaching zero. The linear transformation H governing geometric anisotropy involves estimating two parameters which are listed first in the table (Parameter # 1 in H and Parameter # 2 in H).

4 CEEMDAN decomposition results

The next figures show the results of the decomposition of the abundance indices in intrinsic mode functions (IMFs).

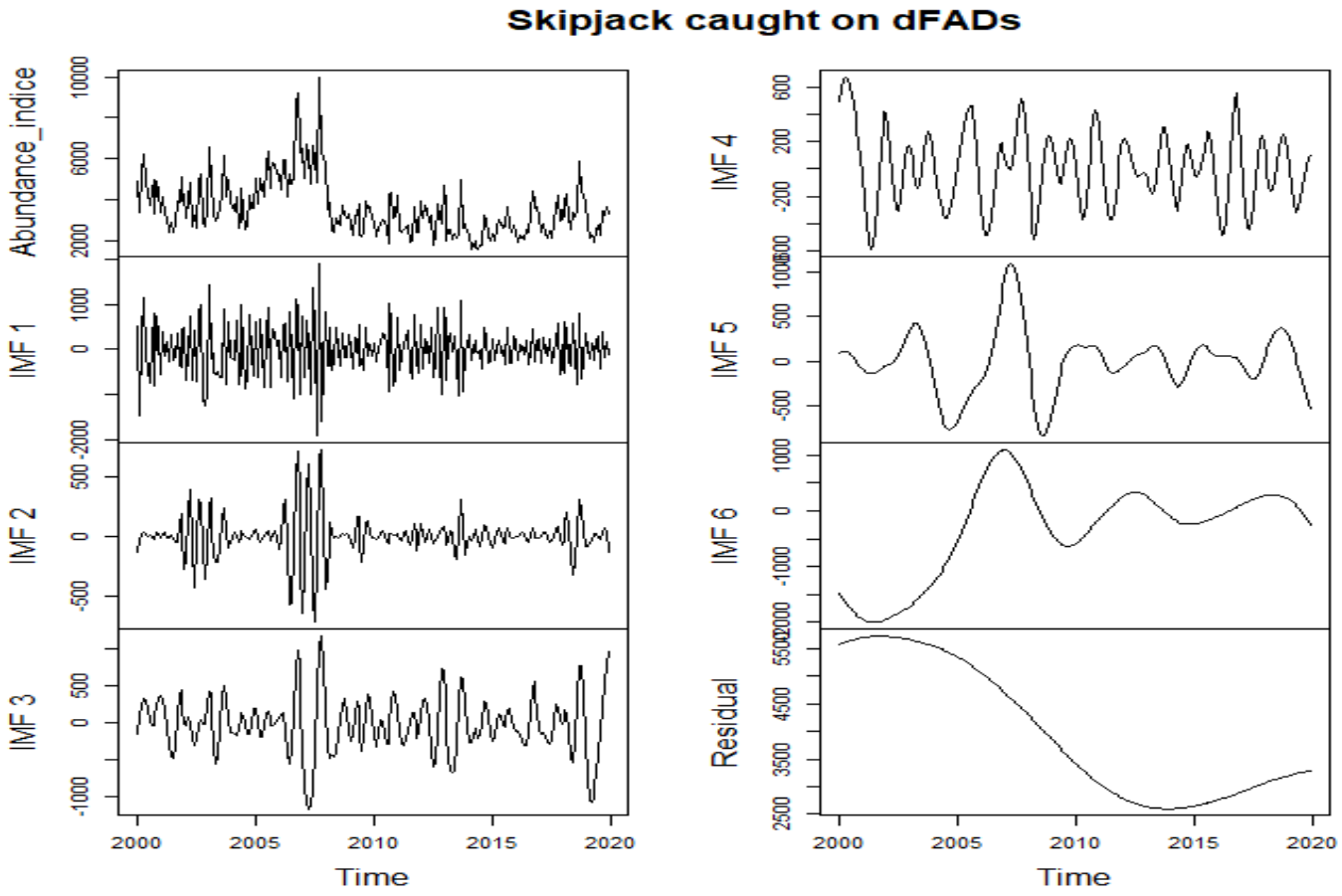
Skipjack caught on dFADs
Abundance_indice
IMF 1
IMF 2
IMF 3
IMF 4
IMF 5
IMF 6
Residual
Time
2000
2005
2010
2015
2020

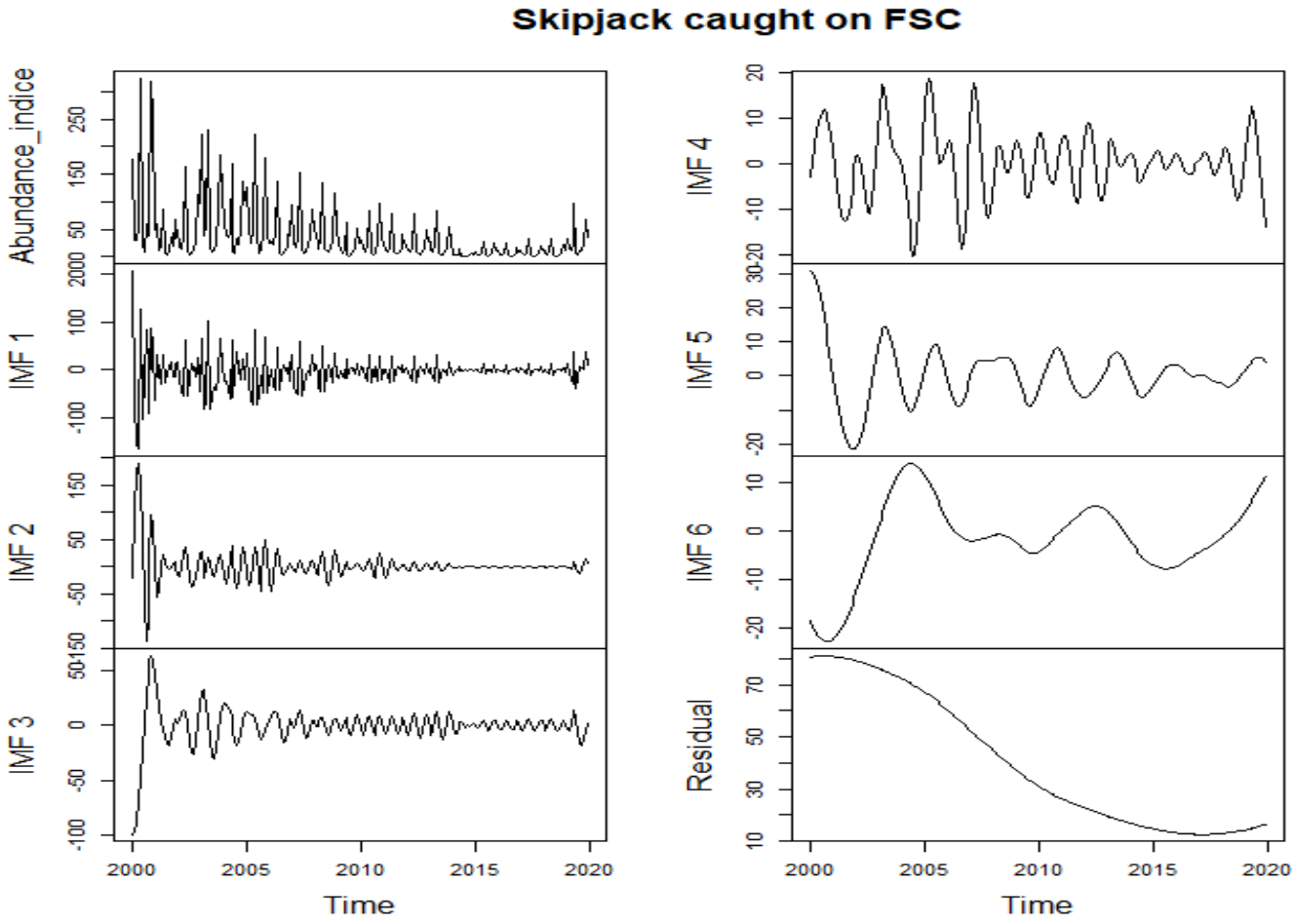
Skipjack caught on FSC
Abundance_indice
IMF 1
IMF 2
IMF 3
IMF 4
IMF 5
IMF 6
Residual
Time
2000
2005
2010
2015
2020

Mature bigeye caught on dFADs

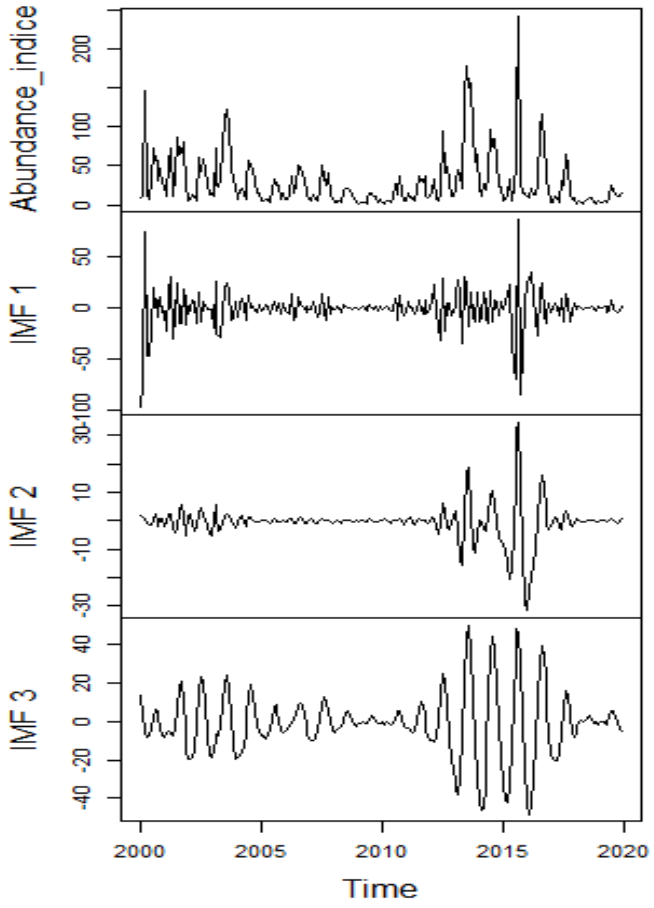

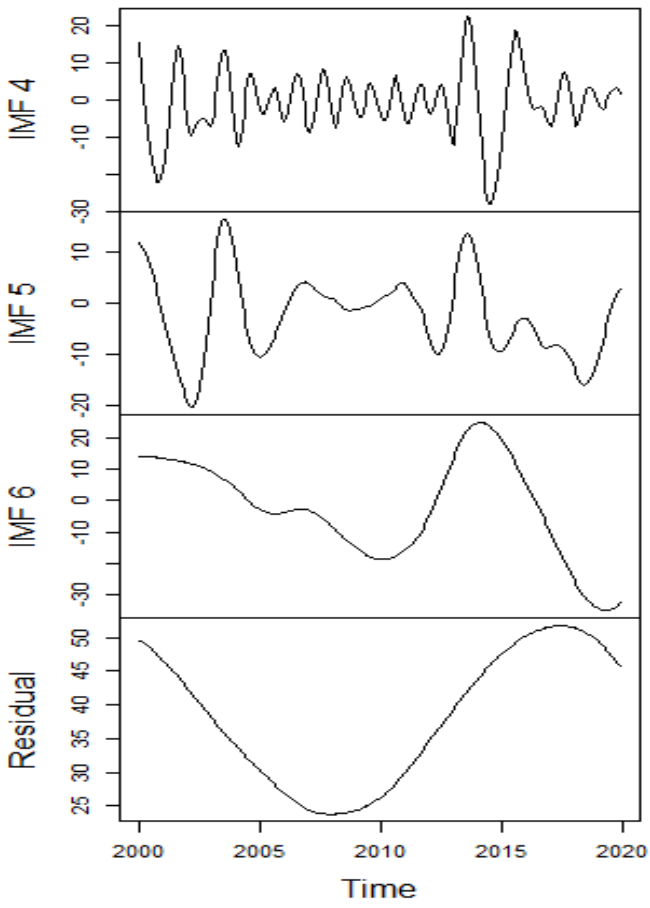

Mature bigeye caught on FSC

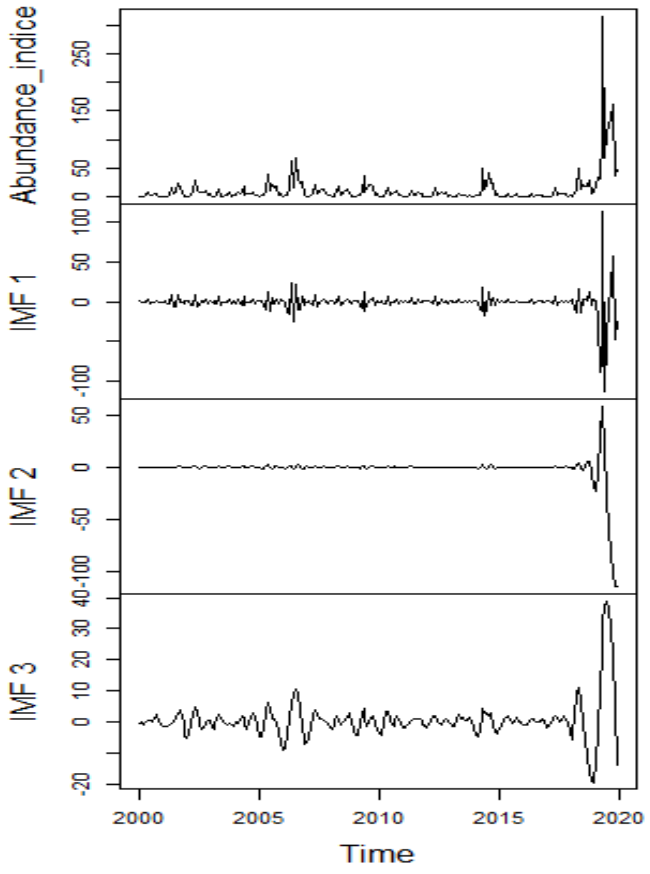

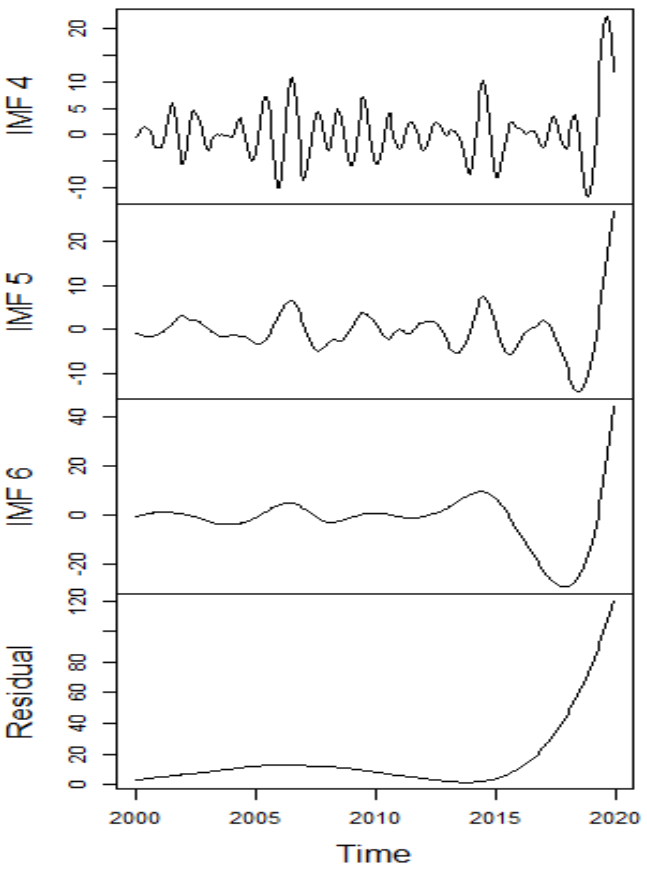

Mature yellowfin caught on dFADs

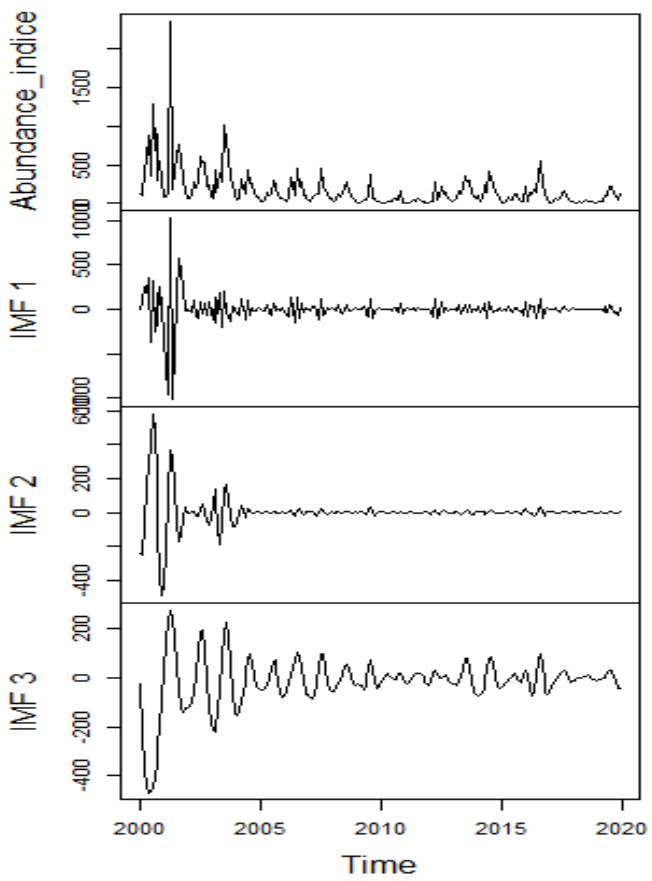

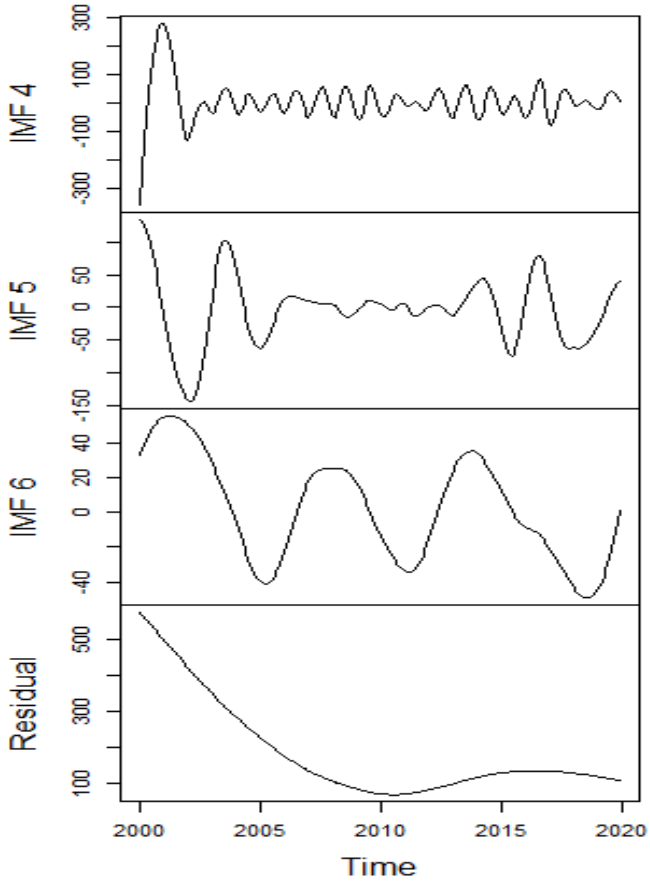

Mature yellowfin caught on FSC

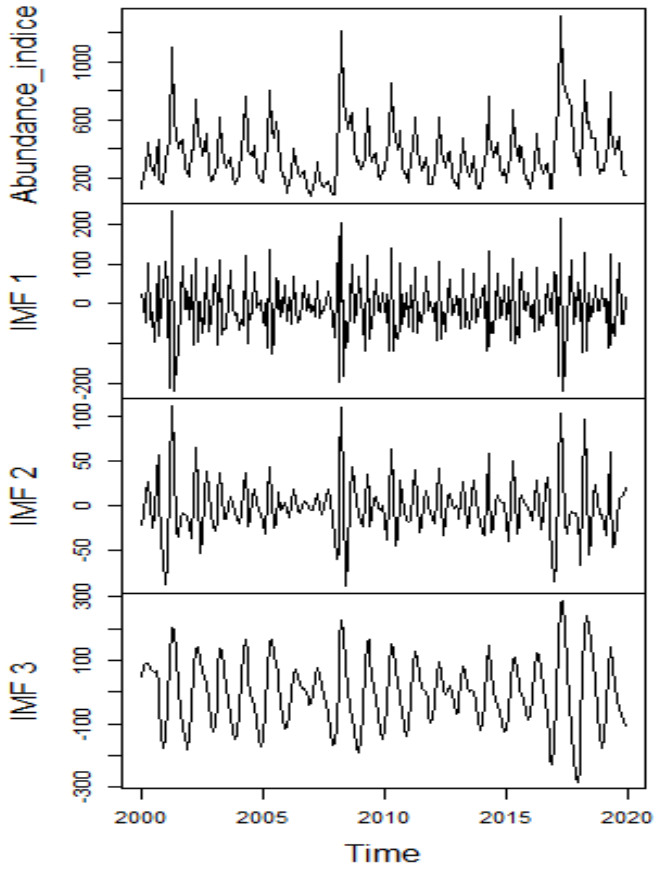

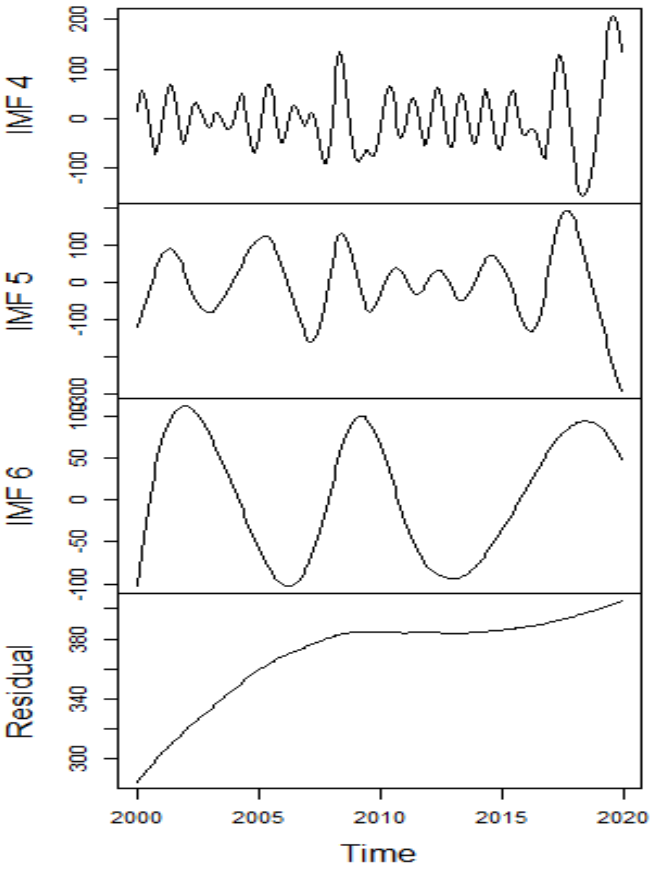

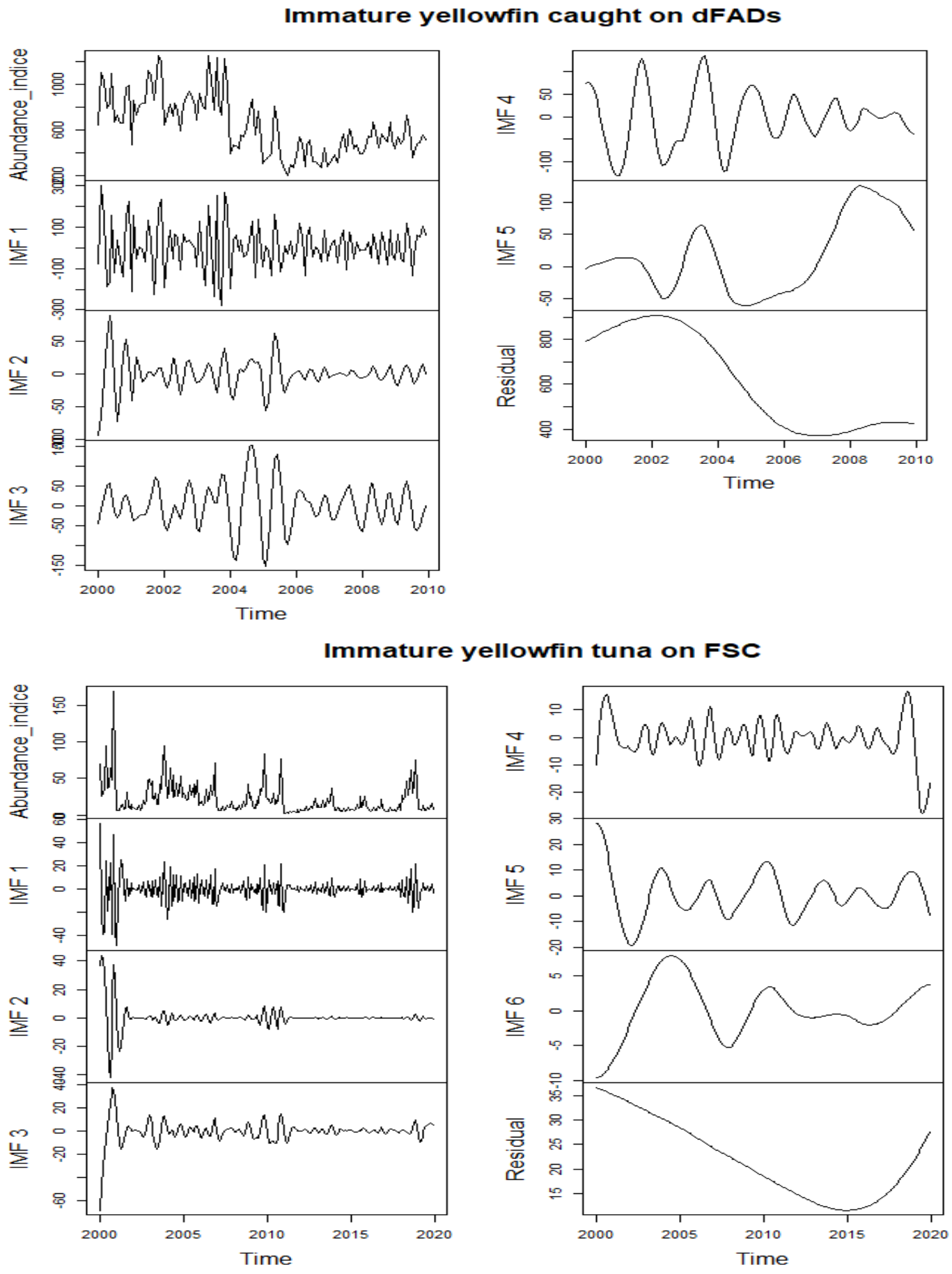

Fig. 7: S2 CEEMDAN decomposition of the abundance indices into intrinsic mode functions and residual. The comment is the same for the 8 figures.